Physics Reference Manual

December 29, 1999

Contents

I Generalities **1**

1 Computing the occurrence of a process **2**
1.1 Particle transport using the *differential* approach 2
1.1.1 The interaction length 2
1.1.2 Determination of the interaction point 3
1.2 Particle transport with *integral* approach 4
1.3 Updating of the proper and laboratory time of the particle . 5
1.4 Status of this document 6

2 SetCuts : conversion from range to kinetic energy **7**
2.1 Charged particles 7
2.1.1 General scheme 7
2.1.2 Energy loss formula for heavy charged particles 8
2.1.3 Energy loss of electrons and positrons 8
2.1.4 Range calculation 8
2.2 Photons 9
2.2.1 General scheme 9
2.2.2 Cross section formula for elements 9
2.2.3 Absorption length vector 9
2.2.4 Meaningful cuts in absorption length 10
2.3 Status of this document 10

II Particle's decay **11**

3 Decay **12**
3.1 Mean free path for decay in flight 12
3.2 Decay Channel 12
3.2.1 Muon Decay 13
3.2.2 Kaon Decay 13

III Electromagnetic Interactions **15**

4 Electromagnetic Interactions: General **16**
4.1 Compute the energy loss . . . 17
4.1.1 Energy loss of electrons/positrons . . . 17
4.1.2 Energy loss of muons . . . 18
4.1.3 Energy loss of charged hadrons . . . 19
4.1.4 Status of this document . . . 19
4.2 Multiple scattering . . . 20
4.2.1 Status of this document . . . 22
4.3 Transition radiation . . . 23
4.3.1 Method . . . 23
4.3.2 Simulation of the X-ray transition radiation production 25
4.3.3 Status of this document . . . 25
4.4 Scintillation . . . 26
4.5 Čerenkov effect . . . 27

5 Electromagnetic Interactions: Gamma incident **29**
5.1 PhotoElectric effect . . . 30
5.1.1 Cross section and Mean free path . . . 30
5.1.2 final state . . . 31
5.1.3 Status of this document . . . 31
5.2 Compton scattering . . . 32
5.2.1 Cross section and Mean free path . . . 32
5.2.2 Sampling the final state . . . 33
5.2.3 Restriction . . . 35
5.2.4 Status of this document . . . 35

6 Electromagnetic Interactions: Electron incident **36**
6.1 Ionisation . . . 37
6.1.1 Method . . . 37
6.1.2 Continuous energy loss . . . 37
6.1.3 Total cross-sections . . . 38
6.1.4 Simulation of the $\delta - ray$ production . . . 39
6.1.5 Status of this document . . . 40
6.2 Bremsstrahlung . . . 41
6.2.1 Cross section and energy loss . . . 41
6.2.2 Simulation of the discrete bremsstrahlung . . . 48
6.2.3 Status of this document . . . 51
6.3 e^+e^- annihilation . . . 53
6.3.1 Cross section and Mean free path . . . 53
6.3.2 Sampling the final state . . . 54
6.3.3 Restrictions . . . 55
6.3.4 Status of this document . . . 55

6.4 Synchrotron radiation . . . 57
6.4.1 Method . . . 57
6.4.2 Simulation of synchrotron radiation . . . 58
6.4.3 Status of this document . . . 58
6.5 Photoabsorption ionization model . . . 60
6.5.1 Method . . . 60
6.5.2 Simulation of energy losses . . . 62
6.5.3 Status of this document . . . 62
6.6 Photoabsorption cross section at low energies . . . 63
6.6.1 Method . . . 63
6.6.2 Status of this document . . . 63

7 Electromagnetic Interactions: Low energy extension 65
7.1 Introduction . . . 66
7.1.1 Physics . . . 66
7.1.2 Common features . . . 66
7.1.3 Software implementation . . . 68
7.2 Status of the document . . . 68
7.3 Compton scattering . . . 69
7.4 Status of the document . . . 69
7.5 Rayleigh effect . . . 70
7.6 Status of the document . . . 70
7.7 Photo-electric effect . . . 71
7.8 Status of the document . . . 71
7.9 Bremsstrahlung . . . 72
7.10 Status of the document . . . 72
7.11 Ionisation . . . 73
7.12 Status of the document . . . 73
7.13 Ionisation (new fits) . . . 74
7.14 Status of the document . . . 75

8 Electromagnetic Interactions: Muon incident 76
8.1 Ionisation . . . 77
8.1.1 Method . . . 77
8.1.2 Continuous energy loss . . . 77
8.1.3 Simulation of the knock-on electrons . . . 79
8.1.4 Status of this document . . . 80
8.2 Bremstrahlung . . . 82
8.2.1 Differential cross section . . . 82
8.2.2 Aplicability and restrictions of the method . . . 83
8.2.3 Continuous energy loss . . . 83
8.2.4 Total cross section . . . 83
8.2.5 Sampling . . . 83
8.2.6 Status of this document . . . 85

8.3 Muon photonuclear interaction . . . 86
8.3.1 Inelastic interaction of muons with nuclei . . . 86
8.3.2 Sampling . . . 87
8.4 e^+e^- pair production by muons . . . 90
8.4.1 Direct electron pair production by muons . . . 90
8.4.2 Differential cross section . . . 91
8.4.3 Sampling of e^+e^- pair production . . . 93

9 Electromagnetic Interactions: Charged hadron incident 96
9.1 Ionisation . . . 97
9.1.1 Method . . . 97
9.1.2 Continuous energy loss . . . 97
9.1.3 Simulation of the delta-ray production . . . 100
9.1.4 Status of this document . . . 100

10 Electromagnetic Interactions: Optical photon 102
10.1 Interactions of optical photons . . . 103
10.1.1 Physics processes for optical photons . . . 103
10.1.2 Photon polarization . . . 104
10.1.3 Tracking of the photons . . . 105

IV Hadronic Interactions 109

11 Lepton Hadron Interactions 110
11.1 Overview . . . 110
11.2 the Interaction model . . . 110
11.2.1 Mean free path . . . 110
11.2.2 Calculation of differential cross section . . . 111
11.3 Status of this document . . . 111

12 Interactions of Stopping Particles 113
12.1 Complementary parameterised and theoretical treatment . . . 113
12.1.1 Pion absorption at rest . . . 115

13 Parametrization Driven Models 117
13.1 High energy hadron nucleus interactions . . . 117

14 Theory Driven Models 119

15 Parton string model. 120
15.1 Reaction initial state simulation. . . . 120
15.1.1 Allowed projectiles and bombarding energy range for interaction with nucleon and nuclear targets. . . . 120
15.1.2 MC initialization procedure for nucleus. . . . 120

15.1.3 Random choice of the impact parameter. 121
15.2 Sample of collision participants in nuclear collisions. 122
15.2.1 MC procedure to define collision participants. 122
15.2.2 Separation of hadron diffraction excitation. 123
15.3 Longitudinal string excitation. 124
15.3.1 Hadron–nucleon inelastic collision. 124
15.3.2 The diffractive string excitation. 124
15.3.3 The string excitation by parton exchange. 124
15.3.4 Transverse momentum sampling. 124
15.3.5 Hadron–nucleus inelastic collisions. 125
15.3.6 The diffractive string excitation. 125
15.3.7 The string excitation by parton rearrangement. 125
15.4 Longitudinal string decay. 126
15.4.1 Hadron production by string fragmentation. 126
15.4.2 The hadron formation time and coordinate. 127
15.5 Status of this document. 128

16 Hadron kinetic model. 130
16.1 Reaction initial state simulation. 130
16.1.1 Allowed projectiles and bombarding energy range for interaction with nucleon and nuclear targets. 130
16.2 Hadron propagation. 130
16.3 Selection of particle collisions and particle decays. 131
16.3.1 Particle collision criterion and collision time. 131
16.3.2 Hadron resonance lifetime. 131
16.4 Hadron interaction cross sections. 132
16.4.1 Hadron interaction tabulated and parametrized cross sections. 132
16.4.2 The interaction cross sections for meson-baryon collisions with quark annihilation. 132
16.4.3 Nucleon-nucleon resonance interaction cross sections. . 133
16.5 Hadron collision simulation. 133
16.5.1 Two-body hadron scatterings. 133
16.6 Resonance decay simulation. 134
16.7 Phenomenological potentials. 134
16.7.1 The nucleon potential. 134
16.8 Pauli blocking procedure. 135
16.9 Residual nucleus parameters in the hadron-nucleus collision. . 135
16.10 Calculation of a residual nucleus excitation energy. 136
16.11 Status of this document. 136

17 Precompound model. **137**
17.1 Reaction initial state. . . . 137
17.2 Simulation of pre-compound reaction. . . . 137
17.2.1 Statistical equilibrium condition. . . . 137
17.2.2 Level density of excited (n-exciton) states. . . . 138
17.2.3 Transition probabilities. . . . 138
17.2.4 Emission probabilities for nucleons. . . . 140
17.2.5 Emission probabilities for complex fragments. . . . 140
17.2.6 The total probability. . . . 140
17.2.7 Calculation of kinetic energies for emitted particle. . . . 141
17.2.8 Parameters of residual nucleus. . . . 141
17.3 Status of this document. . . . 141

18 Evaporation model. **142**
18.1 Reaction initial state. . . . 142
18.2 Simulation of fragment evaporation. . . . 142
18.2.1 Evaporation threshold. . . . 142
18.2.2 Nuclear and fragment mass defects. . . . 143
18.2.3 Coulomb barrier calculation. . . . 143
18.2.4 The fragment evaporation probability. . . . 143
18.2.5 The inverse reaction cross section. . . . 143
18.2.6 The level density. . . . 144
18.2.7 The total evaporation probability. . . . 144
18.2.8 Kinetic energy of emitted fragment. . . . 144
18.2.9 Angular distribution of evaporated fragments. . . . 145
18.2.10 Parameters of residual nucleus. . . . 145
18.3 Fission probability calculation. . . . 145
18.3.1 The fission total probability. . . . 145
18.3.2 The fission barrier. . . . 146
18.4 The total probability for γ evaporation. . . . 146
18.4.1 Energy of evaporated photon. . . . 147
18.5 Discrete photon evaporation. . . . 147
18.6 Status of this document. . . . 147

19 Fission model. **149**
19.1 Reaction initial state. . . . 149
19.2 Fission process simulation. . . . 149
19.2.1 Atomic number distribution of fission products. . . . 149
19.2.2 Charge distribution of fission products. . . . 150
19.2.3 Kinetic energy distribution of fission products. . . . 151
19.2.4 Calculation of the excitation energy of fission products. 152
19.2.5 Excited fragment momenta. . . . 152
19.3 Status of this document. . . . 152

20 Fermi break-up model. 154
20.1 Fermi break-up simulation for light nuclei. 154
20.1.1 Masses of nuclei. 154
20.1.2 Allowed channel. 154
20.1.3 Break-up probability. 155
20.1.4 Fermi break-up model parameter. 156
20.1.5 Fragment characteristics. 156
20.1.6 MC procedure. 156
20.2 Status of this document. 156

21 Multifragmentation model. 158
21.1 Multifragmentation process simulation. 158
21.1.1 Multifragmentation probability. 158
21.1.2 Direct simulation of the low multiplicity multifragment disintegration. 160
21.1.3 Fragment multiplicity distribution. 161
21.1.4 Atomic number distribution of fragments. 161
21.1.5 Charge distribution of fragments. 161
21.1.6 Kinetic energy distribution of fragments. 162
21.1.7 Calculation of the fragment excitation energies. 162
21.2 Status of this document. 162

22 Low Energy Neutron Interactions 164
22.1 Introduction 164
22.2 Physics and Verification 164
22.2.1 Inclusive Cross-sections 164
22.2.2 Elastic Scattering 165
22.2.3 Radiative Capture 165
22.2.4 Fission 167
22.2.5 Inelastic Scattering 169
22.3 Summary 171

V Fast Shower Parametrizations 173

23 Fast Shower Parametrizations 174

Part I

Generalities

Chapter 1

Computing the occurrence of a process

1.1 Particle transport using the *differential* approach

1.1.1 The interaction length

* In a simple material the number of atoms per volume is:

$$n = \frac{\mathcal{N}\rho}{A}$$

where:

$\mathcal{N}$	Avogadro's number
ρ	density of the medium
A	mass of mole

* In a compound material the number of atoms of Element elm per volume is:

$$n_{elm} = \frac{\mathcal{N}\rho w_{elm}}{A_{elm}}$$

where:

$\mathcal{N}$	Avogadro's number
ρ	density of the medium
w_{elm}	proportion by mass of the Element elm
A_{elm}	mass of mole of the Element elm

* The mean free path, λ, of a process can be given in terms of its total cross section.

$$\lambda(E) \equiv \frac{1}{\Sigma(E)} = \frac{1}{\sum_{elm}\left[n_{elm}\sigma(Z_{elm}, E)\right]}$$

where $\sigma(Z, E)$ is the total cross section per atom of the process and $\sum_{elm}$ runs over all Elements the material is made of.

Cross sections per atom and mean free path values are tabulated during initialisation.

1.1.2 Determination of the interaction point

The mean free path of a particle for a given process, λ, depends on the medium and cannot be used directly to sample the probability of an interaction in a heterogeneous detector. The number of mean free paths which a particle travels is:

$$n_\lambda = \int \frac{dx}{\lambda(x)} \tag{1.1}$$

and it is independent of the material traversed. If n_r is a random variable denoting the number of mean free paths from a given point until the point of interaction, it can be shown that n_r has the distribution function

$$P(n_r < n_\lambda) = 1 - e^{-n_\lambda} \tag{1.2}$$

The total number of mean free paths the particle travels before the interaction point, n_λ, is sampled at the beginning of the trajectory as:

$$n_\lambda = -\log(\eta) \tag{1.3}$$

where η is a random number uniformly distributed in the range $(0, 1)$. n_λ is updated after each step Δx according the formula:

$$n'_\lambda = n_\lambda - \frac{\Delta x}{\lambda(x)} \tag{1.4}$$

until the step originating from $s(x) = n_\lambda \lambda(x)$ is the shortest and this triggers the specific process.

The short description given above is the *differential approach* of the particle transport , which is used in most of the simulation codes(e.g. [GEANT3],[EGS4]).

In this approach besides the other (*discrete*) processes the continuous energy loss imposes a limit on the stepsize, too. The reason of this is the energy dependence of the cross sections. It is assumed in this approach that the cross sections of the particles are constant during a step , i.e. the step size should be so small that the relative difference of the cross sections at the beginning of the step and at the end can be small enough.In principle one has to use very small steps in order to have an accurate simulation , but the computing time increases if the stepsize decreases. As a good compromise the stepsize is limited in GEANT4 by the requirement that the stopping

range of the particle can decrease by not more than 20 % during the step. This condition works fine for a particle of kinetic energy $> 0.5MeV - 1.MeV$, but for low energy it gives very short step sizes. To cure this problem a lower limitation on the stepsize is also introduced. The lower limit of the stepsize is the *cut in range* parameter of the program.

There is another disadvantage of this usual differential algorithm , which can be a serious problem in the case of certain processes. If the interaction process has a cross section with narrow peaks in it , in this approach the particle can easily skip over these peaks.(This can happen in the case of a number of hadronic processes.)

To overcome these shortcomings the *integral approach* has been implemented in GEANT4 as an option .

1.2 Particle transport with *integral* approach

In this algorithm the integral in eq. 1.1 is really computed for every process and another equation is used instead of eq. 1.4 when n_λ is updated. This section gives a short overview on the formulae used in this approach.

The change in the number of mean free path after a *small* step can be written as

$$\Delta n_\lambda = \frac{\Delta x}{\lambda(x)}. \tag{1.5}$$

This formula can be rewritten in the following form

$$\Delta n_\lambda = \frac{dx}{dT} \cdot \frac{1}{\lambda(T)} \cdot dT, \tag{1.6}$$

where T kinetic energy of the particle
$\frac{dx}{dT} = \frac{1}{\frac{dT}{dx}}$ inverse of the well-known quantity $\frac{dE}{dx}$.

After these preliminaires the number of mean free paths (eq. 1.1) can be rewritten as

$$n_\lambda(T) = \int_0^T \frac{d\tau}{f(\tau) \cdot \lambda(\tau)} \tag{1.7}$$

or

$$n_\lambda(T) = \int_0^T \frac{\sigma(\tau) \cdot d\tau}{f(\tau)} \tag{1.8}$$

where $\frac{dE}{dx}$ has been denoted by $f()$. Eqs. 1.7 and 1.8 are the basic equations of the integral approach . The meaning of the integrals on the right hand sides of the equations is the number of mean free paths for a given process between the initial state of energy T and the stopping of the particle (energy 0).

The steps of the algorithm using the integral approach are the following:

- the number of mean free paths the particle travels to the interaction point , Δn_λ is sampled using eq. 1.3
- initial value of the quantity $n_\lambda(T_0)$ is computed
- the (possible) final energy T is calculated from

$$\Delta n_\lambda = n_\lambda(T_0) - n_\lambda(T) \tag{1.9}$$

- the step limitation originating from the process is

$$steplimit = r(T_0) - r(T) \tag{1.10}$$

, where the function $r(T)$ gives the range of the particle for a kinetic energy value T.

If the interaction occurred at the end of the step was some other process or the step was limited by the geometry (at medium boundary) , the number of mean free paths Δn_λ should be updated. This update can be easily done using the function $n_\lambda(T)$

$$\Delta n_{\lambda,updated} = \Delta n_\lambda - [n_\lambda(T_0) - n_\lambda(T)] \tag{1.11}$$

1.3 Updating of the proper and laboratory time of the particle

The proper and lab. time of the particle should be updated after each step. This update is done differently in the two approaches.

In the differential approach the following formula is used to update the particle time in the laboratory system

$$\Delta t_{lab} = \frac{\Delta x}{\frac{v_0+v}{2}} \tag{1.12}$$

, where

Δx	step travelled by the particle,
v_0	particle velocity at the beginning of the step
v	particle velocity at the end of the step .

This expression is a good approximation for use in the differential approach , because in this scheme the velocity is not allowed to change too much during the step.This is not the case in the integral approach, the kinetic energy and the velocity of the particle can change a lot here, therefore the update of the laboratory time is done by using the integral expression

$$t = \int_0^s \frac{dx}{v(x)} \tag{1.13}$$

which can be written as

$$t = \int_0^T \frac{f(\tau) \cdot d\tau}{v(\tau)}. \tag{1.14}$$

In the eqs. 1.13 and 1.14

t	time
v	velocity of the particle
s	path length can be travelled by the particle before stopping
T	kinetic energy
$f(T)$	dE/dx

Using eq. 1.14 the expression for Δt_{lab} is

$$\Delta t_{lab} = t(T_0) - t(T). \tag{1.15}$$

The update of the proper time is performed similarly in the two approaches.

1.4 Status of this document

9.10.98 created by L. Urbán.
5.12.98 editing by J.P. Wellisch.

Bibliography

[EGS4] W.R. Nelson et al.:The EGS4 Code System. *SLAC-Report-265 , December 1985*

[GEANT3] GEANT3 manual ,CERN Program Library Long Writeup W5013 (October 1994).

Chapter 2

SetCuts : conversion from range to kinetic energy

2.1 Charged particles

Starting from a particle cut given in stopping range, the method constructs a vector holding the cut values in kinetic energy for every material. The main steps of the algorithm are the same for all the charged particles, the only difference is that different energy loss formulae are used for electrons, positrons and heavy charged particles (muon,pion,proton,...).

In the case of charged hadrons this procedure is applied for the proton and antiproton only , the cut values in kinetic energy for other hadrons are computed using the proton and antiproton energy loss and range tables .

2.1.1 General scheme

1. An energy loss table is created and filled for all the elements in the element table.
2. For every material in the material table the following steps are performed:
   (a) a range vector is constructed using the energy loss table and formulae for the low energy part of the calculations,
   (b) the conversion from stopping range to kinetic energy is performed and the corresponding element of the `KineticEnergyCuts` vector is set (It contains the particle cut value in kinetic energy for the actual material.),
   (c) the range vector is deleted.
3. The energy loss table is deleted at the end of the process.

2.1.2 Energy loss formula for heavy charged particles

The energy loss of the particle is calculated from a simplified Bethe-Bloch formula if the kinetic energy of the particle is above the value :

$$T_{lim} = 2\,MeV \times \left(\frac{\text{particle mass}}{\text{proton mass}}\right)$$

The simplified here means that the low energy shell correction term and the high energy Sternheimer density correction term have been omitted. Below the energy value T_{lim} a simple parametrized energy loss formula is used to compute the loss, which reproduces the energy loss values of the stopping power tables fairly well. The main reason of using a parametrized formula for low energy is that the Bethe-Bloch breaks down at low energy. The formula has the following form :

$$\frac{dE}{dx} = \begin{cases} a * \sqrt{\frac{T}{M}} + b * \frac{T}{M} & \text{for } T \in [0,\, T_0] \\ \\ c * \sqrt{\frac{T}{M}} & \text{for } T \in [T_0,\, T_{lim}] \end{cases}$$

where : M = particle mass,
T = kinetic energy,
$T_0 = 0.1\,MeV \times Z^{1/3} \times$ M/(proton mass)
Z = atomic number.

the paramaters a, b, c have been chosen in such a way that dE/dx is a continuous function of T at $T = T_{lim}$ and $T = T_0$, and dE/dx reaches its maximum at the correct T value.

2.1.3 Energy loss of electrons and positrons

The Berger-Seltzer energy loss formula has been used for T $>$ 10 keV to compute the energy loss comes from the ionization . This formula plays the role of the Bethe-Bloch for electrons (see e.g. the GEANT3 manual).Below 10 keV the simple c/(T/mass of electron) parametrization has been used, where c can be determined from the requirement of continuity at T = 10 keV. As in the case of electrons the radiation loss is important even at relative low (few MeV) energy, a second term has been added to the energy loss formula which accounts for the radiation losses (losses due to bremsstrahlung). This second term is an empirical parametrized formula. For positrons a different formula is used to calculate the ionization loss, the term accounting for the radiation losses is the same than that for electrons.

2.1.4 Range calculation

The stopping range is defined as :

$$R(T) = \int_0^T \frac{1}{(dE/dx)}\, dE$$

The integration has been done analytically for the low energy part and numerically above an energy limit.

2.2 Photons

Starting from a particle cut given in absorption length, the method constructs a vector holding the cut values in kinetic energy for every material. The main steps of the algorithm are the following :

2.2.1 General scheme

1. A cross section table is created and filled for all the elements in the element table.
2. For every material in the material table the following steps are performed:
   (a) an absorption length vector is constructed using the cross section table
   (b) the conversion from absorption length to kinetic energy is performed and the corresponding element of the `KineticEnergyCuts` vector is set (It contains the particle cut value in kinetic energy for the actual material.),
   (c) the absorption length vector is deleted.
3. The cross section table is deleted at the end of the process.

2.2.2 Cross section formula for elements

An approximate empirical formula is used to compute the *absorption cross section* of a photon in an element. The *absorption cross section* means here the sum of the cross sections of the gamma conversion, Compton scattering and photoelectric effect. These processes are the 'destructive' processes for photons , they destroy the photon or decrease its energy. (The coherent or Rayleigh scattering changes the direction of the gamma only , its cross section is not included in the *absorption cross section*.)

2.2.3 Absorption length vector

The `AbsorptionLength` vector is calculated for every material as :

$$\texttt{AbsorptionLength} = 5/(\text{macroscopic absorption cross section})$$

The factor 5 comes from the requirement that the probability of having no 'destructive' interaction should be small, hence

$$\begin{aligned} \exp(-\texttt{AbsorptionLength * MacroscopicCrossSection}) &= \exp(-5) \\ &= 6.7 \times 10^{-3} \end{aligned}$$

2.2.4 Meaningful cuts in absorption length

The photon cross section for a material has a minimum at a certain kinetic energy T_{min}. The `AbsorptionLength` has a maximum at $T = T_{min}$, the value of the maximal `AbsorptionLength` is the biggest "meaningful" cut in absorption length . If the cut given by the user is bigger than this maximum, a warning is printed and the cut in kinetic energy is set to the maximum gamma energy (i.e. all the photons will be killed in the material).

2.3 Status of this document

9.10.98 created by L. Urbán.
5.12.98 editing by J.P. Wellisch.

Part II

Particle's decay

Chapter 3

Decay

The class G4Decay simulates both decay in flight and decay at rest. G4Decay determines decay time in the rest frame of the particle (i.e. proper time) according to its life time τ. Decay length is calculated from the result and its momentum.
Decay modes and their branching ratio is defined in G4DecayTable class, which is a member of G4ParticleDefinition. G4Decay selects a mode among decay modes defined in the decay table. In Geant4, the concept of "decay channel" is used for simulation of decay modes. There are many varieties of kinematics for determination of secondaries, for example V-A theory for muon decay, π^0 dalitz decay, and simple phase space decay. Individual decay channel class derived from G4VDecayChannel is assigned for each decay mechanism and calculates momentum of secondaries.

3.1 Mean free path for decay in flight

Mean free path λ is calculated for each step in the G4Decay class.
$\lambda = \beta c \tau \gamma$
where $\gamma = \sqrt{1 - \beta^2}$.
Mean free path is calculated by using momentum at the beginning of the step.

3.2 Decay Channel

Momentum of daughter particles are calculated in the rest frame of the parent particle by each decay channel class. And all secondaries are boosted into the laboratory frame. Polarization are not be taken into account for parent nor daughters.
In default, there are four decay channel classes in Geant4.

G4PhaseSpaceDecayChannel	: phase space decay
G4DalitzDecayChannel	: dalitz decay
G4MuonDecayChannel	: muon decay
G4KL3DecayChannel	: semi-leptonic decays of kaon

Here, G4PhaseSpaceDecayChannel and G4DalitzDecayChannel adopts same algorism as GENAT3.

3.2.1 Muon Decay

G4MuonDecayChannel simulates muon decay according to V-A theory. The energy of electron is calculated as follows:

$$d\Gamma = \frac{{G_F}^2 {m_\mu}^5}{192\pi^3} 2\epsilon^2(3\epsilon - 2\epsilon)$$

where:

Γ	:	decay rate
ϵ	:	$= E_e/E_{max}$
E_e	:	electron energy
E_{max}	:	maximum electron energy $= m_\mu/2$

Energies of two neutrinos are calculated so that energy/momentum conserves. Neutrino is not used for ordinary simulation (at least transparent for detectors), so energy and angular distribution formula used in this class is a simple one and is different from the V-A theory. Polarization of both muon and electron are not taken into consideration in this class.

3.2.2 Kaon Decay

The class G4KL3DecayChannel simulates following four decay modes of semi-leptonic decay of kaon:

${K^\pm}_{e3}$	:	$K^\pm \to \pi^0 + e^\pm + \nu$
${K^\pm}_{\mu 3}$	:	$K^\pm \to \pi^0 + \mu^\pm + \nu$
${K^0}_{e3}$	:	$K^0_L \to \pi^\pm + e^\mp + \nu$
${K^0}_{\mu 3}$	:	$K^0_L \to \pi^\pm + \mu^\mp + \nu$

Assuming that only vector current contributes to $K \to l\pi\nu$ decays, the matrix element can be described by using two dimensionless form factors of f_+ and f_-, which depend only on momentum transfer $t = (P_K - P_\pi)^2$.
The Dalitz plot density used in this class is as follows [1]:

$$\rho\left(E_\pi, E_\mu\right) \propto f_+^2\left(t\right)[A + B\xi\left(t\right) + C\xi\left(t\right)^2]$$

where: $A = m_K(2E_\mu E_\nu - m_K E'_\pi) + {m_\mu}^2(\frac{1}{4}E'_\pi - E_\nu)$
$B = {m_\mu}^2(E_\nu - \frac{1}{2}E'_\pi)$
$C = \frac{1}{4}{m_\mu}^2 E'_\pi$
$E'_\pi = {E_\pi}^{max} - E_\pi$

Here, $\xi(t)$ is the ratio of the two form factors

$$\xi(t) = f_-(t)/f_+(t)$$

We assume a linear dependence of $f_+(t)$ on t, i.e.

$$f_+(t) = f_+(0)[1 + \lambda_+(t/{m_\pi}^2)]$$

And we assume $f_-(t)$ is a constant due to time reversal invariance.

Then we use two parameters of λ_+ and $\xi(0)$ for describing Dalitz plot density in this class. As for values of these parameters, we adopt world average values given by Particle Data Group [1].

Bibliography

[1] L.M.Chounet, J.M.Gaillard, and M.K.gaillard, Phys. Reports 4C, 199 (1972)

[2] *Review of Particle Physics* Physical Review D54 (1996)

Part III

Electromagnetic Interactions

Chapter 4

Electromagnetic Interactions: General

4.1 Compute the energy loss

The energy loss processes are very similar for $e+/e-$, $\mu+/\mu-$ and charged hadrons , so it is quite natural to have a common description for them and we have chosen this way.

4.1.1 Energy loss of electrons/positrons

The G4eEnergyLoss class computes the continuous energy loss of electrons/positrons. The continuous energy loss is calculated as a sum of the contribution of the different processes. At present there are two processes contributing to the continuous energy loss , they are:

the ionisation process (class G4eIonisation) and the bremsstrahlung process (class G4eBremsstrahlung).

The class G4eIonisation calculates the contribution due to ionisation and it simulates the 'discrete' part of the ionisation , the Moller and Bhabha scattering or delta ray production by e+/e-.

The class G4eBremsstrahlung computes the energy loss contribution due to soft bremsstrahlung and it simulates the 'discrete' or hard bremsstrahlung.

The formulae used to compute the continuous energy loss are the same than those in GEANT3, but the two programs are not the same. The main difference between GEANT3 and GEANT4 is that while in GEANT3 the continuous energy loss, delta ray production and bremsstrahlung are three independent processes , in GEANT4 these processes are closely connected, they form a unified scheme.

The G4eEnergyLoss class constructs dE/dx and range tables for every material. First the dE/dx tables are costructed and filled , the energy loss class simply summes up of the contributions computed by the ionisation and bremsstrahlung processes. After this step G4eEnergyLoss creates range tables of $e+/e-$ for every material and computes the inverse of these range tables as well. All the tables are constructed at the beginning of the GEANT4 run , at initialisation time. Later, during the simulation the energy loss process performs two tasks : it imposes a limit on the stepsize of the particle and computes the energy loss after a step travelled by the particle.

Step limit due to the continuous energy loss

The continuous energy loss imposes a limit on the stepsize. The reason of this is the energy dependence of the cross sections. It is generally assumed in MC programs that the cross sections of the particles are approximately constant during a step , i.e. the step size should be so small that the relative difference of the cross sections at the beginning of the step and at the end should be small enough.In principle one has to use very small steps in order to have an accurate simulation , but the computing time increases if the

stepsize decreases. As a good compromise the stepsize is limited here by the requirement that the stopping range of the particle can decrease by not more than 20 % during the step. This condition works fine for a particle of kinetic energy $> 0.5MeV - 1.MeV$, but for low energy it gives very short step sizes. To cure this problem a lower limitation on the stepsize is also introduced. The choice of this lower limit is quite natural , the stepsize can not be smaller than the *cut in range* parameter of the program. The stepsize limit varies smoothly with decreasing energy from the value given by the condition $\Delta range/range = 0.20$ to the lowest possible value *cut in range* . It is worthwile to mention , that the lower limit used here is much more natural and physical , than the one is used in GEANT3 at the automatic calculation of the tracking parameters.

Computation of the energy loss

The computation of the *mean energy loss* after a given step is done by using the range and inverse range tables. The mean loss ΔT can be written as

$$\Delta T = T_0 - f_T(r_0 - step) \tag{4.1}$$

where T_0 is the kinetic energy, r_0 the range at the beginning of the step *step*, the function $f_T(r)$ is the inverse of the range table (i.e. it gives the kinetic energy of the particle for a range value of r) .

After the mean energy loss has been calculated the process computes the *actual* energy loss , i.e. the loss with fluctuation. The fluctuation is computed from a fluctuation model , from the model *GLANDZ* of the GEANT3 code [GEANT3] , [La95] .

4.1.2 Energy loss of muons

The energy loss of muons is computed by the class G4MuEnergyLoss. The scheme of the computation is the same as in the case of $e+/e-$, the only difference is that now there are three processes contributing to the total continuous energy loss , these are

the ionisation process (class G4MuIonisation), the bremsstrahlung process (class G4MuBremsstrahlung) and the direct pair production of muons (class G4MuPairProduction).

The G4MuIonisation class computes the contribution to the continuous energy loss due to ionisation and simulates the corresponding 'discrete' process, the knock-on electron or δ-ray production by muons.

The G4MuBremsstrahlung class calculates the continuous loss due to the *soft* bremsstrahlung and simulates the 'discrete', *hard* bremsstrahlung.

The G4MuPairProduction class gives the contribution to the continuous energy loss due to *sub-cutoff* $e+/e-$ pairs and performs the simulation of the pair production.

4.1.3 Energy loss of charged hadrons

The continuous energy loss of the charged hadrons are calculated by the class G4hEnergyLoss . The algorithm is the same than in the case of $e+/e-$ energy loss. Here there is only one process , the ionisation (class G4hIonisation) which contributes to the continuous energy loss .

The G4hIonisation class computes the continuous energy loss and simulates the δ-ray producion by hadrons.

In the case of energy loss of the hadrons two dE/dx , range and inverse range tables are constructed only , these are the tables for *proton* and *antiproton* . The energy loss for othe charged hadrons are computed from these tables at the *scaled kinetic energy* T_{scaled}

$$T_{scaled} = \frac{M_{proton}T}{M_{particle}} \tag{4.2}$$

where T is the kinetic energy of the particle, M_{proton} and $M_{particle}$ are the masses of the proton and particle, respectively.

There is an important constraint for this process: *the cut in range must be the same for all the charged hadrons* . This condition is meaningful physically and it makes possible to use the proton/antiproton tables only when computing the energy loss.

4.1.4 Status of this document

9.10.98 created by L. Urbán.
5.12.98 editing by J.P. Wellisch.

Bibliography

[GEANT3] GEANT3 manual ,CERN Program Library Long Writeup W5013 (October 1994).

[La95] K. Lassila-Perini and L. Urban , NIM A362 (1995),416.

4.2 Multiple scattering

The G4MultipleScattering class simulates the multiple scattering of charged particles in material.It uses a new multiple scattering (MSC) model which does not use the Moliere formalism([Mol48]).This MSC model simulates the scattering of the particle after a given step , computes the mean path length correction and the mean lateral displacement as well.

Let us define a few notation first.

The true path length ('t' path length) is the total length travelled by the particle. All the physical processes restrict this 't' step.

The geometrical (or 'z') path length is the straight distance between the starting and endpoint of the step , if there is no magnetic field. The geometry gives a constraint for this 'z' step. It should be noted, that the geometrical step length is meaningful in the case of magnetic field, too, but in this case it is a distance along a curved trajectory.

The mean properties of the multiple scattering process are determined by the transport mean free path , λ , which is a function of the energy in a given material.Some of the mean properties - the mean lateral displacement and the second moment of cos(theta) - depend on the second transport mean free path, too. (The transport mean free path is called first transport mean free path as well.)

The 't'⇒'z' (true path length – geometrical path length) transformation is given by the simple equation

$$z = \lambda * (1. - exp(-t/\lambda)) \tag{4.3}$$

which is an exact result for the mean values of z , if the differential cross section has an axial symmetry and the energy loss can be neglected . This formula and some other expressions for the first moments of the spatial distribution after a given 'true' path length t have been taken from the excellent paper of Fernandez-Varea et al. [Fer93], but the expressions have been calculated originally by Goudsmit and Saunderson [Goud40] and Lewis [Lew50]. Inverting eq. 4.3 the 'z'⇒'t' transformation can be written as

$$t = -\lambda * ln(1. - z/\lambda) \tag{4.4}$$

where $z < \lambda$ should be required (this condition is fulfilled if z has been computed from eq. 4.3).

The mean value of $cos(\theta)$ - θ is the scattering angle after a true step length t - is

$$< cos(\theta) >= exp(-t/\lambda) \tag{4.5}$$

The transport mean free path values have been calculated by Liljequist et al. [Lil90],[Lil87] for electrons and positrons in the kinetic energy range

$0.1keV--20MeV$ in 15 materials . The MSC model uses these values with an appropriate interpolation or extrapolation in the atomic number Z and in the velocity of the particle β , when it is necessary.

The quantity $cos(\theta)$ is sampled in the MSC model according to a model function $f(cos(\theta))$. The shape of this function has been choosen in such a way, that$f(cos(\theta))$ reproduces the results of the direct simulation ot the particle transport rather well and eq. 4.5 is satisfied. The functional form of this model function is

$$f(x) = p\frac{(a+1)^2(a-1)^2}{2a}\frac{1}{(a-x)^3} + (1-p)\frac{1}{2} \tag{4.6}$$

where $x = cos(\theta)$, $0 \leq p \leq 1$ and $a > 1$. The model parameters p and a depend on the path length t , the energy of the particle and the material.They are not independent parameters , they should satisfy the constraint

$$\frac{p}{a} = exp(-\frac{t}{\lambda}) \tag{4.7}$$

which follows from eq. 4.5 .

The mean lateral displacement is given by a more complicated formula (see the paper [Fer93]), but this quantity also can be calculated relatively easily and accurately.

It is worth to note that in this MSC model there is no step limitation originated from the multiple scattering process. Another important feature of this model that the total 'true' path length of the particle does not depend the length of the steps . Most of the algorithms used in simulations do not have these properties.

In the case of heavy charged particles ($\mu, \pi, proton, etc.$) the mean transport free path is calculated from the $e+/e-$ λ values with a 'scaling'.

In its present form the model computes and uses *mean* path length corrections and lateral displacements, the only *random* quantity is the scattering angle θ which is sampled according to the model function f.

The G4MultipleScattering process has 'AlongStep' and 'PostStep' parts.

The AlongStepGetPhysicalInteractionLength function performs the 't' step $\Rightarrow$ 'z' step transformation . It should be called after the other physics GetPhysicalInteractionLength functions but before the GetPhysicalInteractionLength of the transportation process.The reason for this restriction is the following: The physics processes 'feel' the true path length travelled by the particle , the geometry (transport) uses the 'z' step length.If we want to compare the minimum step size coming from the physics with the constraint of the geometry, we have make the transformation.

The AlongStepDoIt function of the process performs the inverse, 'z'$\Rightarrow$'t' transformation.This function should be called after the AlongStepDoIt of the transportation process , i.e. after the particle relocation determined

by the geometrical step length, but before applying any other (physics) AlongStepDoIt.

The PostStepGetPhysicalInteractionLength part of the multiple scattering process is very simple , it sets the force flag to 'Forced' in order to ensure the call of the PostStepDoIt in every step and returns a big value as interaction length (that means that the multiple scattering process does not restrict the step size).

4.2.1 Status of this document

9.10.98 created by L. Urbán.
5.12.98 editing by J.P. Wellisch.

Bibliography

[Mol48] *Z. Naturforsch. 3a (1948) 78.*

[Fer93] J. M. Fernandez-Varea et al. *NIM B73 (1993) 447.*

[Goud40] S. Goudsmit and J. L. Saunderson. *Phys. Rev. 57 (1940) 24.*

[Lew50] H. W. Lewis. *Phys. Rev. 78 (1950) 526.*

[Lil87] D. Liljequist and M. Ismail. *J.Appl.Phys. 62 (1987) 342.*

[Lil90] D. Liljequist et al. *J.Appl.Phys. 68 (1990) 3061.*

4.3 Transition radiation

4.3.1 Method

Let us consider the mean number of XTR (X-ray transition radiation) quanta $d^2\bar{N}/d\omega d\Omega$ generated by relativistic charged particle intersecting the interface between two media 1 and 2 ($1 \to 2$) into forward hemisphere in unit energy ω and solid angle Ω . In the X-ray region, when one could neglect of refraction and reflection of the XTR quanta this value is given by the following expression [Bolot82] :

$$\frac{d^2\bar{N}}{d\omega d\Omega} = \frac{\alpha}{4\pi^2}\beta^2\frac{\sqrt{\varepsilon_2}\sin^2\theta}{\omega}\left|\frac{1}{1-\beta\sqrt{\varepsilon_1-\varepsilon_2\sin^2\theta}} - \frac{1}{1-\beta\sqrt{\varepsilon_2}\cos\theta}\right|^2, \quad (4.8)$$

where α is the fine structure constant, β is the ratio of the particle velocity v to the velocity of light c , ε_1 and ε_2 are the complex dielectric constants in the medium 1 and 2 respectively ($d\Omega = 2\pi\sin\theta d\theta$) . In the X-ray region $\omega > 1$ keV the imaginary part of the dielectric constant is much less than the real part which in turn is practically equal to the well known approximation $(1-\omega^2/\omega_p^2)$, where ω_p is the plasma energy of the medium . In the ultrarelativistic case the radiation is concentrated in the region of small angles $\theta \sim 1/\gamma \ll 1$ (γ is the Lorenz factor of the particle). Then the relation (1.1) can be transformed to the well known form [Avak75], [Ginzb78], [Dolg93]:

$$\frac{d^2\bar{N}}{d\omega d\xi} = \frac{\alpha}{\pi}\frac{\xi}{\omega}\left|\frac{1}{\frac{1}{\gamma^2}+\eta^{(1)}+\xi} - \frac{1}{\frac{1}{\gamma^2}+\eta^{(2)}+\xi}\right|^2, \quad (4.9)$$

where $\eta^{(i)} = (\omega_p^{(i)}/\omega)^2$, and $\omega_p^{(i)}$ is the plasma energy in the i-th medium ($i = 1, 2$). We introduced in addition, suitable for the following calculations, value $\xi = 2(1-\cos\theta) \sim \theta^2 \ll 1$, where the angle θ is counted from the particle direction. Generally, the trivial numerical integration of (1.2) allows us to simulate the energy and angular distributions of the XTR quanta generated. The relation (1.2) however has a sharp peak when the denominators are of the order of $1/\gamma^2$. The proper calculation of the narrow region of the maximum forces one to decrease the integration step resulting in the accumulation of round-off errors and numerical unstability of the results. It is more suitable therefore to use analytical expressions [Bag98].

Let us derive firstly the expressions for the angular density of XTR quanta $d\bar{N}/d\xi$. Introducing the auxiliary coefficients: $x = 1/\omega$; $c = (1/\omega_p^{(1)})^2$; $d = (1/\omega_p^{(2)})^2$; $\sigma(\gamma,\xi) = \xi + 1/\gamma^2$; $a^2 = \sigma c$; $b^2 = \sigma d$, we have

$$\frac{d\bar{N}}{d\xi} = \int_{\omega_1}^{\omega_2}\frac{d^2\bar{N}}{d\omega d\xi}d\omega = \frac{\alpha}{\pi}\xi\left[A+B+C\right], \quad (4.10)$$

$$A = \frac{c^2}{2}\left[\frac{1}{a^2(x^2+a^2)} + \frac{1}{a^4}\ln\frac{x^2}{x^2+a^2}\right]_{x_2}^{x_1},$$

$$B = -\frac{cd}{a^2-b^2}\left[\frac{1}{b^2}\ln\frac{x^2}{x^2+b^2} - \frac{1}{a^2}\ln\frac{x^2}{x^2+a^2}\right]_{x_2}^{x_1},$$

$$C = \frac{d^2}{2}\left[\frac{1}{b^2(x^2+b^2)} + \frac{1}{b^4}\ln\frac{x^2}{x^2+b^2}\right]_{x_2}^{x_1},$$

where $x_i = 1/\omega_i, (i = 1, 2)$. The expression (1.3) is sufficiently smooth to get the integral spectral distribution of XTR quanta $\bar{N}(\xi)$ by numerical integration:

$$\bar{N}(\xi) = \int_{\xi}^{\xi_{max}} \frac{d\bar{N}}{d\xi} d\xi,$$

where $\xi_{max} \sim (100/\gamma)$ is the upper boundary of the angular region where the main part of the XTR quanta is generated.

The spectral density of XTR quanta $d\bar{N}/\omega$ is given by:

$$\frac{d\bar{N}}{d\omega} = \int_0^{\xi_{max}} \frac{d^2\bar{N}}{d\omega d\xi} d\xi = \frac{\alpha}{\pi\omega}\left[\frac{\tilde{a}+\tilde{b}}{\tilde{a}-\tilde{b}}\ln\frac{\omega+\tilde{b}}{\omega+\tilde{a}} + \frac{\tilde{a}}{\omega+\tilde{a}} + \frac{\tilde{b}}{\omega+\tilde{b}}\right]_0^{\xi_{max}}, \tag{4.11}$$

where $\tilde{a} = 1/\gamma^2 + \eta^{(1)}$, $\tilde{b} = 1/\gamma^2 + \eta^{(2)}$. From here for, $\omega < \omega_c^{(2)} << \omega_c^{(1)}$, $(\omega_c^{(i)} = \gamma\omega_p^{(i)}, (i = 1, 2)$ is the characteristic energy of XTR in the i-th medium), we have with logarithmic accuracy

$$\begin{aligned} \bar{N}(\omega) &= \int_{\omega}^{\omega_c^{(1)}} \frac{d\bar{N}}{d\omega} d\omega \\ &= \frac{\alpha}{\pi}\left[2\ln\frac{\omega_c^{(1)}}{\omega}\left(\ln\frac{\omega_c^{(1)}}{\omega_c^{(2)}} - 1\right) - \ln^2\frac{\omega_c^{(1)}}{\omega_c^{(2)}} + 2\ln 2 - \frac{\pi^2}{24}\right]. \end{aligned} \tag{4.12}$$

One can see from the expression (1.5), that the total number of XTR quanta generated by ultrarelativistic particle intersecting the interface between two media is small and of the order of some units of α . For example, for $\omega = 1$ keV, $\gamma = 10^4$ about $0.034 \approx 5\alpha$ is generated from the interface between polypropylene and air.

4.3.2 Simulation of the X-ray transition radiation production

The simulation of XTR quanta generated by relativistic charged particle intersecting the interface between two media can be done according to the following algorithm. We start with the estimation of the total number of XTR quanta based on the Poisson distribution with the mean number according the expression (1.5). In those rare events when the number of XTR quanta is not equal to zero the energy and angle of each XTR quantum are simulated based on the integral distributions obtained by the numerical integration of the expressions (1.4) and (1.3) respectively.

4.3.3 Status of this document

14.10.98 created by V.Grichine
5.12.98 editing by J.P. Wellisch.

Bibliography

[Avak75] Avakian A.L., Garibian G.M., and,Yang C. *Nucl. Instr. and Meth. 129, 303* (1975)

[Bag98] Bagulya A.V. and Grichine V.M. Bulletin of Lebedev Institute, no.1-2, 12 (1998)

[Bolot82] Bolotovsky B.M. *Lebedev Institute Proceedings, vol. 140, 95* (1982)

[Ginzb78] Ginzburg V.L.and Cytovitch V.N. *Soviet Physics (Uspekhi), vol. 126, 553* (1978)

[Dolg93] Dolgoshein B. *Nucl. Instr. and Meth. A326, 434* (1993).

4.4 Scintillation

Every scintillating material has a characteristic light yield, Y $(photons/MeV)$, and an intrinsic resolution which generally broadens the statistical distribution, $\sigma_i/\sigma_s > 1$, due to impurities which are typical for doped crystals like NaI(Tl) and CsI(Tl). The average yield can have a non-linear dependence on the local energy deposition. Scintillator also have a time distribution spectrum with one or more exponential decay time constants, τ_i, with each decay component having its intrinsic photon emission spectrum. These are empirical parameters typical for each material.

A Poisson-distributed number of photons is generated according to the energy lost during the step and the properties of the scintillator material. Each photon's frequency is sampled from the empirical spectra. They originate evenly along the track segment and are emitted uniformly into 4π with a random linear polarization.

4.5 Čerenkov effect

The radiation of Čerenkov light occurs when a charged particle moves through a dispersive medium faster than the speed of light in that same medium (A dispersive medium is one for which the refraction index of the medium is an increasing function of photon momentum). In such a medium, when a particle travels faster than the speed of light several things occur as the particle slows down:

1. A cone of Čerenkov photons is emitted opening at an increasingly acute angle (to the direction of the particle momentum);
2. The momentum of the photons produced increases, while the number produced decreases.

When the particle reaches a speed slower than the local speed of light, photons are no longer emitted. At that point, the Čerenkov cone has collapsed to zero.

For the formulas contained in this chapter, please see [1]. Let n be the refractive index of the dielectric material acting as a radiator ($n = c/c'$ where c' is the group velocity of light in the material: it follows that $1 \leq n$). In a dispersive material n is an increasing function of the photon momentum p_γ, $dn/dp \geq 0$. A particle traveling with speed $\beta = v/c$ will emit photons at an angle θ with respect to its direction, where θ is given by the relation:

$$\cos\theta = \frac{1}{\beta n}$$

from which follows the limitation for the momentum of the emitted photons:

$$n(p_\gamma^{min}) = \frac{1}{\beta}$$

Photons emitted with a momentum beyond a certain value are immediately re-absorbed by the material — this is the window of transparency of the radiator. As a consequence, all photons are contained in a cone of opening $\cos\theta_{max} = 1/(\beta n(p_\gamma^{max}))$.

The average number of photons produced is given by the relations (Gaussian units):

$$dN = \frac{2\pi z^2 e^2}{\hbar c}\sin^2\theta\frac{d\nu}{c}dx = \frac{2\pi z^2 e^2}{\hbar c}(1-\cos^2\theta)\frac{d\nu}{c}dx = \frac{2\pi z^2 e^2}{\hbar c}(1-\frac{1}{n^2\beta^2})\frac{d\nu}{c}dx$$

$$= \frac{2z^2e^2}{\hbar^2c^2}(1-\frac{1}{n^2\beta^2})dp_\gamma dx \approx 370z^2\frac{photons}{cm\,eV}(1-\frac{1}{n^2\beta^2})dp_\gamma dx$$

and

$$\frac{dN}{dx} \approx 370z^2 \int_{p_\gamma^{min}}^{p_\gamma^{max}} dp_\gamma (1 - \frac{1}{n^2\beta^2}) = 370z^2 (p_\gamma^{max} - p_\gamma^{min} - \frac{1}{\beta^2} \int_{p_\gamma^{min}}^{p_\gamma^{max}} dp_\gamma \frac{1}{n(p_\gamma^2)})$$

The number of photons produced is calculated from a Poissonian distribution with average value $\bar{n} = \Delta_{Step} dN/dx$. The momentum distribution of the photon is then sampled from the density function:

$$f(p_\gamma) = (1 - \frac{1}{n^2(p_\gamma)\beta^2})$$

Chapter 5

Electromagnetic Interactions: Gamma incident

5.1 PhotoElectric effect

5.1.1 Cross section and Mean free path

binding energy of the shells

The binding energy of the inner shells have been parameterised as:

$$B_i(Z) = Z^2(a_i + b_i Z + c_i Z^2 + d_i Z^3)$$

where $i = K, L_1, L_2$, and the constants a_i, b_i, c_i, d_i are tabulated inside dedicated functions.

Cross section per atom

Lets E_γ = incident gamma energy, and $\epsilon = E_\gamma / m_e c^2$
The photoelectric total cross-section per atom has been parameterised as:

$$\sigma(Z, \epsilon) = \frac{Z^\alpha}{\epsilon^\beta} F(Z, \epsilon)$$

where α and β are results of a fit, and $F(Z, \epsilon)$ is:

$$\begin{array}{lll}
\text{for} \quad E_\gamma > B_K : & F = p_{1K}/Z + p_{2K}/\epsilon + p_{3K} & +p_{4K} Z + p_{5K}\epsilon + p_{6K} Z^2 \\
 & & +p_{7K} Z\epsilon + p_{8K}\epsilon^2 + p_{9K} Z^3 \\
 & & +p_{10K} Z^2\epsilon + p_{11K} Z/\epsilon^2 + p_{12K}\epsilon^3 \\
\text{for} \quad E_\gamma \in]B_{L1}, B_K] : & F = p_{1L1}/Z + p_{2L1}/\epsilon + p_{3L1} & \\
\text{for} \quad E_\gamma \in]B_{L2}, B_{L1}] : & F = p_{1L2}/Z + p_{2L2}/\epsilon + p_{3L2} & \\
\text{for} \quad E_\gamma \leq B_{L2} : & F = p_{1M} &
\end{array}$$

The fit was made over 301 data points chosen between:

$$5 \leq Z \leq 100 \quad \text{and} \quad 10\ keV \leq E \leq 50\ MeV$$

The values of the parameters are defined within the method which computes the cross section per atom.
The accuracy of the fit is estimated to be:

$$\frac{\Delta\sigma}{\sigma} \leq \begin{cases} 25\% & \text{near to the peaks} \\ 10\% & \text{elsewhere.} \end{cases}$$

Mean free path

* In a simple material the number of atoms per volume is:

$$n = \frac{\mathcal{N}\rho}{A}$$

where:

$\mathcal{N}$	Avogadro's number
ρ	density of the medium
A	mass of mole

* In a compound material the number of atoms of Element elm per volume is:

$$n_{elm} = \frac{\mathcal{N}\rho w_{elm}}{A_{elm}}$$

where:

$\mathcal{N}$	Avogadro's number
ρ	density of the medium
w_{elm}	proportion by mass of the Element elm
A_{elm}	mass of mole of the Element elm

* The mean free path, λ, for a photon to interact via photo electric effect is given by

$$\lambda(E_\gamma) \equiv \frac{1}{\Sigma(E_\gamma)} = \frac{1}{\sum_{elm}[n_{elm}\sigma(Z_{elm}, E_\gamma)]}$$

where $\sum_{elm}$ runs over all Elements the material is made of.

5.1.2 final state

choose an Element

The binding energy of the shells depend of the atomic number Z_{elm}.
In a compound material one choose randomly an Element on the basis of the probability:

$$Prob(Z_{elm}, E_\gamma) = \frac{n_{elm}\sigma(Z_{elm}, E_\gamma)}{\Sigma(E_\gamma)}$$

final state

The simulation is presently rather crude.
A quanta can be absorbed if $E_\gamma > B_{shell}$. The photoelectron is emitted with kinetic energy:

$$T_{photoelectron} = E_\gamma - B_{shell}(Z_{elm})$$

The electron has the same direction as the incident gamma.

5.1.3 Status of this document

9.10.98 created by M.Maire.
5.12.98 editing by J.P. Wellisch.

5.2 Compton scattering

5.2.1 Cross section and Mean free path

Cross section per atom

An empirical cross-section formula is used, which reproduces rather well the cross-section data down to 10 keV:

$$\sigma(Z, E_\gamma) = \left[P_1(Z) \frac{\log(1+2X)}{X} + \frac{P_2(Z) + P_3(Z)X + P_4(Z)X^2}{1 + aX + bX^2 + cX^3} \right]$$

where:

$$\begin{aligned} Z &= \text{atomic number of the medium} \\ E_\gamma &= \text{energy of the photon} \\ m &= \text{electron mass} \\ X &= \frac{E_\gamma}{mc^2} \\ P_i(Z) &= Z(d_i + e_i Z + f_i Z^2) \end{aligned}$$

The values of the parameters are defined within the method which computes the cross section per atome.
The fit was made over 511 data points chosen between:

$$1 \leq Z \leq 100 \qquad ; \qquad 10\,\text{keV} \leq E_\gamma \leq 100\,\text{GeV}$$

The accuracy of the fit is estimated to be:

$$\frac{\Delta\sigma}{\sigma} = \begin{cases} \approx 10\% & \text{for E} \simeq 10\,\text{keV} - 20\,\text{keV} \\ \leq 5 - 6\% & \text{for E} > 20\,\text{keV} \end{cases}$$

Mean free path

* In a simple material the number of atoms per volume is:

$$n = \frac{\mathcal{N}\rho}{A}$$

where:

$$\begin{aligned} \mathcal{N} &\quad \text{Avogadro's number} \\ \rho &\quad \text{density of the medium} \\ A &\quad \text{mass of mole} \end{aligned}$$

* In a compound material the number of atoms of Element elm per volume is:

$$n_{elm} = \frac{\mathcal{N}\rho w_{elm}}{A_{elm}}$$

where:

$\mathcal{N}$	Avogadro's number
ρ	density of the medium
w_{elm}	proportion by mass of the Element elm
A_{elm}	mass of mole of the Element elm

* The mean free path, λ, for a photon to interact via Compton scattering is given by

$$\lambda(E_\gamma) \equiv \frac{1}{\Sigma(E_\gamma)} = \frac{1}{\sum_{elm}\left[n_{elm}\sigma(Z_{elm}, E_\gamma)\right]}$$

where $\sum_{elm}$ runs over all Elements the material is made of.

5.2.2 Sampling the final state

For a complete account of the Monte Carlo methods used the interested user is referred to the publications of Butcher and Messel , Messel and Crawford or Ford and Nelson [Butch60, Mess70, egs4]. Only the basic formalism is outlined here.
The quantum mechanical Klein-Nishina differential cross-section is [Klein29, egs4]:

$$\Phi(E_0, E_1) = \frac{X_0 n \pi r_0^2 m_e c^2}{E_0^2}\left[\frac{1}{\epsilon} + \epsilon\right]\left[1 - \frac{\epsilon \sin^2\theta}{1+\epsilon^2}\right]$$

where:
E_0 = energy of the incident photon
E_1 = energy of the scattered photon
ϵ = E_0/E_1
n = nb of electron per volume
X_0 = radiation length
m_e = electron mass
r_0 = classical electron radius

Assuming an elastic collision, the scattering angle θ is defined by the Compton formula:

$$E_1 = E_0 \frac{m_e c^2}{m_e c^2 + E_0(1 - \cos\theta)}$$

sample the gamma energy

The value of ϵ corresponding to the minimum photon energy (backward scattering) is given by:

$$\epsilon_0 = \frac{m_e c^2}{m_e c^2 + 2E_0}$$

Therefore we have: $\epsilon \in [\epsilon_0, 1]$
Using the combined "composition and rejection" Monte Carlo methods described in the Gamma Conversion chapter, we may set:

$$\Phi(\epsilon) \simeq [\frac{1}{\epsilon} + \epsilon][1 - \frac{\epsilon \sin^2\theta}{1+\epsilon^2}] = f(\epsilon)g(\epsilon) = [\alpha_1 f_1(\epsilon) + \alpha_2 f_2(\epsilon)]g(\epsilon)$$

where:

$$\begin{array}{lll} \alpha_1 = \ln(1/\epsilon_0) & ; & f_1(\epsilon) = 1/(\alpha_1\epsilon) \\ \alpha_2 = (1-\epsilon_0^2)/2 & ; & f_2(\epsilon) = \epsilon/\alpha_2 \\ & & g(\epsilon) = \left[1 - \frac{\epsilon}{1+\epsilon^2}\sin^2\theta\right] \end{array}$$

f_1 and f_2 are probability density functions on $[\epsilon_0, 1]$ and g is a rejection function: $\forall\epsilon \in [\epsilon_0, 1] : 0 < g(\epsilon) \leq 1$
Given a set of 3 random numbers r, r', r'' uniformly distributed in [0,1], the sampling procedure for ϵ is the following:

1. decide which element of the $f(\epsilon)$ distribution to sample from.
   if $r < \frac{\alpha_1}{\alpha_1+\alpha_2}$ select $f_1(\epsilon)$, otherwise select $f_2(\epsilon)$;
2. sample ϵ from the distributions corresponding to f_1 or f_2.
   For $f_1 : \epsilon = \epsilon_0^{r'}$ $\quad (\equiv \exp(-r'\alpha_1))$
   For $f_2 : \epsilon^2 = \epsilon_0^2 + (1-\epsilon_0^2)r'$
3. calculate $\sin^2\theta = t(2-t)$ where $t \equiv (1-\cos\theta) = \frac{m_e c^2}{E_0}\frac{1-\epsilon}{\epsilon}$
4. test the rejection function: if $g(\epsilon) \geq r''$ accept ϵ, otherwise return to step 1.

compute the final kinematic

After the successful sampling of ϵ, the polar angles of the scattered photon with respect to the direction of the parent photon are generated. The azimuthal angle, ϕ, is generated isotropically and θ is as defined in the previous section. The momentum vector of the scattered photon, $\overrightarrow{P_{\gamma 1}}$, is then transformed into the `World` coordinate system.
The kinetic energy and momentum of the recoil electron are then:

$$\begin{array}{rcl} T_{el} & = & E_0 - E_1 \\ \overrightarrow{P_{el}} & = & \overrightarrow{P_{\gamma 0}} - \overrightarrow{P_{\gamma 1}} \end{array}$$

5.2.3 Restriction

The differential cross-section is only valid for those collisions in which the energy of the recoil electron is large compared with its binding energy (which is ignored). However, as pointed out by Rossi [Rossi52], this has a negligible effect because of the small number of recoil electrons produced at very low energies.

5.2.4 Status of this document

9.10.98 created by M.Maire.
5.12.98 editing by J.P. Wellisch.

Bibliography

[Klein29] O. Klein and Y. Nishina. *Z. Physik 52* 853 (1929)

[Rossi52] B. Rossi. *High energy particles, Prentice-Hall* 77-79 (1952)

[Butch60] J.C. Butcher and H. Messel. *Nucl. Phys. 20* 15 (1960)

[Mess70] H. Messel and D. Crawford. *Electron-Photon shower distribution, Pergamon Press* (1970)

[egs4] R. Ford and W. Nelson. *SLAC-265, UC-32* (1985)

Chapter 6

Electromagnetic Interactions: Electron incident

6.1 Ionisation

The class G4eIonisation calculates the continuous energy loss due to ionisation and simulates the 'discrete' part of the ionisation , the Moller and Bhabha scattering or delta ray production by e^-/e^+ . The formulae used here are the same than those in GEANT3 ([GEANT3]).

6.1.1 Method

Let:

$$\frac{d\sigma(E,T)}{dT}$$

be the differential cross-section for the ejection of an electron with kinetic energy T by an incident $e^{\pm}$ of total energy E moving in a medium of density ρ. Let us denote the value of the *kinetic energy cut-off* or *production threshold for δ-rays* by T_{cut}. Below this threshold the soft electrons ejected are simulated as continuous energy loss by the incident e^+/e^-, and above it they are explicitly generated.

The mean value of the energy lost by the incident $e^{\pm}$ to the soft δ-rays is:

$$E_{soft}(E,T_{cut}) = \int_0^{T_{cut}} \frac{d\sigma(E,T)}{dT} T\, dT \tag{6.1}$$

whereas the total cross-section for the ejection of an electron of energy $T > T_{cut}$ is:

$$\sigma(E,T_{cut}) = \int_{T_{cut}}^{T_{Max}} \frac{d\sigma(E,T)}{dT}\, dT \tag{6.2}$$

where T_{Max} is the maximum energy transferable to the free electron:

$$T_{Max} = \begin{cases} E-m & for\ \ e^+ \\ (E-m)/2 & for\ \ e^-, \end{cases} \tag{6.3}$$

where m is the electron mass. The method of calculation of the continuous energy loss and the total cross-section are explained below.

6.1.2 Continuous energy loss

The integration of 6.1 leads to the Berger-Seltzer formulae (see e.g in [Mess70]) :

$$\frac{dE}{dx} = \frac{2\pi r_0^2 mn}{\beta^2}\left[\ln\frac{2(\tau+2)}{(I/m)^2} + F^{\pm}(\tau,\Delta) - \delta\right], \tag{6.4}$$

where

γ	$\frac{E}{m}$
β^2	$1-\frac{1}{\gamma^2}$
τ	$\gamma-1$
τ_c	$\frac{T_{cut}}{m}$
T_{cut}	energy cut for $e^{\pm}$
τ_{max}	maximum possible energy transfer in e^- mass: τ for e^+, $\tau/2$ for e^-
Δ	$\min(\tau_c, \tau_{max})$
n	electron density of the medium
I	average mean ionisation energy
δ	density effect correction.

The functions $F^{\pm}$ are given by

$$F^+(\tau,\Delta) = \ln(\tau\Delta) - \frac{\Delta^2}{\tau}\left[\tau + 2\Delta - \frac{3\Delta^2 y}{2} - \left(\Delta - \frac{\Delta^3}{3}\right)y^2 - \left(\frac{\Delta^2}{2} - \tau\frac{\Delta^3}{3} + \frac{\Delta^4}{4}\right)y^3\right] \tag{6.5}$$

$$F^-(\tau,\Delta) = -1 - \beta^2 + \ln\left[(\tau-\Delta)\Delta\right] + \frac{\tau}{\tau-\Delta} + \frac{\left[\frac{\Delta^2}{2} + (2\tau+1)\ln\left(1-\frac{\Delta}{\tau}\right)\right]}{\gamma^2} \tag{6.6}$$

where $y = 1/(\gamma+1)$.

The density effect correction is calculated according to the formalism of Sternheimer ([Ster71]).

6.1.3 Total cross-sections

The integration of formula 6.2 gives the total cross-section ([Mess70]) for Möller scattering (e^-e^-):

$$\sigma(Z,E,T_{cut}) = \frac{2\pi r_0^2 mZ}{\beta^2(E-m)}\left[\frac{(\gamma-1)}{\gamma^2}\left(\frac{1}{x}-1\right) + \frac{1}{x} - \frac{1}{1-x} - \frac{2\gamma-1}{\gamma^2}\ln\frac{1-x}{x}\right] \tag{6.7}$$

and for Bhabha scattering (e^+e^-) :

$$\sigma(Z,E,T_{cut}) = \frac{2\pi r_0^2 mZ}{(E-m)}\left[\frac{1}{\beta^2}\left(\frac{1}{x}-1\right) + B_1 x + B_2(1-x) - \frac{B_3}{2}(1-x^2) + \frac{B_4}{3}(1-x^3)\right] \tag{6.8}$$

where

$\gamma = \frac{E}{m}$	$\beta^2 = 1 - \frac{1}{\gamma^2}$
$x = \frac{T_{cut}}{E-m}$	$\gamma = \frac{1}{\gamma+1}$
$B_1 = 2 - y^2$	$B_2 = (1-2y)(3+y^2)$
$B_3 = (1-2y)^2 + (1-2y)^3$	$B_4 = (1-2y)^3$

The formulae [6.7] and [6.8] give the total cross-section of the scattering above the threshold energies

$$T^{\rm thr}_{\rm Moller} = 2T_{cut} \qquad \text{and} \qquad T^{\rm thr}_{\rm Bhabha} = T_{cut} \tag{6.9}$$

The interaction length for the production of δ-rays is calculated during initialisation .

6.1.4 Simulation of the $\delta - ray$ production

Differential cross section

The differential cross-section of the δ-ray production can be written as in equation 6.10 , 6.11 ([Mess70]). For the electron/electron (Möller) scattering we have:

$$\frac{d\sigma}{d\epsilon} = \frac{2\pi Z r_0^2 m}{\beta^2 (E-m)} \left[\frac{(\gamma-1)^2}{\gamma^2} + \frac{1}{\epsilon}\left(\frac{1}{\epsilon} - \frac{2\gamma-1}{\gamma^2}\right) + \frac{1}{1-\epsilon}\left(\frac{1}{1-\epsilon}\frac{2\gamma-1}{\gamma^2}\right)\right] \tag{6.10}$$

and for the positron-electron (Bhabha) scattering:

$$\frac{d\sigma}{d\epsilon} = \frac{2\pi Z r_0^2 m}{(E-m)} \left[\frac{1}{\beta^2\epsilon^2} - \frac{B_1}{\epsilon} + B_2 - B_3\epsilon + B_4\epsilon^2 \right] \tag{6.11}$$

where

Z	=	atomic number of the medium	E	=	energy of the incident particle
M	=	rest mass of the incident particle	γ	=	$\frac{E}{M}$
β^2	=	$1 - \frac{1}{\gamma^2}$	y	=	$\frac{1}{\gamma+1}$
B_1	=	$2 - y^2$	B_2	=	$(1-2y)(3+y^2)$
B_3	=	$(1-2y)^2 + (1-2y)^3$	B_4	=	$(1-2y)^3$
ϵ	=	$\frac{T}{E-m}$			

with T the kinematic energy of the scattered electron (of the lower energy in the case of e^+e^- scattering).

The kinematical limits for the variable ϵ are:

$$\epsilon_0 = \frac{T_{cut}}{E-m} \le \epsilon \le \frac{1}{2} \quad \text{for } e^-e^- \qquad\qquad \epsilon_0 = \frac{T_{cut}}{E-m} \le \epsilon \le 1 \quad \text{for } e^+e^-$$

Sampling

Apart from the normalisation, the cross-section can be written as

$$\frac{d\sigma}{d\epsilon} = f(\epsilon)g(\epsilon),$$

where, for e^-e^- scattering,

$$\begin{aligned} f(\epsilon) &= \frac{1}{\epsilon^2}\frac{\epsilon_0}{1-2\epsilon_0} \\ g(\epsilon) &= \frac{4}{9\gamma^2-10\gamma+5}\left[(\gamma-1)^2\epsilon^2-(2\gamma^2+2\gamma-1)\frac{\epsilon}{1-\epsilon}+\frac{\gamma^2}{(1-\epsilon)^2}\right] \end{aligned}$$

and for e^+e^- scattering

$$\begin{aligned} f(\epsilon) &= \frac{1}{\epsilon^2}\frac{\epsilon_0}{1-\epsilon_0} \\ g(\epsilon) &= \frac{B_0-B_1\epsilon+B_2\epsilon^2-B_3\epsilon^3+B_4\epsilon^4}{B_0-B_1\epsilon_0+B_2\epsilon_0^2-B_3\epsilon_0^3+B_4\epsilon_0^4} \end{aligned}$$

Here $B_0=\gamma^2/(\gamma^2-1)$ and all the other quantities have been defined above.

The variable ϵ is sampled by:

1. sample ϵ from $f(\epsilon)$
2. calculate the rejection function $g(\epsilon)$ and accept the sampled ϵ with a probability of $g(\epsilon)$.

After the successful sampling of ϵ, the direction of the scattered electron is generated with respect to the direction of the incident particle. The azimuthal angle ϕ is generated isotropically; the polar angle θ is calculated from the energy momentum conservation. This information is used to calculate the energy and momentum of both scattered particles and to transform them into the *global* coordinate system.

6.1.5 Status of this document

9.10.98 created by L. Urbán.
5.12.98 editing by J.P. Wellisch.

Bibliography

[GEANT3] GEANT3 manual ,CERN Program Library Long Writeup W5013 (October 1994).

[Mess70] H.Messel and D.F.Crawford. Pergamon Press,Oxford,1970.

[Ster71] R.M.Sternheimer. Phys.Rev. B3 (1971) 3681.

6.2 Bremsstrahlung

The class G4eBremsstrahlung calculates the continuous energy loss due to *sub-cutoff* photons and simulates the 'discrete' part of the interaction , the bremsstrahlung by e^-/e^+ . The formulae used here are the very similar to those used in GEANT3 ([GEANT3]). The only *important* difference is that in GEANT4 both of the LPM effect and dielectric supression of the bremsstrahlung ([Gal64],[Ant97]) have been implemented, while GEANT3 contains the latter only (using the name Migdal correction for it) .

6.2.1 Cross section and energy loss

Let's call $d\sigma(Z,T,k)/dk$ the differential cross-section for production of a photon of energy k by an electron of kinetic energy T in the field of an atom of charge Z, and k_c the energy cut-off below which the soft photons are treated as continuous energy loss . Then the mean value of the energy lost by the electron due to soft photons is

$$E^{brem}_{Loss}(Z,T,k_c) = \int_0^{k_c} k\frac{d\sigma(Z,T,k)}{dk}dk \tag{6.12}$$

whereas the total cross-section for the emission of a photon of energy larger than k_c is

$$\sigma_{brem}(Z,T,k_c) = \int_{k_c}^{T} \frac{d\sigma(Z,T,k)}{dk}dk \tag{6.13}$$

Many theories of the bremsstrahlung process exist, each with its own limitations and regions of applicability. Perhaps the best synthesis of these theories can be found in the paper of S.M. Seltzer and M.J. Berger [Sel85]. The authors give a tabulation of the bremsstrahlung cross-section $d\sigma/dk$ differential in the photon energy k, for electrons with kinetic energies T from 1 keV to 10 GeV. For electron energies above 10 GeV the screened Bethe-Heitler differential cross-section can be used ([EGS4] together with the dielectric supression correction ([Mess70] , [Mig56]) . This correction decreases the differential cross-section at photon energies below a certain fraction of the incident electron energy ($d\sigma/dk$ decreases significantly if $k/T \leq 10^{-4}$.)

Parameterisation of energy loss and total cross-section

Using the tabulated cross-section values of Seltzer and Berger together with the corrected Bethe-Heitler formula (which so includes the dilelectric supression,too) we have computed $\sigma(Z,T,k_c)$ and we have used these computed values as "data points" in the fitting procedure. Calculating the "low energy" ($T \leq 10$ GeV) data we have applied the dielectric supression to the results of Seltzer and Berger. We have chosen the parameterisations:

$$\sigma(Z,T,k_c) = \frac{Z(Z+\xi_\sigma)(T+m)^2}{T(T+2m)}[\ln(T/k_c)]^\alpha F_\sigma(Z,X,Y) \quad \text{(barn)} \tag{6.14}$$

and

$$E^{brem}_{Loss}(Z,T,k_c) = \frac{Z(Z+\xi_l)(T+m)^2}{(T+2m)}\left[\frac{k_c C_M}{T}\right]^{\beta} F_l(Z,X,Y) \quad \text{(GeV barn)} \tag{6.15}$$

where m is the mass of the electron,

$$\begin{array}{ll} X=\ln(E/m), & Y=\ln(v_\sigma E/k_c) \qquad \text{for the total cross-section } \sigma \\ X=\ln(T/m), & Y=\ln(k_c/v_l E) \qquad \text{for the energy loss } E^{brem}_{Loss} \end{array}$$

with $E = T + m$. The constants $\xi_\sigma,\ \xi_l,\ \alpha,\ \beta,\ v_\sigma,\ v_l$ are parameters to be fitted.

$$C_M \quad = \quad \frac{1}{1+\frac{nr_0\lambda r^2(T+m)^2}{\pi k_c^2}}$$

is the Midgal correction factor, with

r_o classical electron radius;

λ reduced electron Compton wavelength;

n electron density in the medium.

The factors $(T+m)^2/T(T+2m)$ and $(T+m)^2/(T+2m)$ come from the scaled cross-section computed by Seltzer and Berger:

$$f(k/T) = \frac{\beta^2}{Z^2}k\frac{d\sigma}{dk} = \frac{T(T+2m)}{(T+m)^2Z^2}k\frac{d\sigma}{dk}$$

The functions $F_i(Z,X,Y)$ $(i=\sigma,l)$ have the form

$$F_i(Z,X,Y) = F_{i0}(X,Y) + ZF_{i1}(X,Y) \tag{6.16}$$

where $F_{ij}(X,Y)$ are polynomials of the variables X, Y

$$\begin{aligned} F_{i0}(X,Y) &= (C_1 + C_2X + \ldots + C_6X^5) + (C_7 + C_8X + \ldots + C_{12}X^5)Y \\ &\quad +(C_{13} + C_{14}X + \ldots + C_{18}X^5)Y^2 + \ldots \\ &\quad +(C_{31} + C_{32}X + \ldots + C_{36}X^5)Y^5 \qquad Y \le 0 \\ &= (C_1 + C_2X + \ldots + C_6X^5) + (C_7 + C_8X + \ldots + C_{12}X^5) \\ &\quad +(C_{37} + C_{38}X + \ldots + C_{42}X^5)Y^2 + \ldots + \\ &\quad (C_{55} + C_{56}X + \ldots + C_{60}X^5)Y^5 \qquad Y > 0 \\ F_{i1}(X,Y) &= (C_{61} + C_{62}X + \ldots + C_{65}X^4) + (C_{66} + C_{67}X + \ldots + C_{70}X^4)Y \\ &\quad +(C_{71} + C_{72}X + \ldots + C_{75}X^4)Y^2 + \ldots \end{aligned}$$

$$
\begin{aligned}
& +(C_{81} + C_{82}X + \ldots + C_{85}X^4)Y^4 \\
& \qquad\qquad\qquad\qquad\qquad\qquad\qquad\qquad\qquad\qquad\qquad\qquad Y \leq 0 \\
= \; & (C_{61} + C_{62}X + \ldots + C_{65}X^4) + (C_{66} + C_{67}X + \ldots + C_{70}X^4)Y \\
& +(C_{86} + C_{87}X + \ldots + C_{90}X^4)Y^2 + \ldots \\
& +(C_{96} + C_{97}X + \ldots + C_{100}X^4)Y^4 \\
& \qquad\qquad\qquad\qquad\qquad\qquad\qquad\qquad\qquad\qquad\qquad\qquad Y > 0
\end{aligned}
$$

$F_{ij}(X,Y)$ denotes in fact a function constructed from two polynomials

$$
F_{ij}(X,Y) = \begin{cases} F_{ij}^{neg}(X,Y) & \text{for} \quad Y \leq 0 \\ F_{ij}^{pos}(X,Y) & \text{for} \quad Y > 0 \end{cases}
$$

where the polynomials F_{ij} fulfil the conditions

$$
F_{ij}^{neg}(X,Y)_{Y=0} = F_{ij}^{pos}(X,Y)_{Y=0} \qquad\qquad \left(\frac{\partial F_{ij}^{neg}}{\partial Y}\right)_{Y=0} = \left(\frac{\partial P_{ij}^{pos}}{\partial Y}\right)_{Y=0}
$$

We have computed 4000 "data points" in the range

$$
Z = 6; 13; 29; 47; 74; 92 \qquad 10\,\text{keV} \leq T \leq 10\,\text{TeV} \qquad 10\,\text{keV} \leq k_c \leq T
$$

and we have performed a least-squares fit to determine the parameters.

The values of the parameters (ξ_σ, α, v_σ, C_i for σ and ξ_l, β, V_l, C for E_{Loss}^{brem}) can be found in the code of the class itself.

The errors of the parameterisations (6.14) and (6.15) can be estimated as

$$
\frac{\Delta\sigma}{\sigma} = \begin{cases} 12 - 15\% & \text{for} \quad T \leq 1MeV \\ \leq 5 - 6\% & \text{for} \quad 1MeV < T \leq 10TeV \end{cases}
$$

$$
\frac{\Delta E_{Loss}^{brem}}{E_{Loss}^{brem}} = \begin{cases} 10 - 15\% & \text{for} \quad T \leq 1MeV \\ 5 - 6\% & \text{for} \quad 1MeV < T \leq 100GeV \\ 10\% & \text{for} \quad 100GeV < T \leq 10TeV \end{cases}
$$

The energy loss due to soft photon bremsstrahlung is tabulated at initialisation time as a function of the medium and of the energy.

The mean free path for discrete bremsstrahlung is tabuled at initialisation time as a function of the medium and of the energy, too.

Corrections for e^+e^- differences

The radiative energy loss for electrons or positrons is:

$$\begin{aligned} -\frac{1}{\rho}\left(\frac{dE}{dx}\right)^{\pm}_{rad} &= \frac{N_{Av}\alpha r_e^2}{A}(T+m)Z^2\Phi^{\pm}_{rad}(Z,T) \\ \Phi^{\pm}_{rad}(Z,T) &= \frac{1}{\alpha r_e^2 Z^2(T+m)}\int_0^T k\frac{d\sigma^{\pm}}{dk}dk \end{aligned}$$

Reference [Kim86] says that:
"The differences between the radiative loss of positrons and electrons are considerable and cannot be disregarded.

[...] The ratio of the radiative energy loss for positrons to that for electrons obeys a simple scaling law, [...] is a function only of the quantity T/Z^2"

In other words:

$$\eta = \frac{\Phi^{+}_{rad}(Z,T)}{\Phi^{-}_{rad}(Z,T)} = \eta\left(\frac{T}{Z^2}\right)$$

The authors have calculated this function in the range $10^{-7} \leq \frac{T}{Z^2} \leq 0.5$ (here the kinetic energy T is expressed in MeV). Their *data* can be fairly accurately reproduced using a parametrisation:

$$\eta = \begin{cases} 0 & \text{if} \quad x \leq -8 \\ \frac{1}{2} + \frac{1}{\pi}\arctan\left(a_1 x + a_3 x^3 + a_5 x^5\right) & \text{if} \quad -8 < x < 9 \\ 1 & \text{if} \quad x \geq 9 \end{cases}$$

where:

$$\begin{aligned} x &= \log\left(C\frac{T}{Z^2}\right) \text{ (T in GeV)} \\ C &= 7.5221 \times 10^6 \\ a_1 &= 0.415 \\ a_3 &= 0.0021 \\ a_5 &= 0.00054 \end{aligned}$$

This e^+e^- energy loss difference is not a pure low-energy phenomenon (at least for high Z), as it can be seen from Tables 6.1.

The scaling holds for the ratio of the total radiative energy losses, but it is significantly broken for the photon spectrum in the screened case. In case

$\frac{T}{Z^2}(GeV)$	T	η	$\left(\frac{rad.\ loss}{total\ loss}\right)_{e^-}$
10^{-9}	$\sim 7keV$	~ 0.1	$\sim 0\%$
10^{-8}	$67keV$	~ 0.2	$\sim 1\%$
2×10^{-7}	$1.35MeV$	~ 0.5	$\sim 15\%$
2×10^{-6}	$13.5MeV$	~ 0.8	$\sim 60\%$
2×10^{-5}	$135.MeV$	~ 0.95	$> 90\%$

Table 6.1: ratio of the e^+e^- radiative energy loss in lead (Z=82).

of a point Coulomb charge the scaling would hold also for the spectrum. The scaling can be expressed by:

$$\frac{\Phi^+}{\Phi^-} = \eta\left(\frac{T}{Z^2}\right) \qquad\qquad \frac{\frac{d\sigma^+}{dk}}{\frac{d\sigma^-}{dk}} = \text{does not scale}$$

If we consider the photon spectrum from bremsstrahlung reported in [Kim86] we see that:

$$\frac{d\sigma^\pm}{dk} = S^\pm\left(\frac{k}{T}\right) \qquad \frac{S^+(k)}{S^-(k)} \leq 1 \qquad S^+(1) = 0 \qquad S^-(1) > 0$$

We further assume that:

$$\frac{d\sigma^+}{dk} = f(\epsilon)\frac{d\sigma^-}{dk} \qquad\qquad \epsilon = \frac{k}{T} \tag{6.17}$$

In order to satisfy approximately the scaling law for the ratio of the total radiative energy loss, we require for $f(\epsilon)$:

$$\int_0^1 f(\epsilon)d\epsilon \;\; = \;\; \eta \tag{6.18}$$

From the photon spectra we require:

$$\left.\begin{array}{l} f(0) = 1 \\ f(1) = 0 \end{array}\right\} \qquad \text{for all } Z, T \tag{6.19}$$

We have chosen a simple function f:

$$f(\epsilon) \;\; = \;\; C(1-\epsilon)^\alpha \qquad\qquad C, \alpha > 0 \tag{6.20}$$

from the conditions (6.18), (6.19) we get:

$$\begin{aligned} C &= 1 \\ \alpha &= \frac{1}{\eta} - 1 \qquad\qquad (\alpha > 0 \text{ because } \eta < 1) \\ f(\epsilon) &= (1-\epsilon)^{\frac{1}{\eta}-1} \end{aligned}$$

We have defined weight factors F_l and F_σ for the positron continuous energy loss and discrete bremsstrahlung cross section:

$$F_l = \frac{1}{\epsilon_0}\int_0^{\epsilon_0} f(\epsilon)d\epsilon \qquad\qquad F_\sigma = \frac{1}{1-\epsilon_0}\int_{\epsilon_0}^{1} f(\epsilon)d\epsilon \quad (6.21)$$

where $\epsilon_0 = \frac{k_c}{T}$ and k_c is the photon cut . In this scheme the positron energy loss and discrete bremsstrahlung can be calculated as:

$$\left(-\frac{dE}{dx}\right)^{+} = F_l \left(-\frac{dE}{dx}\right)^{-} \qquad\qquad \sigma^{+}_{brems} = F_\sigma \sigma^{-}_{brems}$$

As in this approximation the photon spectra are identical, the same sampling is used for generating e^-e^+ bremsstrahlung. The following relations hold:

$$\begin{aligned} F_\sigma &= \eta(1-\epsilon_0)^{\frac{1}{\eta}-1} < \eta \\ \epsilon_0 F_l + (1-\epsilon_0)F_\sigma &= \eta \qquad\qquad \text{from the def (6.21)} \\ \Rightarrow F_l &= \eta\frac{1-(1-\epsilon_0)^{\frac{1}{\eta}})}{\epsilon_0} > \eta\frac{1-(1-\epsilon_0)}{\epsilon_0} = \eta \qquad \Rightarrow \begin{cases} F_l > \eta \\ F_\sigma < \eta \end{cases} \end{aligned}$$

which is consistent with the spectra.

The effect of this e^-e^+ bremsstrahlung difference can be also seen in e.m. shower development, when the primary energy is not too high.

Landau Pomeranchuk Migdal effect

The LPM effect (see e.g in [Gal64],[Ant97]) is the supression of the photon production due to the multiple scattering of the electrons.If an electron multiple scatters while traversing the co called formation zone, the bremsstrahlung amplitude from before and after the scattering can interfere, reducing the amplitude for bremsstrahlung photon emission (similar supression occurs for pair production,too). The supression becomes significant for photon energies below a certain value, given by

$$\frac{k}{E} < \frac{E}{E_{LPM}} \qquad (6.22)$$

, where

k	photon energy
E	electron energy
E_{LPM}	characteristic energy for LPM effect (depend on the medium).

The value of the LPM characteristic energy can be written as

$$E_{LPM} = \frac{\alpha m^2 X_0}{4hc} \tag{6.23}$$

, where

α	fine structure constant
m	electron mass
X_0	radiation length in the material
h	Planck constant
c	velocity of light in vacuum.

The LPM supression of the photon spectrum is given by the formula

$$S_{LPM} = \sqrt{\frac{E_{LPM} \cdot k}{E^2}} \tag{6.24}$$

, while the dielectric supression (included already in the parametrisations) can be written as

$$S_p = \frac{k^2}{k^2 + C_p \cdot E^2} \tag{6.25}$$

, where the quantity C_p is given by

$$C_p = \frac{r_0^2 \lambda_e^2 n}{\pi} \tag{6.26}$$

In eq. 6.26 the parameters are

r_0	classical electron radius
λ_e	electron Compton wawelength
n	electrondensity in the material.

Both of the supression effects reduce the effective formation length of the photon , so the supressions *do not simply multiply.* For the total supression S the following equation holds (see [Gal64])

$$\frac{1}{S} = 1 + \frac{1}{S_p} + \frac{S}{S_{LPM}^2} \tag{6.27}$$

which can be solved easily for S

$$S = \frac{\sqrt{S_{LPM}^4 \cdot (1 + \frac{1}{S_p})^2 + 4 \cdot S_{LPM}^2} - S_{LPM}^2 \cdot (1 + \frac{1}{S_p})}{2} \tag{6.28}$$

The implementation of the LPM effect has been done in the following way: The cross section and energy loss should be modified by applying the (energy and material dependent) factor $\frac{S}{S_p}$. This is done at initialisation time for the energy loss by computing the correction factor

$$f_c = \frac{\int_0^{k_cut} n_\gamma(k) \cdot \frac{S}{S_p} dk}{\int_0^{k_cut} n_\gamma(k) dk} \tag{6.29}$$

, wherea $n_\gamma(k)$ is the photon specrum . The total cross section given by the parametrization 6.14 has not been modified , the algorithm of the photon generation takes care of the LPM effect.

6.2.2 Simulation of the discrete bremsstrahlung

The energy of the final state photons is sampled according to the spectrum [Sel85] by Seltzer and Berger. Seltzer and Berger have calculated the bremsstrahlung spectra for materials with atomic numbers Z = 6, 13, 29, 47, 74, 92 in the electron (kinetic) energy range 1 keV - 10 GeV. Their tabulated results have been used as input in a parametrising-fitting procedure. The functional form of the parameterisation for the quantity:

$$S(x) = Ck\frac{d\sigma}{dk}$$

can be written as

$$S(x) = \begin{cases} (1 - a_h\epsilon)F_1(\delta) + b_h\epsilon^2 F_2(\delta) & T \geq 1MeV \\ 1 + a_l x + b_l x^2 & T < 1MeV \end{cases} \tag{6.30}$$

where:

C		normalisation constant	k		photon energy
T, E		kinetic and total energy of the primary electron	x	=	$\frac{k}{T}$
ϵ	=	$\frac{k}{E} = x\frac{T}{E}$			

The $F_i(\delta)$ screening functions depend on the screening variable:

δ	=	$\frac{136m_e}{Z^{1/3}E}\frac{\epsilon}{1-\epsilon}$	
$F_1(\delta)$	=	$F_0(42.392 - 7.796\delta + 1.961\delta^2 - F)$	$\delta \leq 1$
$F_2(\delta)$	=	$F_0(41.734 - 6.484\delta + 1.250\delta^2 - F)$	$\delta \leq 1$
$F_1(\delta)$	=	$F_2(\delta) = F_0(42.24 - 8.368\ln(\delta + 0.952) - F)$	$\delta > 1$
F_0	=	$\frac{1}{42.392-F}$	
F	=	$4\ln Z - 0.55(\ln Z)^2$	

$a_{h,l}$ and $b_{h,l}$ are parameters to be fitted.

The 'high energy' (T > 1 MeV) formula comes from the Coulomb-corrected, sceened Bethe-Heitler formula (see e.g. [Will60, Butc60, EGS4]). However, there are two things in eq. (6.30) which make a difference:

1. a_h, b_h depend on T and on the atomic number Z (in the case of the Bethe-Heitler spectrum $a_h = 1$, $b_h = 0.75$);

2. the function F is not the same than that in the Bethe-Heitler cross-section, this function gives a better behaviour in the high frequency limit, i.e. when $k \to T$ ($x \to 1$).

The T and Z dependence of the parameters are described by the equations:

$$\begin{aligned} a_h &= 1 + \frac{a_{h1}}{u} + \frac{a_{h2}}{u^2} + \frac{a_{h3}}{u^3} \\ b_h &= 0.75 + \frac{b_{h1}}{u} + \frac{b_{h2}}{u^2} + \frac{b_{h3}}{u^3} \\ a_l &= a_{l0} + a_{l1}u + a_{l2}u^2 \\ b_l &= b_{l0} + b_{l1}u + b_{l2}u^2 \\ \text{with} & \\ u &= \ln\left(\frac{T}{m_e}\right) \end{aligned}$$

the $a_{hi}, b_{hi}, a_{li}, b_{li}$ parameters are polynomials of second order in the variable:

$$v = [Z(Z+1)]^{1/3}$$

It can be seen relatively easily that for the limiting case $T \to \infty$, $a_h \to 1, b_h \to 0.75$, so eq. (6.30) gives the Bethe-Heitler cross section.

There are altogether 36 linear parameter in the formulae , their values are given in the code. The parameterisation reproduces the Seltzer-Berger tables within a few % (2-3 % on average, the maximum error being less than 10-12 %), the tables, on the other hand, agree well with the experimental data and theoretical (low- and high-energy) results (less than 10 % below 50 MeV, less than 5 % above 50 MeV).

Apart from the normalisation the cross section differential in photon energy can be written as:

$$\frac{d\sigma}{dk} = \frac{1}{\ln\frac{1}{x_c}}\frac{1}{x}g(x) = \frac{1}{\ln\frac{1}{x_c}}\frac{1}{x}\frac{S(x)}{S_{max}}$$

where $x_c = k_c/T$, k_c is the photon cut-off energy below which the bremsstrahlung is treated as a continuous energy loss . Using this decomposition of the cross section and two random numbers r_1, r_2 uniformly distributed in $]0,1[$, the sampling of x is done as follows:

1. sample x from

$$\frac{1}{\ln\frac{1}{x_c}}\frac{1}{x} \qquad \text{setting} \qquad x = e^{r_1 \ln x_c}$$

2. calculate the rejection function $g(x)$ and:

   - if $r_2 > g(x)$ reject x and go back to 1;
   - if $r_2 \leq g(x)$ accept x.

To apply the dielectric supression [Mig56] all it has to be done is to multiply the rejection function by the supression factor , which is equivalent to the expression 6.25:

$$C_M(\epsilon) = \frac{1 + C_0/\epsilon_c^2}{1 + C_0/\epsilon^2}$$

where

$$C_0 = \frac{nr_0\lambda^2}{\pi}, \qquad \epsilon_c = \frac{k_c}{E}$$

n electron density in the medium

r_0 classical electron radius

λ reduced Compton wavelength of the electron.

This correction decreases the cross-section for low photon energy.

After having ϵ sampled , the supression factor $f_{LPM} = \frac{S}{S_p}$ is used as a rejection function in order to take into account the LPM effect , too. Here the supression factor is compared to a random number r uniformly distributed in the interval $(0, 1)$. If $f_{LPM} \geq r$ the simulation is continuing otherwise the bremsstrahlung process is finished *without photon production* .It can be seen easily that this procedure takes into account the LPM supression correctly.

After the successful sampling of ϵ, the polar angles of the radiated photon are generated with respect to the parent electron's momentum. It is difficult to find in the literature simple formulas for this angle. For example the double differential cross section reported by Tsai [Tsai74, Tsai77] is the following:

$$\begin{aligned}
\frac{d\sigma}{dkd\Omega} &= \frac{2\alpha^2 e^2}{\pi k m^4}\left\{\left[\frac{2\epsilon - 2}{(1+u^2)^2} + \frac{12u^2(1-\epsilon)}{(1+u^2)^4}\right] Z(Z+1)\right. \\
&\quad \left. + \left[\frac{2 - 2\epsilon - \epsilon^2}{(1+u^2)^2} - \frac{4u^2(1-\epsilon)}{(1+u^2)^4}\right]\left[X - 2Z^2 f_c((\alpha Z)^2)\right]\right\} \\
u &= \frac{E\theta}{m} \\
X &= \int_{t_{min}}^{m^2(1+u^2)^2} \left[G_Z^{el}(t) + G_Z^{in}(t)\right] \frac{t - t_{min}}{t^2} dt \\
G_Z^{el,in}(t) &\quad \text{atomic form factors} \\
t_{min} &= \left[\frac{km^2(1+u^2)}{2E(E-k)}\right]^2 = \left[\frac{\epsilon m^2(1+u^2)}{2E(1-\epsilon)}\right]^2
\end{aligned}$$

This distribution is complicated to sample, and it is anyway only an approximation to within few percent, if nothing else, due to the presence of the atomic form-factors. The angular dependence is contained in the variable $u = E\theta m^{-1}$. For a given value of u the dependence of the shape of the function on Z, E, $\epsilon = k/E$ is very weak. Thus, the distribution can be approximated by a function

$$f(u) = C\left(ue^{-au} + due^{-3au}\right) \tag{6.31}$$

where

$$C = \frac{9a^2}{9+d} \qquad a = 0.625 \qquad d = 0.13\left(0.8 + \frac{1.3}{Z}\right)\left(100 + \frac{1}{E}\right)(1+\epsilon)$$

where E is in GeV. While this approximation is good at high energies, it becomes less accurate around few MeV. However in that region the ionisation losses dominate over the radiative losses.

The sampling of the function $f(u)$ can be done in the following way (r_i, $i = 1, 2, 3$ are uniformly distributed random numbers in [0,1]):

1. Choose between ue^{-au} and due^{-3au}:

$$b = \begin{cases} a & \text{if} \quad r_1 < 9/(9+d) \\ 3a & \text{if} \quad r_1 \geq 9/(9+d) \end{cases}$$

2. Sample ue^{-bu}:

$$u = -\frac{\log(r_2 r_3)}{b}$$

3. check that:

$$u \leq u_{max} = \frac{E\pi}{m}$$

   otherwise go back to 1.

The probability of failing in the last test is reported in table 6.2.

The function $f(u)$ can be used also to describe the angular distribution of the photon in μ bremsstrahlung and to describe the angular distribution in photon pair production.

The azimuthal angle, Φ, is generated isotropically. This information is used to calculate the momentum vector of the radiated photon, to transform it to the global coordinate system. Also, the momentum of the parent electron is updated.

6.2.3 Status of this document

9.10.98 created by L. Urbán.
5.12.98 editing by J.P. Wellisch.

$$P = \int_{u_{max}}^{\infty} f(u)\, du$$

E (MeV)	P(%)
0.511	3.4
0.6	2.2
0.8	1.2
1.0	0.7
2.0	< 0.1

Table 6.2: Angular sampling efficiency

Bibliography

[GEANT3] GEANT3 manual ,CERN Program Library Long Writeup W5013 (October 1994).

[Gal64] V.M.Galitsky and I.I.Gurevich. Nuovo Cimento 32 (1964) 1820.

[Ant97] P.L. Anthony et al. SLAC-PUB-7413/LBNL-40054 (February 1997)

[Sel85] S.M.Seltzer and M.J.Berger. Nucl.Inst.Meth. 80 (1985) 12.

[Mess70] H.Messel and D.F.Crawford. Pergamon Press,Oxford,1970.

[EGS4] W.R. Nelson et al.:The EGS4 Code System. *SLAC-Report-265 , December 1985*

[Mig56] A.B. Migdal. Phys.Rev. 103. (1956) 1811.

[Kim86] L. Kim et al. Phys. Rev. A33 (1986) 3002.

[Tsai74] Y-S. Tsai . Rev. Mod. Phys. 46. (1974) 815.

[Tsai77] Y-S. Tsai . Rev. Mod. Phys. 49. (1977) 421.

[Will60] R. W. Williams . Fundamental Formulas of Physics, vol.2. Dover Pubs.Inc,1960.

[Butc60] J. C. Butcher and H. Messel. Nucl.Phys. 20. (1960) 15.

6.3 e^+e^- annihilation

6.3.1 Cross section and Mean free path

Cross section per atom

For the annihilation in fly of e^+e^- into two photons the cross-section formula of Heitler is used [Heit54, egs4]:

$$\begin{aligned}
\sigma(Z,E) &= \frac{Z\pi r_0^2}{\gamma+1}\left[\frac{\gamma^2+4\gamma+1}{\gamma^2-1}\ln\left(\gamma+\sqrt{\gamma^2-1}\right)-\frac{\gamma+3}{\sqrt{\gamma^2-1}}\right] \\
E &= \text{total energy of the incident positron} \\
\gamma &= E/m_ec^2 \\
r_0 &= \text{classical electron radius}
\end{aligned}$$

Mean free path

* In a simple material the number of atoms per volume is:

$$n = \frac{\mathcal{N}\rho}{A}$$

where:

$\mathcal{N}$	Avogadro's number
ρ	density of the medium
A	mass of mole

* In a compound material the number of atoms of Element elm per volume is:

$$n_{elm} = \frac{\mathcal{N}\rho w_{elm}}{A_{elm}}$$

where:

$\mathcal{N}$	Avogadro's number
ρ	density of the medium
w_{elm}	proportion by mass of the Element elm
A_{elm}	mass of mole of the Element elm

* The mean free path, λ, for a positron to be annihilated with an electron is given by

$$\lambda(E_\gamma) \equiv \frac{1}{\Sigma(E_\gamma)} = \frac{1}{\sum_{elm}\left[n_{elm}\sigma(Z_{elm},E_\gamma)\right]}$$

where $\sum_{elm}$ runs over all Elements the material is made of.

6.3.2 Sampling the final state

kinematical limits

$$e^+ \, e^- \rightarrow \gamma_a \, \gamma_b$$

The incident e^+ has a kinetic energy T, a total energy: $E_e = T + mc^2$
and a momentum: $Pc = \sqrt{T(T + 2mc^2)}$
The total available energy is: $E_{tot} = E_e + mc^2 = E_a + E_b$
The momentum conservation is: $\vec{P} = \vec{P}_{\gamma_a} + \vec{P}_{\gamma_b}$
Lets define the ratio of energy transfered to one photon (says γ_a):

$$\epsilon = \frac{E_a}{E_{tot}} \equiv \frac{E_a}{T + 2mc^2}$$

The energy transfered to γ_a is maximum when γ_a is emitted in the direction of the incident e^+. Then $E_a\mathsf{max} = (E_{tot} + Pc)/2$
The energy transfered to γ_a is minimum when γ_a is emitted in the opposite direction of the incident e^+. Then $E_a\mathsf{min} = (E_{tot} - Pc)/2$
Therefore:

$$\begin{aligned} \epsilon_{max} &= \frac{E_a\mathsf{max}}{E_{tot}} = \frac{1}{2}\left[1 + \sqrt{\frac{\gamma - 1}{\gamma + 1}}\right] \\ \epsilon_{min} &= \frac{E_a\mathsf{min}}{E_{tot}} = \frac{1}{2}\left[1 - \sqrt{\frac{\gamma - 1}{\gamma + 1}}\right] \end{aligned}$$

where $\gamma = (T + mc^2)/mc^2$
Therefore the range of ϵ is: $[\epsilon_{min} \; ; \; \epsilon_{max}]$ $(\equiv [\epsilon_{min} \; ; \; 1 - \epsilon_{min}])$

sample the gamma energy

The differential cross-section of the two-photon positron-electron annihilation can be written as [Heit54, egs4]:

$$\frac{d\sigma(Z,\epsilon)}{d\epsilon} = \frac{Z\pi r_0^2}{\gamma - 1}\left(\frac{1}{\epsilon}\right)\left[1 + \frac{2\gamma}{(\gamma+1)^2} - \epsilon - \frac{1}{(\gamma+1)^2}\frac{1}{\epsilon}\right]$$

where Z is the atomic number of the material, r_0 the classical electron radius, and $\epsilon \in [\epsilon_{min} \; ; \; \epsilon_{max}]$
The differential cross-section can be decomposed as:

$$\frac{d\sigma(Z,\epsilon)}{d\epsilon} = \frac{Z\pi r_0^2}{\gamma - 1}\alpha f(\epsilon) g(\epsilon)$$

where:

$$\begin{aligned} \alpha &= \ln(\epsilon_{max}/\epsilon_{min}); \qquad f(\epsilon) = 1/(\alpha\epsilon) \\ g(\epsilon) &= \left[1 + \frac{2\gamma}{(\gamma+1)^2} - \epsilon - \frac{1}{(\gamma+1)^2}\frac{1}{\epsilon}\right] \equiv 1 - \epsilon + \frac{2\gamma\epsilon - 1}{\epsilon(\gamma+1)^2} \end{aligned}$$

Given 2 random numbers $r, r' \in]0,1[$, the photon energies are sampled as follow:

1. sample ϵ from $f(\epsilon) : \epsilon = \epsilon_{min}\left(\frac{\epsilon_{max}}{\epsilon_{min}}\right)^r$
2. test the rejection function: if $g(\epsilon) \geq r'$ accept ϵ, otherwise return to step 1.

Then the photon energies are: $E_a = \epsilon E_{tot} \qquad E_b = (1-\epsilon)E_{tot}$

compute the final kinematic

Lets be θ the angle between the incident e^+ and γ_a. From the energy-momentum conservation we have:

$$\cos\theta = \frac{1}{Pc}\left[T + mc^2\frac{2\epsilon - 1}{\epsilon}\right] = \frac{\epsilon(\gamma+1) - 1}{\epsilon\sqrt{\gamma^2 - 1}}$$

The azimuthal angle, ϕ, is generated isotropically and the momentum vector of the photons, $\vec{P_{\gamma_a}}$ and $\vec{P_{\gamma_b}}$ are computed from the energy-momentum conservation and transformed into the `World` coordinate system.

annihilation at rest

The method **AtRestDoIt** treates the special case when a positron comes at rest before annihilating. It generates two photons with energy $k = m$. The angular distribution is isotropic.

6.3.3 Restrictions

1. The annihilation processes producing one or three or more photons are ignored, because these processes are negligible compared to the annihilation into two photons[egs4, Mess70];
2. In calculating the process it is assumed that the atomic electron initially is free and at rest. This is the usual assumption used in shower programs [egs4];

6.3.4 Status of this document

9.10.98 created by M.Maire.
5.12.98 editing by J.P. Wellisch.

Bibliography

[Heit54] W. Heitler. *The Quantum Theory of Radiation, Clarendon Press, Oxford* (1954)

[Mess70] H. Messel and D. Crawford. *Electron-Photon shower distribution, Pergamon Press* (1970)

[egs4] R. Ford and W. Nelson. *SLAC-265, UC-32* (1985)

6.4 Synchrotron radiation

6.4.1 Method

The spectral distribution of the mean photon number of synchrotron radiation $d\bar{N}/d\omega$ produced by an ultrarelativistic electron moving in a constant uniform magnetic field along a trajectory with length L can be expressed by definition in terms of the spectrum of the mean energy loss of the radiation $d\bar{\Delta}/d\omega$ by the following expression [Maier91]:

$$\frac{d\bar{N}}{d\omega} = \frac{1}{\omega}\frac{d\bar{\Delta}}{d\omega} = \frac{\sqrt{3}}{2\pi}\alpha\left(\frac{L\gamma}{R}\right)\frac{1}{\omega_c}\int_{\omega/\omega_c}^{\infty} K_{5/3}(\eta)d\eta. \tag{6.32}$$

Here:

ω	photon energy
α	fine structure constant
R	instantaneous radius of curvature of the trajectory
K	Macdonald function
ω_c	characteristic energy of synchrotron radiation

$\omega_c = 1.5\beta(\hbar c/R)\gamma^3$, $\hbar$ is the Planck constant, and $\beta = v/c$ is the ratio of the electron velocity v to the speed of light c). In the SI system of units: $R(m) = P(GeV/c)/0.3B_{\perp}(T)$, where $B_{\perp}$ is the component of magnetic flux density perpendicular to the electron velocity, and P is the electron momentum (for the case considered $R \approx const$ along the whole trajectory) . For the simulation of the energy spectrum of synchrotron radiation by the Monte-Carlo method we need to calculate the integral distribution of the mean number of photons with the energy more than the given one: $\bar{N}_{>\omega}$. Transforming $d\bar{N}/d\omega$ by the integral representation of the Macdonald function [Abram64], we have :

$$\begin{aligned}\bar{N}_{>\omega} &= \int_{\omega}^{\infty}\frac{d\bar{N}}{d\omega'}d\omega' \\ &= \frac{\sqrt{3}}{2\pi}\alpha\left(\frac{L\gamma}{R}\right)\int_0^{\infty}\frac{\cosh\left(\frac{5}{3}t\right)}{\cosh^2(t)}\exp\left[-\frac{\omega}{\omega_c}\cosh(t)\right]dt. \end{aligned}\tag{6.33}$$

The latter integral is calculated numerically by the quadrature Laguerre formula [Korn61] . The calculations show that taking into account about 50 roots of the Laguerre polynomials results in an accuracy of the integral estimation better than 10^{-4} [Bag98] . The mean number of synchrotron radiation photons $\bar{N}$ $(= \bar{N}_{>0})$ produced by an ultrarelativistic electron moving

in a constant magnetic field along a trajectory with the length L , is given by :

$$\begin{aligned}\bar{N} = \bar{N}_{>0} &= \frac{\sqrt{3}}{2\pi}\alpha\left(\frac{L\gamma}{R}\right)\int_0^\infty \frac{\cosh\left(\frac{5}{3}t\right)}{\cosh^2(t)}dt \\ &= \frac{5}{2\sqrt{3}}\alpha\left(\frac{L\gamma}{R}\right) \approx 10^{-2}\left(\frac{L\gamma}{R}\right). \qquad (6.34)\end{aligned}$$

Qualitatively this result can be manipulated using the fact that the mean number of photons produced along the formation zone length $z \approx R/\gamma$ is proportional to α . Then for the length L , $\bar{N} \approx \alpha L/(R/\gamma)$. Note, that for the ultrarelativistic case $\gamma \gg 1$, when $R \sim \gamma$, $\bar{N}$ does not depend on the electron energy but is defined by the values of L and $B_\perp$ only. The mean energy loss for synchrotron radiation $\bar{\Delta}$, corresponding to a trajectory with the length L, experiences the essential relativistic rise instead :

$$\bar{\Delta} = \int_0^\infty \omega\frac{d\bar{N}}{d\omega}d\omega = \frac{2}{3}\alpha\hbar c\left(\frac{L\gamma^2}{R^2}\right)\beta\gamma^2 = \frac{8\bar{N}}{15\sqrt{3}}\omega_c \approx 0.31\bar{N}\omega_c \sim \gamma^2 \quad (6.35)$$

The angular distribution of synchrotron radiation produced by ultrarelativistic electron shows the clear 'searchlight' effect. The main number of photons is radiated in the angle limit of the order of $1/\gamma$ around the electron trajectory direction. In the interesting region of $\gamma > 10^3$ the angular resolution of X-ray and gamma detectors usually does not allow us to measure the details of the angular distribution of synchrotron radiation. Therefore, the angular distribution is roughly set to be flat in the range $0 - 1/\gamma$.

6.4.2 Simulation of synchrotron radiation

The distance x along electron/positron trajectory to the next point of creation of synchrotron radiation photon is simulated according to exponential distribution, $exp(-x\bar{N}/L)$. The energy ω of synchrotron radiation photon is simulated according the distribution $\bar{N}_{>\omega}/\bar{N}$. The angles θ and φ counted from the electron trajectory (the electron momentum is considered to be parallel to the local z-axis) are rouhgly set to be distributed randomly in the ranges $0 - 1/\gamma$ and $0 - 2\pi$ respectively

6.4.3 Status of this document

15.10.98 created by V.Grichine
5.12.98 editing by J.P. Wellisch.

Bibliography

[Abram64] Edited by M. Abramovwitz and I.A. Stegan. *Handbook of Mathemaatical Functions, NBS Applied Mathematics Series 55* (1964)

[Bag98] Bagulya A.V. and Grichine V.M. Bulletin of Lebedev Institute, no.9-10, 7 (1998)

[Korn61] G.A. Korn and T.M. Korn. *Mathematical Handbook for scientists and engineers, McGRAW-HILL BOOK COMPANY, INC* (1961)

[Maier91] R. Maier. *Synchrotron Radiation, CERN Report 91-04, 97-115* (1991)

6.5 Photoabsorption ionization model

6.5.1 Method

In the framework of the PhotoAbsorption Ionization (PAI) model we describe the ionization energy loss produced by a relativistic charged particle in matter. The differential cross section $d\sigma_i/d\omega$ of ionizing collisions with the energy transfer ω produced by a relativistic particle in a matter in the most general form can be expressed by the following equations [Asosk82]:

$$\frac{d\sigma_i}{d\omega} = \frac{2\pi Ze^4}{mv^2}\left\{\frac{f(\omega)}{\omega\left|\varepsilon(\omega)\right|^2}\left[\ln\frac{2mv^2}{\omega\left|1-\beta^2\varepsilon\right|}- -\frac{\varepsilon_1-\beta^2\left|\varepsilon\right|^2}{\varepsilon_2}\arg(1-\beta^2\varepsilon^*)\right]+\frac{\tilde{F}(\omega)}{\omega^2}\right\}, \tag{6.36}$$

$$\tilde{F}(\omega)=\int_0^\omega\frac{f(\omega')}{\left|\varepsilon(\omega')\right|^2}d\omega',$$

$$f(\omega)=\frac{m\omega\varepsilon_2(\omega)}{2\pi^2ZN\hbar^2},$$

where m and e are the electron mass and charge respectively, $\hbar$ is the Planck constant, $\beta = v/c$ is ratio of the particle velocity v to the speed of light c, Z is the effective atomic number, N is the number of atoms (molecule) in unit volume, and $\varepsilon = \varepsilon_1 + i\varepsilon_2$ is the complex dielectric constant of the medium. In an isotropic nonmagnetic medium the dielectric constant can be expressed in terms of complex index of refraction, $n(\omega) = n_1 + in_2$, $\varepsilon(\omega) = n^2(\omega)$. In the energy range above the first ionization potential I_1 for all matters of practical interest, particular in all gases, $n_1 \sim 1$. Therefore the imaginary part of the dielectric constant can be expressed in terms of the photoabsorption cross section $\sigma_\gamma(\omega)$:

$$\varepsilon_2(\omega) = 2n_1n_2 \sim 2n_2 = \frac{N\hbar c}{\omega}\sigma_\gamma(\omega).$$

The real part of the dielectric constant is calculated in turn from the dispersion relation:

$$\varepsilon_1(\omega) - 1 = \frac{2N\hbar c}{\pi}V.p.\int_0^\infty\frac{\sigma_\gamma(\omega')}{\omega'^2-\omega^2}d\omega',$$

where the integral of the pole expression is considered in terms of the principal value. In practice it is convenient to calculate the contribution from the continuos part of the spectrum only. Then we have to use the normalised photoabsorption cross section $\tilde{\sigma}_\gamma(\omega)$:

$$\tilde{\sigma}_\gamma(\omega) = \frac{2\pi^2\hbar e^2 Z}{mc}\sigma_\gamma(\omega)\left[\int_{I_1}^{\omega_{max}}\sigma_\gamma(\omega')d\omega'\right]^{-1},\ \omega_{max}\sim 100\ keV,$$

which satisfies the quantum mechanical sum rule [Fano68]:

$$\int_{I_1}^{\omega_{max}}\tilde{\sigma}_\gamma(\omega')d\omega' = \frac{2\pi^2\hbar e^2 Z}{mc}.$$

The differential cross section of ionizing collisions is expressed by the photoabsorption cross section in the continuous spectrum region:

$$\begin{aligned}\frac{d\sigma_i}{d\omega} &= \frac{\alpha}{\pi\beta^2}\left\{\frac{\tilde{\sigma}_\gamma(\omega)}{\omega\left|\varepsilon(\omega)\right|^2}\left[\ln\frac{2mv^2}{\omega\left|1-\beta^2\varepsilon\right|}-\right.\right.\\ &\left.\left.-\frac{\varepsilon_1-\beta^2\left|\varepsilon\right|^2}{\varepsilon_2}\arg(1-\beta^2\varepsilon^*)\right]+\frac{1}{\omega^2}\int_{I_1}^{\omega}\frac{\tilde{\sigma}_\gamma(\omega')}{\left|\varepsilon(\omega')\right|^2}d\omega'\right\}, \quad (6.37)\end{aligned}$$

$$\varepsilon_2(\omega) = \frac{N\hbar c}{\omega}\tilde{\sigma}_\gamma(\omega),$$

$$\varepsilon_1(\omega) - 1 = \frac{2N\hbar c}{\pi}V.p.\int_{I_1}^{\omega_{max}}\frac{\tilde{\sigma}_\gamma(\omega')}{\omega'^2-\omega^2}d\omega'.$$

For practical calculations according (9.2) it is convinient to use the representation of the photoabsorption cross section as polinom of ω^{-1} as was proposed in [Biggs90]:

$$\sigma_\gamma(\omega) = \sum_{k=1}^{4} a_k^{(i)}\omega^{-k},$$

where the coefficients, $a_k^{(i)}$ are fitted with experimental data by the least square method separately in each i-th energy interval. The interval borders are equal as a rule to the corresponding photoabsorption edges. Then the dielectric constant can be calculated analytically in elementary functions for all ω except of photoabsorption edges where the photoabsorption cross section experiences breaks and the integral for the real part is not defined in the sence of the principal value.

The third term in (9.2), which can be calculated numerically only, results in complex procedure of calculation of $d\sigma_i/d\omega$. However, one can see that this term dominates for the energy transfers $\omega > 10\ keV$, where the function $\left|\varepsilon(\omega)\right|^2 \sim 1$. It is clear from physical reasons, since the third term represents the Rutheford cross section on atomic electrons which can be considered as

quasifree for given energy transfer [Allis80]. In addition, for high energy transfers , $\varepsilon(\omega) = 1 - \omega_p^2/\omega^2 \sim 1$, where ω_p is the plasma energy of the matter. Therefore the factor $|\varepsilon(\omega)|^{-2}$ can be moved from the integral and the differential cross section of ionizing collisions can be expressed as:

$$\frac{d\sigma_i}{d\omega} = \frac{\alpha}{\pi\beta^2 |\varepsilon(\omega)|^2} \left\{ \frac{\tilde{\sigma}_\gamma(\omega)}{\omega} \left[\ln \frac{2mv^2}{\omega |1-\beta^2\varepsilon|} - \right.\right. \\ \left.\left. - \frac{\varepsilon_1 - \beta^2 |\varepsilon|^2}{\varepsilon_2} \arg(1-\beta^2\varepsilon^*) \right] + \frac{1}{\omega^2} \int_{I_1}^{\omega} \tilde{\sigma}_\gamma(\omega') d\omega' \right\}, \quad (6.38)$$

which is especially simple in gases when $|\varepsilon(\omega)|^{-2} \sim 1$ for all $\omega > I_1$ [Allis80].

6.5.2 Simulation of energy losses

For given length of track the number of ionizing collisions is simulated by the Poisson distribution with the mean number proportional to the total cross section of ionizing collisions:

$$\sigma_i = \int_{I_1}^{\omega_{max}} \frac{d\sigma(\omega')}{d\omega'} d\omega',$$

while the energy transfer in each collision is simulated according the distribution proportional to:

$$\sigma_i(>\omega) = \int_{\omega}^{\omega_{max}} \frac{d\sigma(\omega')}{d\omega'} d\omega'.$$

The sum of the energy transfers is equal to energy loss.

6.5.3 Status of this document

16.11.98 created by V. Grichine .
5.12.98 editing by J.P. Wellisch.

Bibliography

[Asosk82] Asoskov V.S., Chechin V.A., Grichine V.M. at el, Lebedev Institute annual report, v. 140, p. 3 (1982)

[Allis80] Allison W.W.M., and Cobb J. Ann.Rev.Nucl.Part.Sci., v.30,p.253 (1980)

[Fano68] Fano U., and Cooper J.W. Rev.Mod.Phys., v. 40, p. 441 (1968)

[Biggs90] Biggs F., and Lighthill R., Preprint Sandia Laboratory, SAND 87-0070 (1990)

6.6 Photoabsorption cross section at low energies

6.6.1 Method

The photoabsorption cross section, $\sigma_\gamma(\omega)$, where ω is the photon energy , is used in GEANT-4 package for description of X-ray transportation and ionization effects in very thin absorbers. For practical calculations it is convenient to use the representation of the photoabsorption cross section as polinom of ω^{-1} as was proposed in [Biggs90](Sandia table):

$$\sigma_\gamma(\omega) = \sum_{k=1}^{4} a_k^{(i)} \omega^{-k},$$

where the coefficients, $a_k^{(i)}$ are fitted with experimental data by the least square method separately in each i-th energy interval. The interval borders are equal as a rule to the corresponding photoabsorption edges.

Calculations of primary ionization and energy loss distributions produced by relativistic charged particles in gaseous detectors based on original data of Sandia table showed that there is clear disagreement with experimental data, especially for gas mixtures with xenon.

The special investigation was performed [Grich94] for fitting of coefficients $a_k^{(i)}$ in the energy range of $10 - 50\ eV$ based on modern experimental data from synchrotron radiation experiments. The elements usually used in operation mixture of gaseous detectors were checked.

For hydrogen, fluorine, carbon, nitrogen and oxygen the data from the synchrotron radiation experiments with molecular gases such as N_2, O_2, CO_2, CH_4, and CF_4 were used: [Lee73],[Lee77]. The noble gases were checked using data given in the tables [Marr76] and [West80].

6.6.2 Status of this document

18.11.98 created by V. Grichine .
5.12.98 editing by J.P. Wellisch.

Bibliography

[Biggs90] Biggs F., and Lighthill R. Preprint Sandia Laboratory, SAND 87-0070 (1990)

[Grich94] Grichine V.M., Kostin A.P., Kotelnikov S.K. at el Bulletin of the Lebedev Institute no. 2-3, 34 (1994)

[Lee73] Lee L.C. at el J.Q.S.R.T., v. 13, p. 1023 (1973)

[Lee77] Lee L.C. at el Journ. of Chem. Phys., v. 67, p. 1237 (1977)

[Marr76] Marr G.V. and West J.B. Atom. Data Nucl. Data Tabl., v. 18, p. 497 (1976)

[West80] West J.B. and Morton J. Atom. Data Nucl. Data Tabl., v. 30, p. 253 (1980)

Chapter 7

Electromagnetic Interactions: Low energy extension

7.1 Introduction

A set of physics processes for photons and electrons is implemented in Geant4 to extend the validity range of photon and electron interactions down to lower energy than the standard Geant4 electromagnetic processes. They include photoelectric effect, Compton scattering, Rayleigh effect, Bremsstrahlung and ionization. Some features common to all the Low Energy processes currently implemented in Geant4 are summarized in this section; more detailed information specific to each process is given in the following sections.

7.1.1 Physics

The low energy processes of the Geant4 represent electromagnetic interactions down to lower energies than the ones covered by the equivalent Geant4 standard electromagnetic processes.

The current implementation of the Low Energy processes should be valid for energies down to between 250 eV (and could be used up to 100 GeV), unless differently specified in the following sections devoted to the detailed descriptions below. It covers elements with atomic number between 1 and 100.

7.1.2 Common features

All processes involve two distinct phases:

- the calculation and use of total cross sections,
- the generation of the final state.

Both phases are based on the exploitation of evaluated data.

Data sources

The data for the determination of cross sections and the sampling of the final state are extracted from a set of of publically distributed evaluated data libraries: EPDL97 (Evaluated Photons Data Library) [1] EEDL (Evaluated Electrons Data Library) [2] and EADL (Evaluated Atomic Data Library) [3]

These libraries provide the following data relevant for the simulation of the Geant4 Low Energy processes:

- total cross sections for photoelectric effect, Compton scattering, Rayleigh effect and Bremsstrahlung,
- subshell integrated cross sections for photoelectric effect and ionisation,

- energy spectra of the secondaries for electron processes,
- scattering functions for the Compton effect,
- form factors for the Rayleigh effect,
- binding energies for electrons for all subshells,
- transition probabilities between subshells for fluorescence and the Auger effect.

The energy range covered by the data libraries extends from 100 GeV down to 1 eV for Rayleigh and Compton effects, down to the lowest binding energy for each element for photoelectric effect, down to 10 eV for Bremsstrahlung and down to the lowest subshell binding energy for each element for ionization. For a rough estimate of the accuracy of EPDL97 data libraries in different energy regimes, see [4].

Distribution policy of the data sets

The author of the EPDL97 who has also the responsability of EEDL and EADL [1]-[3] data libraries Dr. Red Cullen has kindly permitted that the libraries and their related documentation be distributed with the Geant4 toolkit. They can be downloaded from the source code section of the official Geant4 page: http://wwwinfo.cern.ch/asd/geant4/geant4.html.

The EADL, EEDL and EPDL97 are also available from several public distribution centres in a different format not usable with Geant4. [5].

Calculation of total cross sections

The total cross sections as a function of energy are derived from the evaluated data for all processes.

Since the libraries provide cross sections for a discrete set of incident energies, the total cross sections at a given energy E are obtained by interpolating the available data, according to the formula [6]:

$$\log(\sigma(E)) = log(\sigma_1)\frac{log(E_2) - log(E)}{log(E_2) - log(E_1)} + log(\sigma_2)\frac{log(E) - log(E_1)}{log(E_2) - log(E_1)} \quad (7.1)$$

where E_1 and E_2 are the closest lower and higher energy respectively for which data are available.

In the case of ionization partial cross sections for each subshell of an atom of the element considered are first calculated at a given energy by interpolating the data according to the formula above, then the corresponding total cross section is obtained by summing the partial cross sections over all the shells.

Sampling of relevant physics quantities

The final state products of the processes are generated according to sampling distributions derived from the evaluated data.

The energy dependence of the parameters characterizing the sampling distributions is taken into account either by interpolation to the data available in the libraries directly or by interpolation to values obtained from fits to the data.

7.1.3 Software implementation

For each process an energy production threshold is defined; by default it is set equal to the lowest limit of the energy validity range of the process (250 eV in the current implementation), but a higher value can be set by the user.

For a particle of energy E above the production threshold the mean free path for interacting via a given process is calculated, like in the standard processes [7], as:

$$\lambda = \frac{1}{\Sigma_i \sigma_i(E) \cdot n_i} \tag{7.2}$$

where $\sigma_i(E)$ is the microscopic integrated cross section of the process considered at energy E and n_i is the atomic density number of the $i-th$ element contributing to the material composition; the sum runs over all the elements the material is composed of. The cross sections are determined as described in section 7.1.2. Particles with energy below the production threshold are assigned a mean free path corresponding to zero (compatible with machine precision); their energy is converted into a local energy deposit and they are not further tracked.

In the phase of generation of the final state the atom of the material involved in the interaction with the incident particle is selected randomly.

The final state is generated sampling the relevant physics quantities (energies and angular distributions of the secondaries) from the distributions derived from the evaluated data. The energy dependence of these distributions is taken into account by interpolating or fitting the data.

The secondaries generated with energy below the production threshold are not further tracked and their energy is converted into a local energy deposited.

7.2 Status of the document

30.9.99 created by Alessandra Forti

7.3 Compton scattering

The total cross section at a given energy E is calculated as described in section 7.1.2.

The scattered photon energy is sampled according to the product of the Klein-Nishina formula **??**:

$$\Phi(\epsilon) \cong [\frac{1}{\epsilon} + \epsilon][1 - \frac{\epsilon}{1+\epsilon^2} sin^2(\theta)] \tag{7.3}$$

times the scattering functions, where ϵ is the ratio between the scattered photon energy and the incident photon energy. Values of the scattering functions at each momentum transferred $q = E \times \sin^2(\theta/2)$ are obtained interpolating the values of the data.

Total angular and energy distribution of the incoherent scattered photons is the product of the Klein-Nishina formula and of the scattering functions.

$$P(\epsilon, q) = \Phi(\epsilon) \times SF(q) \tag{7.4}$$

The effect of the scattering functions is to multiply Klein-Nishina distribution for the square of the energy of the scattered photon at very low energies, to suppress forward angles at high energies and at very high energies the effect can be ignored because scattering functions becomes isotropic.

The method applied for the sampling is a combination of the composition and rejection Monte Carlo methods [8] as in the standard process. The difference between the standard Compton effect and the low energy Compton at sampling time is that, to take into account the effect of the scattering function, the rejection function **??**:

$$g(\epsilon) = \left[1 - \frac{\epsilon}{1+\epsilon^2} \sin^2\theta\right] \tag{7.5}$$

is multiplied by the scattering functions and the product of the two function:

$$g(\epsilon) \times SF(q) \tag{7.6}$$

is compared with a random number r times the atomic number of the element that is the maximum value the scattering function can reach. If the value of the new rejection function is smaller than $Z \times r$ the procedure is repeated otherwise the value of the angle and of the energy are kept.

7.4 Status of the document

30.9.99 created by Alessandra Forti

7.5 Rayleigh effect

The total cross section at a given energy E is calculated as described in section 7.1.2.

The coherent scattered photon angle sampled according to the product of the Rayleigh formula $1+\cos^2(\theta)$ multiplied by squared form factors $FF(q)$ from EPDL data libraries [9] [10].

$$\Phi(E,\theta) = [1 + \cos^2(\theta)] \times FF^2(q) \tag{7.7}$$

Values at each momentum transferred $q = E \times \sin^2(\theta/2)$ of the form factors are obtained interpolating the data. Form factors introduce a dependency on the initial energy of the photon that is not taken into account in the Rayleigh formula. At low energies form factors are isotropic and doesn't affect angular distribution, while at high energies they are forward peaked.

At sampling time the angle θ is generated according to uniform distribution. The resulting value of the distribution at that angle and at that incident energy is compared with a second random number r_2 times the square of the atomic number of the element that is the maximum value that the Rayleigh effect can reach.

If the value of the distribution is smaller than $Z^2 \times r_2$ the procedure is repeated with other two random numbers, otherwise the value of the current angle is kept.

7.6 Status of the document

30.9.99 created by Alessandra Forti

7.7 Photo-electric effect

The total cross section at a given kinetic energy T is calculated as described in section 7.1.2.

The incident photon is absorbed and an electron of energy and direction equal to the incident photon's ones is emitted. The subshell from which the electron is emitted is randomly selected according to the cross sections of the subshells, determined at the energy T by interpolating the evaluated cross section data from the EPDL97 data library.

The interaction leaves the atom in an excited state, with excitation energy equal to the binding energy of the subshell from which the electron has been emitted.

The deexcitation of the atom proceeds via the emission of fluorescence photons. The transition probabilities from a subshell to lower energy ones are extracted from the EADL data library. Procedure adopted [11] assumes that the atom is initially in its neutral state. Transitions are selected with a random number and the corresponding transition energy is assigned to the photon emitted. Procedure is repeated until the last vacancy is filled and the atom is again in its neutral state. Last energy transition correspond to the binding energy of the subshell.

7.8 Status of the document

30.9.99 created by Alessandra Forti

7.9 Bremsstrahlung

The total cross section at a given electron kinetic energy T is calculated as described in section 7.1.2.

The energy spectra of the outcoming photons from the EEDL library are used to sample photon energies. The probability of the emission of a photon with kinetic energy t, considering an electron of incident kinetic energy T is generated according to:

$$Prob(T,t) = \frac{a(T)}{t} + b(T) \tag{7.8}$$

The energy distributions of the emitted photon available in the EEDL library for a few incident electron energies are fitted to determine the values of the a and b coefficients at the corresponding incident energy. In the fits the Pearson χ^2 was utilized.

The energy dependence of the a and b coefficients is then determined by a logarithmic interpolation for a and by a further fit for b.

The direction of the outcoming electron is the same as the direction of the incoming one.

The angular distribution of the emitted photons with respect to the incident electron is generated according to a simplified [8] formula based on Tsai cross section [12], which is expected to become isotropic in the low energy limit.

7.10 Status of the document

30.9.99 created by Alessandra Forti

7.11 Ionisation

The total cross section at a given incident kinetic energy T is calculated by summing the partial cross sections at such energy for all the subshells of an element. The partial subshell cross sections at incident energy T are obtained from an interpolation of the evaluated cross section data in the EEDL library, according to the formula 7.1.

The subshell from which the electron is emitted is randomly selected according to the cross sections of the subshells, determined at the energy T by interpolating the evaluated cross section data from the EEDL data library.

The probability of emission of an electron (δ ray) with kinetic energy t from a subshell of binding energy B_i as the result of the interaction of an incoming electron of kinetic energy T is described by:

$$Prob(T, t, B_i) = \sum_{j=2}^{7} \frac{a_j(T)}{(t + b_i)^j} \tag{7.9}$$

for $t < t_0$ and

$$Prob(T, t, B_i) = \frac{c(T)}{t^2} \tag{7.10}$$

for $t > t_0$, where t_0 is a parameter. Both formulas result from empirical fits to the EEDL data and are normalized to 1. The a, b and c coefficients are determined by fitting the data; their energy dependence is evaluated from a semilogarithmic interpolation of the fitted data.

The sampling of the final state proceeds through two steps: first the range of the energy ($t < t_0$ or $t > t_0$) is determined by a random number extraction, taking into account the relative area determined by the two functions 7.9 and 7.10, then the energy of the δ ray is generated according to the corresponding probability distribution.

The angle of emission of the scattered electron and of the δ ray is determined by energy-momentum conservation.

The interaction leaves the atom in an excited state, with excitation energy equal to the binding energy of the subshell from which the electron has been emitted. The deexcitation of the atom proceeds via the emission of fluorescence photons, as described in section 7.7.

7.12 Status of the document

30.9.99 created by Alessandra Forti

7.13 Ionisation (new fits)

The total cross section at a given incident kinetic energy T is calculated by summing the partial cross sections at such energy for all the subshells of an element. The partial subshell cross sections at incident energy T are obtained from an interpolation of the evaluated cross section data in the EEDL library, according to the formula 7.1.
The subshell from which the electron is emitted is randomly selected according to the cross sections of the subshells, determined at the energy T by interpolating the evaluated cross section data from the EEDL data library.
The probability of emission of an electron (δ ray) with kinetic energy t from a subshell of binding energy B_i as the result of the interaction of an incoming electron of kinetic energy T is obtained using from one up to three functions depending on the subshell data behaviour. Usually three functions are needed in few cases to better describe the peak of the spectrum that mainly conditions the sampling. Starting from this point of view subshells have been divided in three categories:

- subshells that need only one function: 71%
- subshells that need two functions: 28%
- subshells the nedd three functions: 0.5%

The three functions used are:

$$Prob(T,t,B_i) = \sum_{j=2}^{7} \frac{A_j(T)}{(t+B_i)^j} \tag{7.11}$$

for $t < t_1$

$$Prob(T,t) = C_1 \cdot t^{C_2} \tag{7.12}$$

for $t_1 < t < t_2$ and

$$Prob(T,t,B_i) = \sum_{j=2}^{5} \frac{D_j(T)}{(t+B_i)^j} \tag{7.13}$$

for $t_2 < t$ where t_1 and t_2 are parameters.
Function (7.11) appears in all the cases, function (7.12) only when three functions are needed and function (7.13) is used when two or three functions are needed. All the three formulas are empirical and result from fits to the EEDL data and they are normalized to 1. The A, C and D coefficients dependence on the incident energy T is evaluated from a semilogarithmic interpolation of the fits coefficient.
The sampling of the final state proceeds through two steps: first the function to be used (when there is more than one) is determined by a random number extraction, taking into account the relative area determined by the two functions 7.11, 7.12 and 7.13. When one of the three function is not needed

its area is automatically put to zero. The second step is to generate the energy of the δ ray according to the selected probability distribution.
The angle of emission of the scattered electron and of the δ ray is determined by energy-momentum conservation.
The interaction leaves the atom in an excited state, with excitation energy equal to the binding energy of the subshell from which the electron has been emitted. The deexcitation of the atom proceeds via the emission of fluorescence photons, as described in section 7.7.

7.14 Status of the document

30.9.99 created by Alessandra Forti

Bibliography

[1] http://reddog1.llnl.gov/homepage.red/photon.htm

[2] http://reddog1.llnl.gov/homepage.red/Electron.htm

[3] http://reddog1.llnl.gov/homepage.red/ATOMIC.htm

[4] http://reddog1.llnl.gov/homepage.red/DOCUMENT/EDPL97/epdl97.htm

[5] http://reddog1.llnl.gov/homepage.red/gowhere.htm

[6] Private communication, to be submitted for publication by J. Stepanek

[7] http://wwwinfo.cern.ch/asd/geant4/G4UsersDocuments/UsersGuides/PhysicsReferenceManual/html/index.html

[8] Geant3, CERN Program Library Long Writeup W5013

[9] P. P. Kane et al. Phys. Rep. (Review Section of Phys Lett.) 140, N 2 (1986) 75

[10] D. E. Cullen Nucl. Instr. Meth. Phys Res. B 101 (1995) 499

[11] J. Stepanek Comp. Phys. Comm. 1206, (1997)

[12] Y.S. Tsai, Rev. Mod. Phys. 46 (1974) 815 and Rev. Mod. Phys. 49 (1977) 421

[13] Y. Kim and M.E. Rudd, Phys. Rev. 50 (1994) 3954

[14] EGS4 W.R. Nelson et al. The EGS4 Code System. SLAC-Report-265 , December 1985

Chapter 8

Electromagnetic Interactions: Muon incident

8.1 Ionisation

The class G4MuIonisation calculates the continuous energy loss due to ionisation and simulates the 'discrete' part of the ionisation , the delta ray production or knock-on electron production by muons . The formulae used here are essentially the same than those in GEANT3 ([GEANT3]).

8.1.1 Method

In `GEANT4`, δ-rays are generated generally only above a threshold energy T_{cut} which value is calculated from the parameter *cut in range* for all charged particles. The total cross-section for the production of a δ-ray electron of kinetic energy $T > T_{cut} =$ by a particle of kinetic energy E is:

$$\sigma(E, T_{cut}) = \int_{T_{cut}}^{T_{max}} \frac{d\sigma(E,T)}{dT} dT \tag{8.1}$$

where T_{max} is the maximum energy transferable to the free electron:

$$T_{max} = \frac{2m(\gamma^2 - 1)}{1 + 2\gamma\frac{m}{M} + (\frac{m}{M})^2} \tag{8.2}$$

The energy lost in ionising collisions producing δ-rays below T_{cut} are included in the continuous energy loss. The mean value of the energy lost due to these *soft* collisions is:

$$E_{loss}(E, T_{cut}) = \int_0^{T_{cut}} T \frac{d\sigma(E,T)}{dT} dT \tag{8.3}$$

where m is the electron mass and M is the mass of the muon.

8.1.2 Continuous energy loss

The integration of (8.4) leads to the Bethe-Bloch stopping power or to the restricted energy loss formula [PDGB88]:

$$\left(\frac{dE}{dx}\right) = \begin{cases} N_{el}\frac{Z_{inc}^2}{\beta^2}\left[\ln\left(\frac{2m_e\beta^2\gamma^2 T_{max}}{I^2}\right) - 2\beta^2 - \delta - \frac{2C_e}{Z}\right] & \text{if} \quad T_{cut} \geq T_{max} \\ N_{el}\frac{Z_{inc}^2}{\beta^2}\left[\ln\left(\frac{2m_e\beta^2\gamma^2 T_c}{I^2}\right) - \beta^2\left(1 + \frac{T_c}{T_{max}}\right) - \delta - \frac{2C_e}{Z}\right] & \text{if} \quad T_{cut} < T_{max} \end{cases} \tag{8.4}$$

where, N_{el} is the electron density in the medium , $T_c = \min(T_{cut}, T_{max})$, m_e the electron mass and I is the average ionisation potential . There exists a variety of phenomenological approximations for this. At present the simple expression $I = 16\ Z^{0.9}$ eV is used for all the elements.

δ is a correction term which takes account of the reduction in energy loss due to the so-called density effect. This becomes important at high

energy because media have a tendency to become polarised as the incident particle velocity increases. As a consequence, the atoms in a medium can no longer be considered as isolated. To correct for this effect the formulation of Sternheimer [Ster71] is used:

$$\delta = \begin{cases} 0 & \text{if} \quad X < X_0 \\ 4.606X + C + a(X_1 - X)^m & \text{if} \quad X_0 \leq X < X_1 \\ 4.606X + C & \text{if} \quad X \geq X_1 \end{cases} \tag{8.5}$$

where the medium-dependent constants are calculated as follows:

$$\begin{array}{lcllcl} X & = & \log_{10}(\gamma\beta) = \ln(\gamma^2\beta^2)/4.606 & \nu_p & = & \sqrt{\frac{N_{el}e^2}{\pi m}} \ \text{s}^{-1} \ \text{plasma frequency} \\ N_{el} & = & \text{electron density in the material} & C & = & -2\ln\left(\frac{I}{h\nu_p}\right) - 1 \\ a & = & \frac{4.606(X_a - X_0)}{(X_1 - X_0)^m} & 4.606\ X_a & = & -C \end{array}$$

For condensed media we have:

$$I < 100 \text{ eV} \quad \begin{cases} X_0 = \begin{cases} 0.2 & \text{if} \quad -C \leq 3.681 \\ -0.326C - 1.0 & \text{if} \quad -C > 3.681 \end{cases} \\ X_1 = 2.0 \\ m = 3.0 \end{cases}$$

$$I \geq 100 \text{ eV} \quad \begin{cases} X_0 = \begin{cases} 0.2 & \text{if} \quad -C \leq 5.215 \\ -0.326C - 1.5 & \text{if} \quad -C > 5.215 \end{cases} \\ X_1 = 3.0 \\ m = 3.0 \end{cases}$$

and in the case of gaseous media $m = 3$ and:

$$\begin{array}{llllll} X_0 = 1.6 & X_1 = 4 & \text{for} & & C & \leq 9.5 \\ X_0 = 1.7 & X_1 = 4 & \text{for} & 9.5 < & C & \leq 10 \\ X_0 = 1.8 & X_1 = 4 & \text{for} & 10 < & C & \leq 10.5 \\ X_0 = 1.9 & X_1 = 4 & \text{for} & 10.5 < & C & \leq 11 \\ X_0 = 2. & X_1 = 4 & \text{for} & 11 < & C & \leq 12.25 \\ X_0 = 2. & X_1 = 5 & \text{for} & 12.25 < & C & \leq 13.804 \\ X_0 = 0.326C - 2.5 & X_1 = 5 & \text{for} & 13.804 < & C & \end{array}$$

C_e/Z is a so-called *shell correction term* which accounts for the fact that, at low energies for light elements and at all energies for heavy ones, the probability of collision with the electrons of the inner atomic shells (K, L, etc.) is negligible. The semi-empirical formula used in `GEANT4`, applicable to all materials, is due to Barkas [Bark62]:

$$\begin{array}{rcl} C_e(I,\eta) & = & (0.42237\eta^{-2} + 0.0304\eta^{-4} - 0.00038\eta^{-6})10^{-6}I^2 \\ & + & (3.858\eta^{-2} - 0.1668\eta^{-4} + 0.00158\eta^{-6})10^{-9}I^3 \\ \eta & = & \gamma\beta \end{array}$$

This formula breaks down at low energies, and it only applies for values of $\eta > 0.13$ (i.e. $T > 0.9$ MeV for a muon). For $\eta \leq 0.13$ the shell correction term is calculated as:

$$C_e(I,\eta)\Big|_{\eta\leq 0.13} = C_e(I,\eta=0.13)\frac{\ln\left(\frac{T}{T_{2l}}\right)}{\ln\left(\frac{7.9\ 10^{-3}\ \mathrm{GeV}}{T_{2l}}\right)}$$

i.e. the correction is *switched off* logarithmically from $T = 0.9$ MeV to $T = T_{2l} = 0.225$ MeV, the latter value is the limit between the use of the Bethe-Bloch formula and the low energy parametrisation .

The mean energy loss can be described by the Bethe-Bloch formula (8.4) only if the projectile velocity is larger than that of orbital electrons. In the low-energy region where this is not verified, a different kind of parameterisation should be used. Presently a simple phenomenological parametrisation has been chosen which gives the energy loss as a function of the variable $\tau = \frac{T}{M}$. The parametrisation is given by the expression

$$\frac{dE}{dx} = N_{el}\cdot(A\sqrt{\tau} + B\tau) \quad \text{for} \quad \tau \leq \tau_0 \tag{8.6}$$

$$\frac{dE}{dx} = N_{el}\cdot\frac{C}{\sqrt{\tau}} \quad \text{for} \quad \tau_0 < \tau \leq \tau_1 \tag{8.7}$$

,the values of the A, B, C and τ_0, τ_1 parameters are the same than in the case of charged hadrons .This parametrisation is used for $T < \tau_1 \cdot M$ and the Bethe-Bloch formula is used above this kinetic energy .

The energy lost due to the soft δ-rays is tabulated during initialisation as a function of the medium and of the energy .

Total cross-section

The integration of formula (8.1) gives the total cross-section :

$$\sigma(Z,E,T_{cut}) = 2\pi r_0^2 m\frac{Z}{\beta^2}\left(\frac{1-Y+\beta^2 Y\ln Y}{T_{cut}} + \frac{T_{max}-T_{cut}}{2E^2}\right) \tag{8.8}$$

, where $Y = \frac{T_{cut}}{T_{max}}$.

The mean free path is tabulated during initialisation as a function of the medium and of the energy .

8.1.3 Simulation of the knock-on electrons

Differential cross-section

The differential cross-section can be written as:

$$\frac{d\sigma}{dT} = 2\pi Z r_0^2 m \frac{1}{\beta^2}\frac{1}{T^2}\left[1 - \beta^2\frac{T}{T_{max}} + \frac{T^2}{2E^2}\right] \tag{8.9}$$

where T_{max} is the maximum energy transferable to the free electron (8.3) and T_{cut} the energy threshold for the δ-ray emission: $T_{cut} \leq T \leq T_{max}$

Sampling

Apart from the normalisation, the cross-section can be written as

$$\begin{aligned} f(T) &= \left(\frac{1}{T_{cut}} - \frac{1}{T_{max}}\right)\frac{1}{T} \\ g(T) &= 1 - \beta^2\frac{T}{T_{max}} + \frac{T^2}{2E^2} \end{aligned}$$

The variable ϵ is sampled by:

1. sample ϵ from $f(\epsilon)$
2. calculate the rejection function $g(\epsilon)$ and accept the sampled ϵ with a probability of $g(\epsilon)$.

After the successful sampling of ϵ, the polar angles of the scattered electron are generated with respect to the direction of the incident particle. The azimuthal angle ϕ is generated isotropically; the polar angle θ is calculated from the energy momentum conservation. This information is used to calculate the energy and momentum of both scattered particles and to transform them into the global coordinate system.

8.1.4 Status of this document

9.10.98 created by L. Urbán.
5.12.98 editing by J.P. Wellisch.

Bibliography

[GEANT3] GEANT3 manual ,CERN Program Library Long Writeup W5013 (October 1994).

[Mess70] H.Messel and D.F.Crawford. Pergamon Press,Oxford,1970.

[Ster71] R.M.Sternheimer. Phys.Rev. B3 (1971) 3681.

[PDGB88] Particle Data Group . Rev. of Particle Properties. Eur. Phys. J. C 3. (1988) 1.

[Bark62] W. H. Barkas. Technical Report 10292,UCRL, August 1962.

[Serr67] C.R.Serre. Techical Report 67 5 , CERN, March 1967.

[Serr71] C.R.Serre. Techical Report 71 18, CERN, September 1971.

8.2 Bremstrahlung

Bremsstrahlung dominates other muon interaction processes in the region of catastrophic collisions ($v \geq 0.1$); at "moderate" muon energies - above knock–on electron production kinematic limit. At high energies ($E \geq 1$ TeV) this process contributes about 40% to average muon energy loss.

8.2.1 Differential cross section

The differential cross section for muon bremsstrahlung (in units $cm^2/(g\,GeV)$) can be written as :

$$\begin{aligned} \frac{d\sigma(E,\epsilon,Z,A)}{d\epsilon} &= \frac{16}{3}\alpha N_A(\frac{m}{\mu}r_e)^2\frac{1}{\epsilon A}Z(Z\Phi_n+\Phi_e)(1-v+\frac{3}{4}v^2) \quad (8.10)\\ \frac{d\sigma(E,\epsilon,Z,A)}{d\epsilon} &= 0 \quad if \quad \epsilon \geq \epsilon_{max} = E-\mu \end{aligned}$$

where μ and m are muon and electron masses, Z and A are atomic number and atomic weight of the material and N_A is Avogadro's number. If we indicate with E and T the initial total and kinetic energy of muon and with ϵ the emitted photon energy we have: $\epsilon = E - E'$ and relative energy transfer $v = \epsilon/E$.

Functions Φ_n and Φ_e represent contribution of nucleus and electrons and can be expressed as :

$$\begin{aligned} \Phi_n &= \ln\frac{BZ^{-1/3}(\mu+\delta(D'_n\sqrt{e}-2))}{D'_n(m+\delta\sqrt{e}BZ^{-1/3})};\\ &= 0 \quad if \quad negative; \end{aligned}$$

$$\begin{aligned} \Phi_e &= \ln\frac{B'Z^{-2/3}\mu}{(1+\frac{\delta\mu}{m^2\sqrt{e}})(m+\delta\sqrt{e}B'Z^{-2/3})}\\ &= 0 \quad if \quad \epsilon \geq \epsilon'_{max} = E/(1+\mu^2/2mE)\\ &= 0 \quad if \quad negative \end{aligned}$$

$$\begin{aligned} \delta &= \mu^2\epsilon/2EE' = \mu^2 v/2(E-\epsilon)\\ D'_n &= D_n^{(1-1/Z)}, \quad D_n = 1.54A^{0.27}\\ B &= 183, \quad B' = 1429, \quad \sqrt{e} = 1.648(721271). \end{aligned}$$

Special case for hydrogen (Z=1): $B = 202.4,\ B' = 446,\ D'_n = D_n$.

Formulae are mostly taken from ([Keln95]) and ([Keln97]). They include improved in comparison with ([Petr68])(in the region $v \sim 1$ and low Z)

correction for nuclear size. Bremsstrahlung on atomic electrons (taking into account target recoil and atomic binding) is introduced instead of a rough substitution $Z(Z+1)$. Also ([Andr94]) correction for processes with nucleus excitation is included.

8.2.2 Aplicability and restrictions of the method

1. $E \gg \mu$, ultrarelativistic approximation is used in the formulas;
2. $E \leq 10^{20}$ eV, above LPM cross section suppression can be expected;
3. $v \geq 10^{-6}$; below , Ter-Mikaelyan suppression can be expected. However, in the latter region the cross section of muon bremsstrahlung is several orders of magnitude less than for other processes.
4. Coulomb corrections is not included. However existing calculations [Andr96] show that it is small for muon bremsstrahlung.

8.2.3 Continuous energy loss

The restricted energy loss for muon bremsstrahlung $(dE/dx)_{rest}$ with relative transfers $v = \epsilon/(T+\mu) \leq v_{cut}$ can be calculated as follows :

$$\frac{dE}{dx} = \int_0^{\epsilon_{cut}} \epsilon\sigma(E,\epsilon)\, d\epsilon = (T+\mu)\int_0^{v_{cut}} v\sigma(E,v)\, dv$$

If user's cut $v_{cut} \geq v_{max} = T/(T+\mu)$, total average energy loss is calculated. Integration is done on the basis of Gaussian quadratures, binnig provides the accuracy better than about 0.03% for $T = 1$ GeV, $Z = 1$ (rapidly improving with increasing T and Z).

8.2.4 Total cross section

The integration of differential cross section (1) over $d\epsilon$ gives the total cross section for muon bremsstrahlung:

$$\sigma_{tot}(E,\epsilon_{cut}) = \int_{\epsilon_{cut}}^{\epsilon_{max}} \sigma(E,\epsilon)\, d\epsilon = \int_{\ln v_{cut}}^{\ln v_{max}} v\sigma(E,v)\, d(\ln v)\,, \qquad (8.11)$$

where $v_{max} = T/(T+\mu)$. If $v_{cut} \geq v_{max}$, $\sigma_{tot} = 0$.

8.2.5 Sampling

Random photon energy ϵ_p is found from the numerical solution of the equation :

$$P = \int_{\epsilon_p}^{\epsilon_{max}} \sigma(E,\epsilon,Z,A)\, d\epsilon \,/\, \int_{\epsilon_{cut.}}^{\epsilon_{max}} \sigma(E,\epsilon,Z,A)\, d\epsilon.$$

Here P is random uniform probability, $\epsilon_{max} = T$, $\epsilon_{cut} = (T+\mu)\cdot v_{cut}$; $v_{min.cut} = 10^{-5}$ being a minimal relative transfer adopted in the algorithm.

For fast sampling, solution of (2) is tabulated at initialization for a set of Z, T, P. In simulation, sampling subroutine returns random ϵ_p corresponding to probability P, interpolation in the table being used.

Tabulation routine (which works at initialization step) uses function (1) for differential cross section. The table contains the values :

$$x_p = \ln(v_p/v_{max})/\ln(v_{max}/v_{cut}), \tag{8.12}$$

where $v_p = \epsilon_p/(T+\mu)$, $v_{max} = T/(T+\mu)$. Tabulation is performed in the range $Z = 1 \div 128$, $T = 1 \div 10^6\ GeV$, $P = 10^{-5} \div 1$ with constant step in logarithmic scale.

Atomic weight (which is the necessary parameters in (1)) is estimated here with iterative solution of the known approximate relation:

$$A = Z(2 + 0.015A^{2/3});$$

for $Z = 1$, $A = 1$ is used. To find x_p (and, respectively, ϵ_p) corresponding to a given probability P, in sampling subroutine the linear interpolation in $\ln Z, \ln T$, and cubic (4 points Lagrange) interpolation in $\ln P$ is realised. For $P \leq P_{min}$, linear interpolation in (P, x) - coordinates is used; noticeably, $x = 0$ at $P = 0$. Then, random energy ϵ_p is obtained from the inverse transformation of (3) :

$$\epsilon_p = (T+\mu)v_{max}(v_{max}/v_{cut})^{x_p}$$

The algorithm with the parameters described above has been tested for various Z and T. It provides the reproduction of the differential cross section with about 0.2 - 0.7 % accuracy for $T \geq 10$ GeV, the average total energy loss being kept within 0.3%. Accuracy improves with the increase of T, satisfactory results are obtained also for $1 \leq T \leq 10$ GeV.

It is important to note that this sampling scheme allows to generate ϵ_p for different user's cuts on v greater than $v_{min.cut}$. To realize such simulation, it is sufficient to re-define probability variable :

$$P' = P\ \sigma_{tot}\ (v_{user.cut})/\sigma_{tot}(v_{min.cut})$$

and just use P' in sampling subroutine. Thus, time consuming re-calculation of 3-dimensional table is not required (only tabulation of $\sigma_{tot}(v_{user.cut})$ is needed).

After the successful sampling of ϵ, the direction of the emitted photon is generated with respect to the direction of the incident particle. The azimuthal angle ϕ is generated isotropically; the polar angle θ is calculated from the energy momentum conservation. This information is used to calculate the energy and momentum of both scattered particles and to transform them into the *global* coordinate system.

8.2.6 Status of this document

9.10.98 created by R.Kokoulin and A.Rybin .
27/04/99 edited by L. Urban L. Urban

Bibliography

[Keln95] S.R.Kelner, R.P.Kokoulin, A.A.Petrukhin. Preprint MEPhI 024-95, Moscow, 1995.

[Keln97] S.R.Kelner, R.P.Kokoulin, A.A.Petrukhin. Phys. Atomic Nuclei, 60(1997)576.

[Petr68] A.A.Petrukhin, V.V.Shestakov. Canad.J.Phys., 46(1968)S377.

[Andr94] Yu.M.Andreyev, L.B.Bezrukov, E.V.Bugaev. Phys. Atomic Nuclei, 57(1994)2066.

[Andr96] Yu.M.Andreyev, E.V.Bugaev, 1996. Submitted to Phys.Rev.D.

8.3 Muon photonuclear interaction

8.3.1 Inelastic interaction of muons with nuclei

The process is important for high muon energies $E(E \geq 10\,GeV)$, at relatively high energy transfers ν ($\nu/E \geq 10^{-2}$), in particular, in light materials, from view–point of the detector response for high energy muons, muon propagation and muon–induced hadronic background. Average energy loss for this process is almost lineary increasing with energy, and at TeV muon energies constituets about 10% in standard rock.

The main contribution to the cross section $\sigma(E,\nu)$ and energy loss is given by low Q^2–region ($Q^2 \ll 1\ GeV^2$). In this domain, many simplifications can be done in theoretical consideration of the process to obtain convenient and simple formulae for the cross section.

Most widely used are the expressions given by Borog and Petrukhin (1975) [BOR75] and Bezrukov and Bugaev [BEZ81]. Results of these authors agree within 10% for differential cross sections and within about 5% for the average energy loss (if the same photonuclear cross section $\sigma_{\gamma N}$ is used in calculations).

Differential cross section

Borog and Petrukhin formula for the cross section is based on Hand's formalism [HAND63] for inelastic muon scattering, semi–phenomenological inelastic formfactor (VDM with parameters estimated from experimental data), and includes also nuclear shadowing effect with a reasonable theoretical parameterisation [BROD72].

For E $\geq$ 10 GeV, Borog and Petrukhin give for differential cross section $(cm^2/g\,GeV)$

$$\sigma(E,\nu) = \Psi(\nu)\cdot\Phi(E,v) \tag{1}$$

$$\Psi(\nu) \;=\; \frac{\alpha}{\pi}\cdot\frac{A_{eff}\cdot N_{AV}}{A}\cdot\sigma_{\gamma N}(\nu)\cdot\frac{1}{\nu} \tag{2}$$

$$\Phi(\ E,v\ ) = v - 1 + [1 - v + \frac{v^2}{2}\cdot(1+\frac{2\mu^2}{\Lambda^2})]\cdot ln\frac{\frac{E^2(1-v)}{\mu^2}[1+\frac{\mu^2 v^2}{\Lambda^2(1-v)}]}{1+\frac{Ev}{\Lambda}[1+\frac{\Lambda}{2M}+\frac{Ev}{\Lambda}]} \tag{3}$$

where :
ν – energy lost by muon,
$v = \nu$/E,
ν, M – muon and nucleon (proton) masses,
Λ – a VDM parameter in inelastic formfactor estimated as $\Lambda^2 = 0.4\,GeV^2$.

For A_{eff}, taking into account the nuclear shadowing effect, we will keep Borog and Petrukhin choice, namely Brodsky e.a. parameterization

[BROD72]:

$$A_{eff} = 0.22 \cdot A + 0.78 \cdot A^{0.89}.$$

For $\sigma_{\gamma N}$ it seems reasonable to take a more accurate parameterization given by Caldwell e.a. [CALD79] on the basis of experimental data on photoproduction by real photons : $\sigma_{\gamma N} = \left(49.2 + 11.1 ln K \cdot 151.8/\sqrt{K}\right) \cdot 10^{-30} cm^2$, K in GeV.

Upper transferred energy limit $\nu_{max} = E - M/2$; the choice of ν_{min} is a more generic since the formula itself is not valid in this domain; $\nu_{min} =$ 0.2 GeV seems reasonable. Fortunatly, ν_{min} only logarithmically influences the total cross section and practically does not affect average energy loss for high energy muons.

In Eq.2, $A_{eff} \cdot \sigma_{\gamma N}$ are factorized. A more rigorous theoretical consideration may lead to some dependence of the shadowing effect on (ν, E); therefore in differential cross sections routine and in sampling procedure is better to foresee such a possibility and to keep atomic weight of the element A as an evident parameter.

The total cross section is obtained by integration of (1) between ν_{min} and ν_{max}; to facilitate the computation, $\ln(\nu)$– substitution is useful.

8.3.2 Sampling

Sampling of transferred energy

Random transferred energy ν_p is found from the numerical solution of the equation :

$$P = \int_{\nu_p}^{\nu_{max}} \sigma(E,\nu)\, d\nu \;/\; \int_{\nu_{min}}^{\nu_{max}} \sigma(E,\nu)\, d\nu. \qquad (4)$$

Here P is random uniform probability, $\nu_{max} = E - M/2$, $\nu_{min} = 0.2\, GeV$.

For fast sampling, solution of (4) is tabulated at initialization stage. In simulation, sampling routine returns random ν_p corresponding to probability P, interpolation in the table being used.

Tabulation routine uses function (1) for differential cross section. The table contains the values :

$$x_p = \ln(\nu_p/\nu_{max})/\ln(\nu_{max}/\nu_{min}). \qquad (5)$$

Tabulation is made with a constant step in $\ln(T), \ln(A), \ln(P)$. In sampling, linear interpolations in $\ln(T)$ and $\ln(A)$ and cubic interpolation in $\ln(P)$ are used. After that, transferred energy is calculated as inverse transformation of (5) : $\nu_p = \nu_{max}(\nu_{max}/\nu_{min})^{x_p}$. Tabulation parameters provide the accuracy of the reproduction of the theoretical dependence better than 2 % for $T > 1$ GeV and better than 1% for $T > 10$ GeV.

Sampling of muon scattering angle

According to consideration [BOR75], [BOR77], in the region of not very large transferred four momentum ($Q^2 \leq 3\ GeV^2$), t – dependence of the cross section may be described as:

$$\frac{d\sigma}{dt} \sim \frac{(1 - t/t_{max})}{t(1 + t/\nu^2)(1 + t/m_0^2)}[(1 - y)(1 - t_{min}/t) + y^2/2], \tag{6}$$

where
$t \equiv Q^2 = 2(EE' - PP'cos\theta - \mu^2)$;
$t_{min} = (\mu y)^2/(1 - y);\ y = \nu/E$;
$t_{max} = 2M\nu$;
$\nu = E - E'$ is the energy lost by muon;
E is the total initial muon energy ;
M – nucleon (proton) mass.
$m_0^2 \equiv \Lambda^2 \simeq 0.4\ GeV^2$ is a phenomenological parameter determing the inelastic formfactor behaviour.
Factors which do not depend (or slowly depend) on t are omitted.

To simulate random t (and hence the random muon deflection angle), it is covenient to represent Eq.6 in the form :

$$\sigma(t) \sim f(t)\, g(t); \tag{7}$$

$$f(t) = \frac{1}{t(1 + \frac{t}{t_1})}; \tag{8}$$

$$g(t) = \frac{(1 - t/t_{max})}{(1 + t/t_2)} \frac{[(1 - y)(1 - t_{min}/t) + y^2/2]}{[(1 - y) + y^2/2]};$$

$$t_1 = min(\nu^2, m_0^2); t_2 = max(\nu^2, m_0^2). \tag{9}$$

Random t_P is found analytically from Eq.8 :

$$t_P = \frac{t_{max} t_1}{(t_{max} + t_1)[\frac{t_{max}(t_{min} + t_1)}{t_{min}(t_{max} + t_1)}]^P - t_{max}},$$

where P is random uniform number between 0 and 1, and then is accepted with probability $g(t)$. Conditions (9) make use of a symmetry between ν^2 and m_0^2 in Eq.(6) and allow to increase selection efficiency, which is typically ≥ 0.7 . Polar muon deflection angle θ can be easily found from [1]

$$sin^2(\theta/2) = \frac{t_P - t_{min}}{4(EE' - \mu^2) - 2t_{min}}.$$

[1] This convenient formula has been shown to authors by D.A.Timashkov.

Bibliography

[BOR75] V.V. Borog and A.A. Petrukhin, Proc. 14th Int.Conf. on Cosmic Rays, Munich,1975, **vol.6**, p.1949.

[BOR77] V.V Borog, V.G. Kirillov–Ugryumov, A.A. Petrukhin, Sov. J. Nucl. Phys., **25**, 1977, p.46.

[BEZ81] L.B. Bezrukov and E.V. Bugaev, Sov. J. Nucl. Phys., **33**, 1981, p.635.

[BROD72] S.J. Brodsky, F.E. Close, J.F. Gunion, Phys.Rev.,**D6**, 1972, p.177.

[CALD79] D.O. Caldwell e.a., Phys.Rev.Lett.,**42**, 1979, p.553.

[HAND63] L.N.Hand.Phys.Rev.,**129**(1963)1834.

8.4 e^+e^- pair production by muons

8.4.1 Direct electron pair production by muons

Electron pair production is one of the most important processes of muon interaction. At TeV muon energies, pair production cross section exceeds those of other muon interaction processes in a wide region of energy transfers 100 MeV $\leq \epsilon \leq 0.1 \cdot E_\mu$. Average energy loss for pair production increases linearly with muon energy, and in TeV region this process contributes over 50 % to the total energy loss rate. Main contribution to the total cross section is given by transfered energies 5 MeV $\leq \epsilon \leq 0.01 \cdot E_\mu$.

The contribution of various values of relative energy transfers to average muon energy loss is determined mostly by region $10^{-3} \cdot E_\mu \leq \epsilon \leq 0.1 \cdot E_\mu$. Thus, to adequatly describe the number of pairs produced, average energy loss and stohastic energy loss distribution we need to reproduce with a sufficient accuracy the differential cross section behaviour in a wide range of energy transfers 5 MeV $\leq \epsilon \leq 0.1 \cdot E_\mu$.

For theoretical description of the cross section, we use formulae given by [KOKO69] with a correction for finite nuclear size [KOKO71]. To take into account electron pair production in a field of atoimic electrons (inelastic atomic formfactor contribution), results obtained in [KELN97] are used.

8.4.2 Differential cross section

Definitions :
- m and μ – electron and muon masses.
- $E \equiv E_\mu$ – total muon energy; $E = T + \mu$.
- Z, A – atomic number and weight of material.
- ϵ – total pair energy or $\approx$ muon energy loss $(E - E')$.
- $v = \epsilon/E$.
- e = 2.718....
- $A^\star = 183$.

Applicability and restrictions of the method:
- $E_\mu \gg \mu$, that means $E \geq 2$ – 5 GeV.
- $E_\mu \leq 10^{14}$ – 10^{16} eV, if $E \geq 10^{14}$– 10^{16} eV (depending on the material), LPM effect may appear important.
- $\epsilon_{min} = 4{\cdot}$m , (formally, in fact, $\epsilon \gg 2{\cdot}$m).
- $\epsilon_{max} = E_\mu - \frac{3\sqrt{e}}{4}\ \mu\ Z^{1/3}$ (also formally, in fact $E'_\mu \gg \mu$).
- $Z \leq 30$ – 40. For higher Z Coulomb correction is important (not sufficiently studied theoretically at the moment).

The differential cross section for electron pair production by muons $\sigma(Z, A, E, \epsilon)$ can be written as :

$$\sigma(Z, A, E, \epsilon) = \frac{4}{3\pi} \cdot \frac{Z(Z+\zeta)}{A} \cdot N_A(\alpha r_0)^2 \cdot \frac{1-v}{\epsilon} \int_0^{\rho_{max}} G(Z, E, v, \rho)\ d\rho \quad (1)$$

$$G(Z, E, v, \rho) \ = \ \Phi_e + (m/\mu)^2 \cdot \Phi_\mu$$

In principle, there is a possibility that in a futher theoretical refinement the function G will also depend on A.

$$\Phi_{e,\mu} \ = \ B_{e,\mu} \cdot L'_{e,\mu};$$
$$\Phi_{e,\mu} \ = \ 0\, if negative;$$

$$B_e \ = \ [(2+\rho^2)(1+\beta) + \xi(3+\rho^2)] ln(1+\frac{1}{\xi}) + \frac{1-\rho^2-\beta}{1+\xi} - (3+\rho^2);$$

$$B_e \ \approx \ \frac{1}{2\xi}[(3-\rho^2) + 2\beta(1+\rho^2)] \ \ for\ \xi \geq \ 10^3;$$

$$B_\mu \ = \ [(1+\rho^2)(1+\frac{3\beta}{2}) - \frac{1}{\xi}(1+2\beta)(1-\rho^2)] ln(1+\xi) + \frac{\xi(1-\rho^2-\beta)}{1+\xi} + (1+2\beta)(1-\rho^2);$$

$$B_\mu \ \approx \ \frac{\xi}{2}[(5-\rho^2) + \beta(3+\rho^2)] \ \ for\ \xi \ \leq \ 10^{-3};$$

$B_{e,\mu}$ do not depend on Z, A.

$$\xi \;=\; \frac{\mu^2 v^2}{4m^2}\frac{(1-\rho^2)}{(1-v)}; \quad \beta \;=\; \frac{v^2}{2(1-v)};$$

$$L'_e \;=\; ln\frac{A^* Z^{-1/3}\sqrt{(1+\xi)(1+Y_e)}}{1+\frac{2m\sqrt{e}A^* Z^{-1/3}(1+\xi)(1+Y_e)}{Ev(1-\rho^2)}} \;-\; \frac{1}{2}ln[1+(\frac{3mZ^{1/3}}{2\mu})^2(1+\xi)(1+Y_e)];$$

$$L'_\mu \;=\; ln\frac{(\mu/m)A^* Z^{-1/3}\sqrt{(1+1/\xi)(1+Y_\mu)}}{1+\frac{2m\sqrt{e}A^* Z^{-1/3}(1+\xi)(1+Y_\mu)}{Ev(1-\rho^2)}} - ln[\frac{3}{2}Z^{1/3}\sqrt{(1+1/\xi)(1+Y_\mu)}].$$

For faster computing, expressions for $L'_{e,\mu}$ may be further algebraically transformed. Functions $L'_{e,\mu}$ include nuclear size correction ([KOKO71]) in comparison with parameterization ([KOKO69]).

$$Y_e \;=\; \frac{5-\rho^2+4\beta(1+\rho^2)}{2(1+3\beta)ln(3+\frac{1}{\xi})-\rho^2-2\beta(2-\rho^2)};$$

$$Y_\mu \;=\; \frac{4+\rho^2+3\beta(1+\rho^2)}{(1+\rho^2)(\frac{3}{2}+2\beta)ln(3+\xi)+1-\frac{3}{2}\rho^2}.$$

$Y_{e,\mu}$ – approximations ([KOKO69]); there is a possibility that they will be improved , as well as corrections (second terms) in $L_{e,\mu}$.

$$\rho_{max} \;=\; [1-6\mu^2/E^2(1-v)]\sqrt{1-4m/Ev}$$

Comment to calculation of integral $\int d\rho$ in Eq.1 :

It is much better to compute integral $\int_0^{\rho_{max}} G(Z,E,v,\rho)\; d\rho$ with the substitution :

$$\begin{gathered} \text{t} = \ln(1 - \rho), \\ 1 - \rho = \exp(\text{t}) \\ 1 + \rho = 2 - \exp(\text{t}) \\ 1 - \rho^2 = e^t(2 \;-\; e^t) \end{gathered}$$

After that ,

$$\int_0^{\rho_{max}} G(Z,E,v,\rho)\; d\rho \;=\; \int_{t_{min}}^{0} G(Z,E,v,\rho)e^t\; dt; \qquad (2)$$

$$t_{min} \;=\; ln\frac{\frac{4m}{\epsilon}+\frac{12\mu^2}{EE'}(1-\frac{4m}{\epsilon})}{1+(1-\frac{6\mu^2}{EE'})\sqrt{1-\frac{4m}{\epsilon}}}.$$

To compute integral (2) with accuracy better than 0.5%, Gaussian quadrature with number of points N = 8 is sufficient.

Function $\zeta(E,Z)$ serves to take into account the process on atomic electrons (inelastic atomic formfactor contribution). To keep correctly energy loss balance, the following approximation should be used (some algebraic transformation of ([KELN97])):

$$\zeta(E,Z) \;=\; \frac{0.073 ln\frac{E/\mu}{1+\gamma_1 Z^{2/3}\frac{E}{\mu}} \;- 0.26}{0.058 ln\frac{E/\mu}{1+\gamma_2 Z^{1/3}\frac{E}{\mu}} \;- 0.14};$$

$$\zeta(E,Z) \;=\; 0 \, if \; the \; nominator \; is \; negative.$$

For E $\leq$ 35μ, $\zeta(E,Z) \;=\; 0$.
$\gamma_1 \;=\; 1.95 \cdot 10^{-5}$; $\gamma_2 \;=\; 5.30 \cdot 10^{-5}$;
The above formulas make use of Thomas-Fermi model which is not sufficiently good for light elements. For hydrogen (Z = 1) we should change :
$A^* \;=\; 183 \;\Rightarrow\; 202.4$;
$\gamma_1 \;=\; 1.95 \cdot 10^{-5} \;\Rightarrow\; 4.4 \cdot 10^{-5}$;
$\gamma_2 \;=\; 5.30 \cdot 10^{-5} \;\Rightarrow\; 4.8 \cdot 10^{-5}$.

8.4.3 Sampling of e^+e^- pair production

Sampling of e^+e^- pair energy (when interaction occurs) is based on numerical solution of the equation for a given probability P :

$$P = \int_{\epsilon_P}^{\epsilon_{max}} \sigma(Z,A,T,\epsilon)d\epsilon \;/\; \int_{cut}^{\epsilon_{max}} \sigma(Z,A,T,\epsilon)d\epsilon, \qquad (3)$$

or

$$(1-P) = \int_{cut}^{\epsilon_P} \sigma(Z,A,T,\epsilon)d\epsilon \;/\; \int_{cut}^{\epsilon_{max}} \sigma(Z,A,T,\epsilon)d\epsilon. \qquad (4)$$

To reach high sampling speed, solutions of Eqs.3,4 are tabulated at initialization step: two 3-dimensional tables (Table A,B) of $\epsilon_P(P,T,Z)$ are created, and then interpolation is used to sample ϵ_P.

The knots of the tables are chosen in the following way.
1) Constant step in $\ln T$; 4 points per decade in the range T_{min} – T_{max} is to be sufficient.
2) Constant step in $\ln Z$. Dependence of the shape of of sampling distribution on Z is very weak(but exists !), and 8 points in the range $1 \leq Z \leq 128$ should be sufficient. There is practically no dependence on atomic weight A.
3) For probabilities $P \leq 0.5$, Eq.3 is used. The Table A is computed with a constant step in $\ln P$ in the range $10^{-7} \leq P \leq 0.5$. The number of points in the $\ln P$ for Table A is equal to about 100.

4) For $P \geq 0.5$, solutions of Eq.4 are tabulated with constant step in $\ln(1-P)$ in the range $(1-P) = 10^{-5} \div 0.5$; 50 points is enough. In both Table A and Table B the values of $\ln(\epsilon_P - cut)$ are stored.

To create the "probability tables", for every T, Z the following procedure is used:
1) A temporaly table (length $\sim$ 2000 elements) is constructed with a constant step (~ 0.02) in $\ln\epsilon$ in the range (cut, ϵ_{max}) of the values $\epsilon \cdot \sigma$(Z,A,T,ϵ), ϵ is taken in the middle of corresponding $\ln\epsilon$ – bin.
2) Accumulated cross sections

$$\sigma_1 = \int_{ln\epsilon}^{ln\epsilon_{max}} \epsilon \cdot \sigma(Z, A, T, \epsilon) \cdot d(ln\epsilon)$$

and

$$\sigma_2 = \int_{cut}^{ln\epsilon} \epsilon \cdot \sigma(Z, A, T, \epsilon) \cdot d(ln\epsilon)$$

are calculated by summation of this temporaly table (in two directions), and then normalized to obtain accumulated probability functions (A and B, respectively).
3) Finally, $\ln(\epsilon_P - cut)$ for corresponding knots in $\ln P$, $\ln(1-P)$ are calculated by linear interpolation of the above accumulated probabilities to form Tables A and B. Here, to speed up interpolation procedure, making use of the monotonous dependence of accumulated cross sections is of great help.

Random transferred energy is then found by linear interpolation in $\ln Z$, $\ln T$ and cubic interpolation in $\ln P$ or $\ln(1-P)$ for tables A and B, respectively, over 3–dimentional constant step tables. For $P \leq 10^{-7}$ and $(1-P) \leq 10^{-5}$, linear extrapolation with edge knots of the Tables may be safely used. Electron pair energy is related with the auxilary variable $x = \ln(\epsilon_P - cut)$ found by interpolation in a trivial way: $\epsilon_P = e^x + cut$.

Similar to muon bremsstrahlung (this manual), this sampling algorithm allows to not re–initialize the tables for any $user.cut > cut.min$. Instead, it is sufficient to re–define probability variable as

$$P' = P\sigma_{tot}(user.cut)/\sigma_{tot}(cut.min),$$

and to use P' in the sampling routine.

Bibliography

[KOKO69] R.P. Kokoulin and A.A. Petrukhin, Proc. 11th Intern.Conf. on Cosmic Rays, Budapest, 1969 [Acta Phys. Acad. Sci. Hung.,**29, Suppl.4**, p.277, 1970].

[KOKO71] R.P. Kokoulin and A.A. Petrukhin, Proc. 12th Int.Conf. on Cosmic Rays, Hobart, 1971, **vol.6**, p.2436.

[KELN97] S.R. Kelner, Phys.Atomic Nuclei, **61**(1998)448.

Chapter 9

Electromagnetic Interactions: Charged hadron incident

9.1 Ionisation

The class G4hIonisation calculates the continuous energy loss due to ionisation and simulates the 'discrete' part of the ionisation , the delta ray production by charged hadrons . The formulae used here are essentially the same than those in GEANT3 ([GEANT3]).

9.1.1 Method

In `GEANT4`, δ-rays are generated generally only above a threshold energy T_{cut} which value is calculated from the parameter *cut in range* for all charged particles. The total cross-section for the production of a δ-ray electron of kinetic energy $T > T_{cut} =$ by a particle of kinetic energy E is:

$$\sigma(E, T_{cut}) = \int_{T_{cut}}^{T_{max}} \frac{d\sigma(E,T)}{dT} dT \tag{9.1}$$

where T_{max} is the maximum energy transferable to the free electron:

$$T_{max} = \frac{2m(\gamma^2 - 1)}{1 + 2\gamma\frac{m}{M} + (\frac{m}{M})^2} \tag{9.2}$$

The energy lost in ionising collisions producing δ-rays below T_{cut} are included in the continuous energy loss. The mean value of the energy lost due to these *soft* collisions is:

$$E_{loss}(E, T_{cut}) = \int_0^{T_{cut}} T \frac{d\sigma(E,T)}{dT} dT \tag{9.3}$$

where m is the electron mass and M is the mass of the incident particle.

9.1.2 Continuous energy loss

The integration of (9.3) leads to the Bethe-Bloch stopping power or to the restricted energy loss formula [PDGB88]:

$$\left(\frac{dE}{dx}\right) = \begin{cases} N_{el}\frac{Z_{inc}^2}{\beta^2}\left[\ln\left(\frac{2m_e\beta^2\gamma^2 T_{max}}{I^2}\right) - 2\beta^2 - \delta - \frac{2C_e}{Z}\right] & \text{if} \quad T_{cut} \geq T_{max} \\ N_{el}\frac{Z_{inc}^2}{\beta^2}\left[\ln\left(\frac{2m_e\beta^2\gamma^2 T_c}{I^2}\right) - \beta^2\left(1 + \frac{T_c}{T_{max}}\right) - \delta - \frac{2C_e}{Z}\right] & \text{if} \quad T_{cut} < T_{max} \end{cases} \tag{9.4}$$

where, N_{el} is the electron density in the medium , $T_c = \min(T_{cut}, T_{max})$, m_e the electron mass and I is the average ionisation potential . There exists a variety of phenomenological approximations for this. At present the simple expression $I = 16\ Z^{0.9}$ eV is used for all the elements.

δ is a correction term which takes account of the reduction in energy loss due to the so-called density effect. This becomes important at high

energy because media have a tendency to become polarised as the incident particle velocity increases. As a consequence, the atoms in a medium can no longer be considered as isolated. To correct for this effect the formulation of Sternheimer [Ster71] is used:

$$\delta = \begin{cases} 0 & \text{if} \quad X < X_0 \\ 4.606X + C + a(X_1 - X)^m & \text{if} \quad X_0 \leq X < X_1 \\ 4.606X + C & \text{if} \quad X \geq X_1 \end{cases} \tag{9.5}$$

where the medium-dependent constants are calculated as follows:

$$\begin{array}{lcllcl} X & = & \log_{10}(\gamma\beta) = \ln(\gamma^2\beta^2)/4.606 & \nu_p & = & \sqrt{\frac{N_{el}e^2}{\pi m}} \ \text{s}^{-1} \ \text{plasma frequency} \\ N_{el} & = & \text{electron density in the material} & C & = & -2\ln\left(\frac{I}{h\nu_p}\right) - 1 \\ a & = & \frac{4.606(X_a - X_0)}{(X_1 - X_0)^m} & 4.606\ X_a & = & -C \end{array}$$

For condensed media we have:

$$I < 100 \text{ eV} \quad \begin{cases} X_0 = \begin{cases} 0.2 & \text{if} \quad -C \leq 3.681 \\ -0.326C - 1.0 & \text{if} \quad -C > 3.681 \end{cases} \\ X_1 = 2.0 \\ m = 3.0 \end{cases}$$

$$I \geq 100 \text{ eV} \quad \begin{cases} X_0 = \begin{cases} 0.2 & \text{if} \quad -C \leq 5.215 \\ -0.326C - 1.5 & \text{if} \quad -C > 5.215 \end{cases} \\ X_1 = 3.0 \\ m = 3.0 \end{cases}$$

and in the case of gaseous media $m = 3$ and:

$$\begin{array}{llllll} X_0 = 1.6 & X_1 = 4 & \text{for} & & C & \leq 9.5 \\ X_0 = 1.7 & X_1 = 4 & \text{for} & 9.5 < & C & \leq 10 \\ X_0 = 1.8 & X_1 = 4 & \text{for} & 10 < & C & \leq 10.5 \\ X_0 = 1.9 & X_1 = 4 & \text{for} & 10.5 < & C & \leq 11 \\ X_0 = 2. & X_1 = 4 & \text{for} & 11 < & C & \leq 12.25 \\ X_0 = 2. & X_1 = 5 & \text{for} & 12.25 < & C & \leq 13.804 \\ X_0 = 0.326C - 2.5 & X_1 = 5 & \text{for} & 13.804 < & C & \end{array}$$

C_e/Z is a so-called *shell correction term* which accounts for the fact that, at low energies for light elements and at all energies for heavy ones, the probability of collision with the electrons of the inner atomic shells (K, L, etc.) is negligible. The semi-empirical formula used in `GEANT4`, applicable to all materials, is due to Barkas [Bark62]:

$$\begin{array}{rcl} C_e(I,\eta) & = & (0.42237\eta^{-2} + 0.0304\eta^{-4} - 0.00038\eta^{-6})10^{-6}I^2 \\ & + & (3.858\eta^{-2} - 0.1668\eta^{-4} + 0.00158\eta^{-6})10^{-9}I^3 \\ \eta & = & \gamma\beta \end{array}$$

This formula breaks down at low energies, and it only applies for values of $\eta > 0.13$ (i.e. $T > 7.9$ MeV for a proton). For $\eta \leq 0.13$ the shell correction term is calculated as:

$$C_e(I,\eta)\Big|_{\eta\leq 0.13} = C_e(I,\eta=0.13)\frac{\ln\left(\frac{T}{T_{2l}}\right)}{\ln\left(\frac{7.9\,10^{-3}\,\mathrm{GeV}}{T_{2l}}\right)}$$

i.e. the correction is *switched off* logarithmically from $T = 7.9$ MeV to $T = T_{2l} = 2$ MeV.

The mean energy loss can be described by the Bethe-Bloch formula (9.4) only if the projectile velocity is larger than that of orbital electrons. In the low-energy region where this is not verified, a different kind of parameterisation should be used. Presently a simple phenomenological parametrisation has been chosen which gives the energy loss as a function of the variable $\tau = \frac{T}{M_{proton}}$. The parametrisation is given by the expression

$$\frac{dE}{dx} = N_{el}\cdot(A\sqrt{\tau} + B\tau) \quad \text{for} \quad \tau \leq \tau_0 \tag{9.6}$$

$$\frac{dE}{dx} = N_{el}\cdot\frac{C}{\sqrt{\tau}} \quad \text{for} \quad \tau_0 < \tau \leq \tau_1 \tag{9.7}$$

,the values of the A, B, C and τ_0, τ_1 parameters can be found in the code, here only the value of τ_1 is given: $\tau_1 = \frac{2\cdot MeV}{M_{proton}}$. The parameters A, B, C have been chosen in such a way that $\frac{dE}{dx}$ is a continuous function of the kinetic energy T at $T_0 = \tau_0 \cdot M_{proton}$ and $T_1 = \tau_1 \cdot M_{proton}$ (above T_1 the Bethe-Bloch formula is used).

The energy lost due to the soft δ-rays is tabulated during initialisation as a function of the medium and of the energy .

The energy loss of all charged hadrons is obtained from that of protons by calculating the kinetic energy of a proton with the same β, and using this value to interpolate the tables (see the description for the energy loss process):

$$T_{proton} = \frac{M_{\mathrm{p}}}{M}T \tag{9.8}$$

Total cross-section

The integration of formula (9.1) gives the total cross-section :

$$\sigma(Z,E,T_{cut}) = \begin{cases} 2\pi r_0^2 m\frac{Z}{\beta^2}\frac{1-Y+\beta^2 Y\ln Y}{T_{cut}} & \text{for spin-0 particles} \\ 2\pi r_0^2 m\frac{Z}{\beta^2}\left(\frac{1-Y+\beta^2 Y\ln Y}{T_{cut}} + \frac{T_{max}-T_{cut}}{2E^2}\right) & \text{for spin-}\frac{1}{2}\text{ particles} \end{cases} \tag{9.9}$$

, where $Y = \frac{T_{cut}}{T_{max}}$.

The mean free path is tabulated during initialisation as a function of the medium and of the energy for all the charged hadrons.

9.1.3 Simulation of the delta-ray production

Differential cross-section

For heavy charged particles the differential cross-section can be written:

$$\begin{aligned}
\frac{d\sigma}{dT} &= 2\pi Z r_0^2 m \frac{1}{\beta^2}\frac{1}{T^2}\left[1-\beta^2\frac{T}{T_{max}}\right] && \text{for spin 0 particle}\\
\frac{d\sigma}{dT} &= 2\pi Z r_0^2 m \frac{1}{\beta^2}\frac{1}{T^2}\left[1-\beta^2\frac{T}{T_{max}}+\frac{T^2}{2E^2}\right] && \text{for spin 1/2 particle}
\end{aligned}$$

where T_{max} is the maximum energy transferable to the free electron:

$$T_{max} = \frac{2m(\gamma^2-1)}{1+2\gamma(m/M)+(m/M)^2}$$

and T_{cut} the energy threshold for the δ-ray emission: $T_{cut} \le T \le T_{max}$

Sampling

Apart from the normalisation, the cross-section can be written as

$$\begin{aligned}
f(T) &= \left(\frac{1}{T_{cut}}-\frac{1}{T_{max}}\right)\frac{1}{T}\\
g(T) &= 1-\beta^2\frac{T}{T_{max}}+\frac{T^2}{2E^2} \quad \text{(last term for spin-}\tfrac{1}{2}\text{ particle only)}
\end{aligned}$$

The variable ϵ is sampled by:

1. sample ϵ from $f(\epsilon)$
2. calculate the rejection function $g(\epsilon)$ and accept the sampled ϵ with a probability of $g(\epsilon)$.

After the successful sampling of ϵ, the polar angles of the scattered electron are generated with respect to the direction of the incident particle. The azimuthal angle ϕ is generated isotropically; the polar angle θ is calculated from the energy momentum conservation. This information is used to calculate the energy and momentum of both scattered particles and to transform them into the global coordinate system.

9.1.4 Status of this document

9.10.98 created by L.Urbán.
5.12.98 editing by J.P. Wellisch.

Bibliography

[GEANT3] GEANT3 manual ,CERN Program Library Long Writeup W5013 (October 1994).

[Mess70] H.Messel and D.F.Crawford. Pergamon Press,Oxford,1970.

[Ster71] R.M.Sternheimer. Phys.Rev. B3 (1971) 3681.

[PDGB88] Particle Data Group . Rev. of Particle Properties. Eur. Phys. J. C 3. (1988) 1.

[Bark62] W. H. Barkas. Technical Report 10292,UCRL, August 1962.

[Serr67] C.R.Serre. Techical Report 67 5 , CERN, March 1967.

[Serr71] C.R.Serre. Techical Report 71 18, CERN, September 1971.

Chapter 10

Electromagnetic Interactions: Optical photon

10.1 Interactions of optical photons

Optical photons are produced when a charged particle traverses:

1. a dielectric material with velocity above the Čerenkov threshold;
2. a scintillating material.

10.1.1 Physics processes for optical photons

A photon is called optical when its wavelength is much greater than the typical atomic spacing, for instance when $\lambda \geq 10nm$ which corresponds to an energy $E \leq 100eV$. Production of an optical photon in a HEP detector is primarily due to:

1. Čerenkov effect;
2. Scintillation.

Optical photons undergo three kinds of interactions:

1. Elastic (Rayleigh) scattering;
2. Absorption;
3. Medium boundary interactions.

Rayleigh scattering

For optical photons Rayleigh scattering is usually unimportant. For $\lambda = .2\mu m$ we have $\sigma_{Rayleigh} \approx .2b$ for N_2 or O_2 which gives a mean free path of $\approx 1.7km$ in air and $\approx 1m$ in quartz. Two important exceptions are aerogel, which is used as a Čerenkov radiator for some special applications and large water Čerenkov detectors for neutrino detection.

The differential cross section in Rayleigh scattering, $d\sigma/d\Omega$, is proportional to $\cos^2\theta$, where θ is the polar angle of the new polarization with respect to the old polarization.

Absorption

Absorption is important for optical photons because it determines the lower λ limit in the window of transparency of the radiator. Absorption competes with photo-ionization in producing the signal in the detector, so it must be treated properly in the tracking of optical photons.

Medium boundary effects

When a photon arrives at the boundary of a dielectric medium, its behaviour depends on the nature of the two materials which join at that boundary:

- Case dielectric → dielectric.
  The photon can be transmitted (refracted ray) or reflected (reflected ray). In case where the photon can only be reflected, total internal reflection takes place.

- Case dielectric → metal.
  The photon can be absorbed by the metal or reflected back into the dielectric. If the photon is absorbed it can be detected according to the photoelectron efficiency of the metal.

- Case dielectric → black material.
  A black material is a tracking medium for which the user has not defined any optical property. In this case the photon is immediately absorbed undetected.

10.1.2 Photon polarization

The photon polarization is defined as a two component vector normal to the direction of the photon:

$$\begin{pmatrix} a_1 e^{i\Phi_1} \\ a_2 e^{i\Phi_2} \end{pmatrix} = e^{\Phi_o} \begin{pmatrix} a_1 e^{i\Phi_c} \\ a_2 e^{-i\Phi_c} \end{pmatrix}$$

where $\Phi_c = (\Phi_1 - \Phi_2)/2$ is called circularity and $\Phi_o = (\Phi_1 + \Phi_2)/2$ is called overall phase. Circularity gives the left- or right-polarization characteristic of the photon. RICH materials usually do not distinguish between the two polarizations and photons produced by the Čerenkov effect and scintillation are linearly polarized, that is $\Phi_c = 0$.

The overall phase is important in determining interference effects between coherent waves. These are important only in layers of thickness comparable with the wavelength, such as interference filters on mirrors. The effects of such coatings can be accounted for by the empirical reflectivity factor for the surface, and do not require a microscopic simulation. GEANT4 does not keep track of the overall phase.

Vector polarization is described by the polarization angle $\tan \Psi = a_2/a_1$. Reflection/transmission probabilities are sensitive to the state of linear polarization, so this has to be taken into account. One parameter is sufficient to describe vector polarization, but to avoid too many trigonometrical transformations, a unit vector perpendicular to the direction of the photon is used in GEANT4. The polarization vector is a data member of `G4DynamicParticle`.

10.1.3 Tracking of the photons

Optical photons are subject to in flight absorption, Rayleigh scattering and boundary action. As explained above, the status of the photon is defined by two vectors, the photon momentum ($\vec{p} = \hbar\vec{k}$) and photon polarization ($\vec{e}$). By convention the direction of the polarization vector is that of the electric field. Let also $\vec{u}$ be the normal to the material boundary at the point of intersection, pointing out of the material which the photon is leaving and toward the one which the photon is entering. The behaviour of a photon at the surface boundary is determined by three quantities:

1. refraction or reflection angle, this represents the kinematics of the effect;
2. amplitude of the reflected and refracted waves, this is the dynamics of the effect;
3. probability of the photon to be refracted or reflected, this is the quantum mechanical effect which we have to take into account if we want to describe the photon as a particle and not as a wave.

As said above, we distinguish three kinds of boundary action, dielectric → black material, dielectric → metal, dielectric → dielectric. The first case is trivial, in the sense that the photon is immediately absorbed and it goes undetected.

To determine the behaviour of the photon at the boundary, we will at first treat it as an homogeneous monochromatic plane wave:

$$\vec{E} = \vec{E}_0 e^{i\vec{k}\cdot\vec{x} - i\omega t}$$

$$\vec{B} = \sqrt{\mu\epsilon}\frac{\vec{k}\times\vec{E}}{k}$$

Case dielectric → dielectric

In the classical description the incoming wave splits into a reflected wave (quantities with a double prime) and a refracted wave (quantities with a single prime). Our problem is solved if we find the following quantities:

$$\vec{E}' = \vec{E}'_0 e^{i\vec{k}'\cdot\vec{x} - i\omega t}$$

$$\vec{E}'' = \vec{E}''_0 e^{i\vec{k}''\cdot\vec{x} - i\omega t}$$

For the wave numbers the following relations hold:

$$|\vec{k}| = |\vec{k}''| = k = \frac{\omega}{c}\sqrt{\mu\epsilon}$$

$$|\vec{k'}| = k' = \frac{\omega}{c}\sqrt{\mu'\epsilon'}$$

Where the speed of the wave in the medium is $v = c/\sqrt{\mu\epsilon}$ and the quantity $n = c/v = \sqrt{\mu\epsilon}$ is called refractive index of the medium. The condition that the three waves, refracted, reflected and incident have the same phase at the surface of the medium, gives us the well known Fresnel law:

$$(\vec{k} \cdot \vec{x})_{surf} = (\vec{k'} \cdot \vec{x})_{surf} = (\vec{k''} \cdot \vec{x})_{surf}$$

$$k \sin i = k' \sin r = k'' \sin r'$$

where i, r, r' are, respectively, the angle of the incident, refracted and reflected ray with the normal to the surface. From this formula the well known condition emerges:

$$i = r'$$

$$\frac{\sin i}{\sin r} = \sqrt{\frac{\mu'\epsilon'}{\mu\epsilon}} = \frac{n'}{n}$$

The dynamic properties of the wave at the boundary are derived from Maxwell's equations which impose the continuity of the normal components of $\vec{D}$ and $\vec{B}$ and of the tangential components of $\vec{E}$ and $\vec{H}$ at the surface boundary. The resulting ratios between the amplitudes of the the generated waves with respect to the incoming one are expressed in the two following cases:

1. a plane wave with the electric field (polarization vector) perpendicular to the plane defined by the photon direction and the normal to the boundary:

$$\frac{E'_0}{E_0} = \frac{2n\cos i}{n\cos i = \frac{\mu}{\mu'}n'\cos r} = \frac{2n\cos i}{n\cos i + n'\cos r}$$

$$\frac{E''_0}{E_0} = \frac{n\cos i - \frac{\mu}{\mu'}n'\cos r}{n\cos i + \frac{\mu}{\mu'}n'\cos r} = \frac{n\cos i - n'\cos r}{n\cos i + n'\cos r}$$

   where we suppose, as it is legitimate for visible or near-visible light, that $\mu/\mu' \approx 1$;

2. a plane wave with the electric field parallel to the above surface:

$$\frac{E'_0}{E_0} = \frac{2n\cos i}{\frac{\mu}{\mu'}n'\cos i + n\cos r} = \frac{2n\cos i}{n'\cos i + n\cos r}$$

$$\frac{E_0''}{E_0} = \frac{\frac{\mu}{\mu'} n' \cos i - n \cos r}{\frac{\mu}{\mu'} n' \cos i + n \cos r} = \frac{n' \cos i - n \cos r}{n' \cos i + n \cos r}$$

with the same approximation as above.

We note that in case of photon perpendicular to the surface, the following relations hold:

$$\frac{E_0'}{E_0} = \frac{2n}{n' + n} \qquad \frac{E_0''}{E_0} = \frac{n' - n}{n' + n}$$

where the sign convention for the parallel field has been adopted. This means that if $n' > n$ there is a phase inversion for the reflected wave.

Any incoming wave can be separated into one piece polarized parallel to the plane and one polarized perpendicular, and the two components treated accordingly.

To maintain the particle description of the photon, the probability to have a refracted or reflected photon must be calculated. The constraint is that the number of photons be conserved, and this can be imposed via the conservation of the energy flux at the boundary, as the number of photons is proportional to the energy. The energy current is given by the expression:

$$\vec{S} = \frac{1}{2} \frac{c}{4\pi} \sqrt{\mu\epsilon} \vec{E} \times \vec{H} = \frac{c}{8\pi} \sqrt{\frac{\epsilon}{\mu}} E_0^2 \hat{k}$$

and the energy balance on a unit area of the boundary requires that:

$$\vec{S} \cdot \vec{u} = \vec{S}' \cdot \vec{u} - \vec{S}'' \cdot \vec{u}$$

$$S \cos i = S' cosr + S'' cosi$$

$$\frac{c}{8\pi} \frac{1}{\mu} n E_0^2 \cos i = \frac{c}{8\pi} \frac{1}{\mu'} n' E_0'^2 \cos r + \frac{c}{8\pi} \frac{1}{\mu} n E_0''^2 \cos i$$

If we set again $\mu/\mu' \approx 1$, then the transmission probability for the photon will be:

$$T = (\frac{E_0'}{E_0})^2 \frac{n' \cos r}{n \cos i}$$

and the corresponding probability to be reflected will be $R = 1 - T$.

In case of reflection, the relation between the incoming photon $(\vec{k}, \vec{e})$, the refracted one $(\vec{k}', \vec{e}')$ and the reflected one $(\vec{k}'', \vec{e}'')$ is given by the following relations:

$$\vec{q} = \vec{k} \times \vec{u}$$

$$\vec{e}_\perp = (\frac{\vec{e} \cdot \vec{q}}{|\vec{q}|}) \frac{\vec{q}}{|\vec{q}|}$$

$$\vec{e}_{\parallel} = \vec{e} - \vec{e}_{\perp}$$

$$e'_{\parallel} = e_{\parallel} \frac{2n \cos i}{n' \cos i + n \cos r}$$

$$e'_{\perp|} = e_{\perp} \frac{2n \cos i}{n \cos i + n' \cos r}$$

$$e''_{\parallel} = \frac{n'}{n} e'_{\parallel} - e_{\parallel}$$

$$e''_{\perp} = e'_{\perp} - e_{\perp}$$

After transmission or reflection of the photon, the polarization vector is re-normalized to 1. In the case where $\sin r = n \sin i / n' > 1$ then there cannot be a refracted wave, and in this case we have a total internal reflection according to the following formulas:

$$\vec{k}'' = \vec{k} - 2(\vec{k} \cdot \vec{u})\vec{u}$$

$$\vec{e}'' = -\vec{e} + 2(\vec{e} \cdot \vec{u})\vec{u}$$

Case dielectric → metal

In this case the photon cannot be transmitted. So the probability for the photon to be absorbed by the metal is estimated according to the table provided by the user. If the photon is not absorbed, it is reflected.

Bibliography

[1] J.D. Jackson, *Classical Electrodynamics*, J. Wiley & Sons Inc., New York, 1975.

Part IV

Hadronic Interactions

Chapter 11

Lepton Hadron Interactions

This category contains only one process, photonuclear interaction of muons. It consists of process itself and the interaction model.

11.1 Overview

The class G4MuonNucleusProcess simulates the photonuclear interaction of muons. It calculates the discrete energy loss and determinates final state of the muon. The result of the simulation is quite dependent on the interaction model. Such model-dependent part is enclosed in the class G4MuonNucleusInteractionModel, which can be replaced with the alternative one easily. The class G4MuonNucleusInteractionModel provides the practical description of the interaction to calculate cross section and final states. The adopted model is that of GEISHA Monte Carlo Program [1].
In order to determinate the final state of hadronic system, the exchanged virtual photon is replaced with a pion with same Q^2. Then some routines developed for hadronic processes are used to simulate the inelastic interaction between the intermediate pion and the nucleus. Either π^+ or π^- is determinated randomly. The classes invoked to compute pion-nucleus interaction are:

$$\begin{cases} \text{G4LEPionMinus(Plus)Inelastic} & (E \leq 25GeV) \\ \text{G4HEPionMinus(Plus)Inelastic} & (E > 25GeV) \end{cases}$$

11.2 the Interaction model

11.2.1 Mean free path

Microscopic cross section is the function of muon energy and calculated as following:

$$\sigma_{\mu N} = \begin{cases} 0.3 & (E \leq 30GeV) \\ 0.3(E/30)^{0.25} & (E > 30GeV) \end{cases} \quad [\mu b]$$

Macroscopic cross section is roughly proportional to the atomic mass number A of the material.

$$\sigma_{\mu A} = A\sigma_{\mu N}$$

11.2.2 Calculation of differential cross section

The differential cross section in terms of muon energy and emission angle can be expressed as:

$$\frac{d\sigma}{d\Omega dE} = \Gamma\left(\sigma_T + \epsilon\sigma_L\right)$$

where:
- Γ : flux of transverse photon
- ϵ : polarization of intermediate photon
- σ_L : photoabsorption cross section for longitudinal photon
- σ_T : photoabsorption cross section for transverse photon

They are given by:

$$\begin{aligned}
\Gamma &= \frac{K\alpha}{2\pi}\frac{E'}{E}\frac{1}{1-\epsilon} \\
\epsilon &= \left[1 + 2\frac{Q^2+\nu^2}{Q^2}tan^2\frac{\theta}{2}\right]^{-1} \\
\sigma_L &= 0.3\left(1 - \frac{1}{1.868}Q^2\nu\right)\sigma_T \\
\sigma_T &\sim const = 0.12mb
\end{aligned}$$

Q^2 and ν are the scaling variables:

$$\begin{aligned}
Q^2 &= -q^2 = 2(EE' - PP'cos\theta - m_\mu^2) \\
\nu &= E - E'
\end{aligned}$$

The flux of incident photon K is given using the Gilman's convention:

$$K = \nu + \frac{Q^2}{2\nu}$$

11.3 Status of this document

23.10.98 created by M.Takahata

Bibliography

[1] H.Fesefeldt *GHEISHA The Simulation of Hadronic Showers* 149 *RWTH/PITHA 85/02* (1985)

Chapter 12

Interactions of Stopping Particles

Documentation to be completed.

12.1 Complementary parameterised and theoretical treatment

Absorption of negative pions and kaons at rest from a nucleus is described in literature [1], [2], [3], [4] as consisting of two main components:

- a primary absorption process, involving the interaction of the incident stopped hadron with one or more nucleons of the target nucleus;
- the deexcitation of the remnant nucleus, left in an excitated state as a result of the occurrence of the primary absorption process.

This interpretation is supported by several experiments [5], [6], [7], [8], [9], [10], [11], that have measured various features characterizing these processes. In many cases the experimental measurements are capable to distinguish the final products originating from the primary absorption process and those resulting from the nuclear deexcitation component.

A set of stopped particle absorption processes is implemented in GEANT4, based on this two-component model (PiMinusAbsorptionAtRest and KaonMinusAbsorptionAtRest classes, for π^- and K^- respectively. Both implementations adopt the same approach: the primary absorption component of the process is parameterised, based on available experimental data; the nuclear deexcitation component is handled through the theoretical models described elsewhere in this Manual.

Bibliography

[1] E. Gadioli and E. Gadioli Erba *Phys. Rev. C 36* 741 (1987)

[2] H.C. Chiang and J. Hufner *Nucl. Phys. A352* 442 (1981)

[3] D. Ashery and J. P. Schiffer *Ann. Rev. Nucl. Part. Sci. 36* 207 (1986)

[4] H. J. Weyer *Phys. Rep. 195* 295 (1990)

[5] R. Hartmann et al., *Nucl. Phys. A300* 345 (1978)

[6] R. Madley et al., *Phys. Rev. C 25* 3050 (1982)

[7] F. W. Schleputz et al., *Phys. Rev. C 19* 135 (1979)

[8] C.J. Orth et al., *Phys. Rev. C 21* 2524 (1980)

[9] H.S. Pruys et al., *Nucl. Phys. A316* 365 (1979)

[10] P. Heusi et al., *Nucl. Phys. A407* 429 (1983)

[11] H.P. Isaak et al., *Nucl. Phys. A392* 368 (1983)

12.1.1 Pion absorption at rest

The absorption of stopped negative pions in nuclei is interpreted [1], [2], [3], [4] as starting with the absorption of the pion by two or more correlated nucleons; the total energy of the pion is transferred to the absorbing nucleons, which then may leave the nucleus directly, or undergo final-state interactions with the residual nucleus. The remaining nucleus de-excites by evaporation of low energetic particles.

G4PiMinusAbsorptionAtRest generates the primary absorption component of the process through the parameterisation of existing experimental data; the primary absorption component is handled by class G4PiMinusStopAbsorption. In the current implementation only absorption on a nucleon pair is considered, while contributions from absorption on nucleon clusters are neglected; this approximation is supported by experimental results [1], [2] showing that it is the dominating contribution.

Several features of stopped pion absorption are known from experimental measurements on various materials [3], [4], [7], [8], [7], [8], [9], [10]:

- the average number of nucleons emitted, as resulting from the primary absorption process;
- the ratio of nn vs np as nucleon pairs involved in the absorption process;
- the energy spectrum of the resulting nucleons emitted and their opening angle distribution.

The corresponding final state products and related distributions are generated according to a parameterisation of the available experimental measurements listed above. The dependence on the material is handled by a strategy pattern: the features pertaining to material for which experimental data are available are treated in G4PiMinusStopX classes (where X represents an element), inheriting from G4StopMaterial base class. In case of absorption on an element for which experimental data are not available, the experimental distributions for the elements closest in Z are used.

The excitation energy of the residual nucleus is calculated by difference between the initial energy and the energy of the final state products of the primary absorption process.

Another strategy handles the nucleus deexcitation; the current default implementation consists in handling the deexcitatoin component of the process through the evaporation model described elsewhere in this Manual.

Bibliography

[1] E. Gadioli and E. Gadioli Erba *Phys. Rev. C 36* 741 (1987)

[2] H. Machner *Nucl. Phys. A395* 457 (1983)

[3] R. Hartmann et al., *Nucl. Phys. A300* 345 (1978)

[4] R. Madley et al., *Phys. Rev. C 25* 3050 (1982)

[5] F. W. Schleputz et al., *Phys. Rev. C 19* 135 (1979)

[6] C.J. Orth et al., *Phys. Rev. C 21* 2524 (1980)

[7] H.S. Pruys et al., *Nucl. Phys. A316* 365 (1979)

[8] P. Heusi et al., *Nucl. Phys. A407* 429 (1983)

[9] H.P. Isaak et al., *Nucl. Phys. A392* 368 (1983)

[10] H.P. Isaak et al., *Helvetica Physica Acta 55* 477 (1982)

Chapter 13

Parametrization Driven Models

Documentation to be completed.

13.1 High energy hadron nucleus interactions

For the simulation of high energy hadron nucleus interactions the well known GHEISHA model from GEANT3 is included, recoded in C++. This code consists of sampling distribution functions of

- the combined multiplicity $w(\vec{a}, n_i)$ for all particles i, $i = \pi^+, \pi^0, \pi^-, p, n, ...$, including the correlations between them;
- the additive quantum numbers (energy E, charge Q, strangeness S and baryon number B) in the whole phase space region;
- evaporation and nuclear fission.

A universal function $f(\vec{b}, x/p_T, m_T)$ is used for the distribution of the additive quantum numbers, with the Feynman variable x, the transverse momentum p_T and transverse mass m_T. $\vec{a}$ and $\vec{b}$ are parameter vectors, which depend on the particle type of the incoming beam and the atomic number A of the target. Any dependence on the beam energy is completely restricted to the multiplicity distribution and the available phase space. The underlying model for establishing the parametrizations is an old fashioned multi chain model, where the beam particle undergoes multiple collisions with nucleons inside the nucleus; each of these interactions form a fragmenting chain and one recoil nucleon. All produced particles are able to reinteract, thus developing an intranuclear cascade. The formation zone concept is taken into account, which means that the produced particles need some time and thus also some range to hadonize into real particles. It is, however, important to realize that there are numerous tunable parameters in all steps

of the code. This restricts the use of this program as generator for hadron nucleus interactions, since it is not always clear how to relate the parameters to physical quantities. On the other hand a precise simulation of minimum bias events is possible, with a large predictive power for calorimetry. For the tuning of the parameters a database consisting of results from hadron nucleus scattering experiments and from calorimetric test beam data has been collected in the last years. Comparisons with calculations from GEANT3 and GEANT4 will be published elsewhere.

Chapter 14

Theory Driven Models

Chapter 15

Parton string model.

15.1 Reaction initial state simulation.

15.1.1 Allowed projectiles and bombarding energy range for interaction with nucleon and nuclear targets.

The GEANT4 parton string model is capable to predict final states (produced hadrons which belong to the scalar and vector meson nonets and the baryon (antibaryon) octet and decuplet) of reactions on nucleon and nuclear targets with nucleon, pion and kaon projectiles. The allowed bombarding energy $\sqrt{s} > 5$ GeV is recommended.

15.1.2 MC initialization procedure for nucleus.

The initialization of each nucleus, consisting from A nucleons and Z protons with coordinates $\mathbf{r}_i$ and momenta $\mathbf{p}_i$, where $i = 1, 2, ..., A$ is performed. We use the standard initialization Monte Carlo procedure, which is realized in the most of the high energy nuclear interaction models:

- Nucleon radii r_i are selected randomly in the rest of nucleus according to proton or neutron density $\rho(r_i)$. For heavy nuclei with $A > 16$ [1] nucleon density is

$$\rho(r_i) = \frac{\rho_0}{1 + \exp\left[(r_i - R)/a\right]} \tag{15.1}$$

where

$$\rho_0 \approx \frac{3}{4\pi R^3}(1 + \frac{a^2\pi^2}{R^2})^{-1}. \tag{15.2}$$

Here $R = r_0 A^{1/3}$ fm and $r_0 = 1.16(1 - 1.16A^{-2/3})$ fm and $a \approx 0.545$ fm. For light nuclei with $A < 17$ nucleon density is given by a harmonic oscillator shell model [2], e. g.

$$\rho(r_i) = (\pi R^2)^{-3/2} \exp\left(-r_i^2/R^2\right), \tag{15.3}$$

where $R^2 = 2/3 < r^2 >= 0.8133A^{2/3}$ fm^2. To take into account nucleon repulsive core it is assumed that internucleon distance $d > 0.8$ fm;

- The initial momenta of the nucleons are randomly choosen between 0 and p_F^{max}, where the maximal momenta of nucleons (in the local Thomas-Fermi approximation [3]) depends from the proton or neutron density ρ according to

$$p_F^{max} = \hbar c(3\pi^2\rho)^{1/3} \tag{15.4}$$

with $\hbar c = 0.197327$ MeVfm;

- To obtain coordinate and momentum components, it is assumed that nucleons are distributed isotropicaly in configuration and momentum spaces;

- Then perform shifts of nucleon coordinates $\mathbf{r'_i} = \mathbf{r_i} - 1/A\sum_i \mathbf{r_i}$ and momenta $\mathbf{p'_i} = \mathbf{p_i} - 1/A\sum_i \mathbf{p_i}$ of nucleon momenta. The nucleus must be centered in configuration space around $\mathbf{0}$, *i. e.* $\sum_i \mathbf{r}_i = \mathbf{0}$ and the nucleus must be at rest, i. e. $\sum_i \mathbf{p_i} = \mathbf{0}$;

- We compute energy per nucleon $e = E/A = m_N + B(A,Z)/A$, where m_N is nucleon mass and the nucleus binding energy $B(A,Z)$ is given by the Bethe-Weizsäcker formula[4]:

$$B(A,Z) = \\ = -0.01587A + 0.01834A^{2/3} + 0.09286(Z - \tfrac{A}{2})^2 + 0.00071Z^2/A^{1/3}, \tag{15.5}$$

and find the effective mass of each nucleon $m_i^{eff} = \sqrt{(E/A)^2 - p_i^{2\prime}}$.

15.1.3 Random choice of the impact parameter.

The impact parameter $0 \leq b \leq R_t$ is randomly selected according to the probability:

$$P(\mathbf{b})d\mathbf{b} = bd\mathbf{b}, \tag{15.6}$$

where R_t is the target radius, respectively. In the case of nuclear projectile or target the nuclear radius is determined from condition:

$$\frac{\rho(R)}{\rho(0)} = 0.01. \tag{15.7}$$

15.2 Sample of collision participants in nuclear collisions.

15.2.1 MC procedure to define collision participants.

The inelastic hadron–nucleus interactions at ultra–relativistic energies are considered as independent hadron–nucleon collisions. It was shown long time ago [5] for the hadron–nucleus collision that such a picture can be obtained starting from the Regge–Gribov approach [6], when one assumes that the hadron-nucleus elastic scattering amplitude is a result of reggeon exchanges between the initial hadron and nucleons from target–nucleus. This result leads to simple and efficient MC procedure [7] to define the interaction cross sections and the number of the nucleons participating in the inelastic hadron–nucleus collision:

- We should randomly distribute B nucleons from the target-nucleus on the impact parameter plane according to the weight function $T([\vec{b}_j^B])$. This function represents probability density to find sets of the nucleon impact parameters $[\vec{b}_j^B]$, where $j = 1, 2, ..., B$.

- For each pair of projectile hadron i and target nucleon j with choosen impact parameters $\vec{b}_i$ and $\vec{b}_j^B$ we should check whether they interact inelastically or not using the probability $p_{ij}(\vec{b}_i - \vec{b}_j^B, s)$, where $s_{ij} = (p_i + p_j)^2$ is the squared total c.m. energy of the given pair with the 4–momenta p_i and p_j, respectively.

In the Regge–Gribov approach[6] the probability for an inelastic collision of pair of i and j as a function at the squared impact parameter difference $b_{ij}^2 = (\vec{b}_i - \vec{b}_j^B)^2$ and s is given by

$$p_{ij}(\vec{b}_i - \vec{b}_j^B, s) = c^{-1}[1 - \exp\{-2u(b_{ij}^2, s)\}] = \sum_{n=1}^{\infty} p_{ij}^{(n)}(\vec{b}_i - \vec{b}_j^B, s), \quad (15.8)$$

where

$$p_{ij}^{(n)}(\vec{b}_i - \vec{b}_j^B, s) = c^{-1} \exp\{-2u(b_{ij}^2, s)\} \frac{[2u(b_{ij}^2, s)]^n}{n!}. \quad (15.9)$$

is the probability to find the n cut Pomerons or the probability for $2n$ strings produced in an inelastic hadron-nucleon collision. These probabilities are defined in terms of the (eikonal) amplitude of hadron–nucleon elastic scattering with Pomeron exchange:

$$u(b_{ij}^2, s) = \frac{z(s)}{2} \exp(-b_{ij}^2/4\lambda(s)). \quad (15.10)$$

The quantities $z(s)$ and $\lambda(s)$ are expressed through the parameters of the Pomeron trajectory, $\alpha_P^{'} = 0.25\ GeV^{-2}$ and $\alpha_P(0) = 1.0808$, and the param-

eters of the Pomeron-hadron vertex R_P and γ_P:

$$z(s) = \frac{2c\gamma_P}{\lambda(s)}(s/s_0)^{\alpha_P(0)-1} \tag{15.11}$$

$$\lambda(s) = R_P^2 + \alpha_P^{'} \ln(s/s_0), \tag{15.12}$$

respectively, where s_0 is a dimensional parameter.

In Eqs. (15.8,15.9) the so–called shower enhancement coefficient c is introduced to determine the contribution of diffractive dissociation[6]. Thus, the probability for diffractive dissociation of a pair of nucleons can be computed as

$$p_{ij}^d(\vec{b}_i - \vec{b}_j^B, s) = \frac{c-1}{c}[p_{ij}^{tot}(\vec{b}_i - \vec{b}_j^B, s) - p_{ij}(\vec{b}_i - \vec{b}_j^B, s)], \tag{15.13}$$

where

$$p_{ij}^{tot}(\vec{b}_i - \vec{b}_j^B, s) = (2/c)[1 - \exp\{-u(b_{ij}^2, s)\}]. \tag{15.14}$$

The Pomeron parameters are found from a global fit of the total, elastic, differential elastic and diffractive cross sections of the hadron–nucleon interaction at different energies.

For the nucleon-nucleon, pion-nucleon and kaon-nucleon collisions the Pomeron vertex parameters and shower enhancement coefficients are found: $R_P^{2N} = 3.56\ GeV^{-2}$, $\gamma_P^N = 3.96\ GeV^{-2}$, $s_0^N = 3.0\ GeV^2$, $c^N = 1.4$ and $R_P^{2\pi} = 2.36\ GeV^{-2}$, $\gamma_P^\pi = 2.17\ GeV^{-2}$, and $R_P^{2K} = 1.96\ GeV^{-2}$, $\gamma_P^K = 1.92\ GeV^{-2}$, $s_0^K = 2.3\ GeV^2$, $c^\pi = 1.8$.

15.2.2 Separation of hadron diffraction excitation.

For each pair of target hadron i and projectile nucleon j with choosen impact parameters $\vec{b}_i$ and $\vec{b}_j^B$ we should check whether they interact inelastically or not using the probability

$$p_{ij}^{in}(\vec{b}_i - \vec{b}_j^B, s) = p_{ij}(\vec{b}_i - \vec{b}_j^B, s) + p_{ij}^d(\vec{b}_i^A - \vec{b}_j^B, s). \tag{15.15}$$

If interaction will be realized, then we have to consider it to be diffractive or nondiffractive with probabilities

$$\frac{p_{ij}^d(\vec{b}_i - \vec{b}_j^B, s)}{p_{ij}^{in}(\vec{b}_i^A - \vec{b}_j^B, s)} \tag{15.16}$$

and

$$\frac{p_{ij}(\vec{b}_i - \vec{b}_j^B, s)}{p_{ij}^{in}(\vec{b}_i^A - \vec{b}_j^B, s)}. \tag{15.17}$$

15.3 Longitudinal string excitation.

15.3.1 Hadron–nucleon inelastic collision.

Let us consider collision of two hadrons with their c. m. momenta $P_1 = \{E_1^+, m_1^2/E_1^+, \mathbf{0}\}$ and $P_2 = \{E_2^-, m_2^2/E_2^-, \mathbf{0}\}$, where the light-cone variables $E_{1,2}^{\pm} = E_{1,2} \pm P_{z1,2}$ are defined through hadron energies $E_{1,2} = \sqrt{m_{1,2}^2 + P_{z1,2}^2}$, hadron longitudinal momenta $P_{z1,2}$ and hadron masses $m_{1,2}$, respectively. Two hadrons collide by two partons with momenta $p_1 = \{x^+E_1^+, 0, \mathbf{0}\}$ and $p_2 = \{0, x^-E_2^-, \mathbf{0}\}$, respectively.

15.3.2 The diffractive string excitation.

In the diffractive string excitation (the Fritiof approach [9]) only momentum can be transferred:

$$\begin{array}{c} P_1' = P_1 + q \\ P_2' = P_2 - q, \end{array} \tag{15.18}$$

where

$$q = \{-q_t^2/(x^-E_2^-), q_t^2/(x^+E_1^+), \mathbf{q_t}\} \tag{15.19}$$

is parton momentum transferred and $\mathbf{q_t}$ is its transverse component. We use the Fritiof approach to simulate the diffractive excitation of particles.

15.3.3 The string excitation by parton exchange.

For this case the parton exchange (rearrangement) and the momentum exchange are allowed [10],[11],[7]:

$$\begin{array}{c} P_1' = P_1 - p_1 + p_2 + q \\ P_2' = P_2 + p_1 - p_2 - q, \end{array} \tag{15.20}$$

where $q = \{0, 0, \mathbf{q_t}\}$ is parton momentum transferred, i. e. only its transverse components $\mathbf{q_t} = 0$ is taken into account.

15.3.4 Transverse momentum sampling.

The transverse component of the parton momentum transferred is generated according to probability

$$P(\mathbf{q_t})d\mathbf{q_t} = \sqrt{\frac{a}{\pi}} \exp\left(-aq_t^2\right) d\mathbf{q_t}, \tag{15.21}$$

where parameter $a = 0.6$ GeV^{-2}.

x^+ and x^- samplings.

Light cone parton quantities x^+ and x^- are generated independently and according to distribution:

$$u(x) \sim x^{\alpha}(1-x)^{\beta}, \tag{15.22}$$

where $x = x^+$ or $x = x^-$. Parameters $\alpha = -1$ and $\beta = 0$ are chosen for the FRITIOF approach [9]. In the case of the QGSM approach [7] $\alpha = -0.5$ and $\beta = 1.5$ or $\beta = 2.5$. Masses of the excited strings should satisfy the kinematical constraints:

$$P_1'^+ P_1'^- \geq m_{h1}^2 + q_t^2 \tag{15.23}$$

and

$$P_2'^+ P_2'^- \geq m_{h2}^2 + q_t^2, \tag{15.24}$$

where hadronic masses m_{h1} and m_{h2} (model parameters) are defined by string quark contents. Thus, the random selection of the values x^+ and x^- is limited by above constraints.

15.3.5 Hadron–nucleus inelastic collisions.

Hadron-nucleus collisions in the both approaches (diffractive and parton exchange) are considered as a set of the independent hadron-nucleon collisions. However, the string excitation procedures in these approaches are rather different.

15.3.6 The diffractive string excitation.

In the diffractive string excitation (the FRITIOF approach [9]) for each inelastic hadron–nucleon collision we have to select randomly the transverse momentum transferred $\mathbf{q_t}$ (in accordance with the probability given by Eq. (15.21)) and select randomly the values of $x^\pm$ (in accordance with distribution defined by Eq. (15.22)). Then we have to calculate the parton momentum transferred q using Eq. (15.19) and update scattered hadron and nucleon or scatterred nucleon and nucleon momenta using Eq. (15.20). For each collision we have to check the constraints (15.23) and (15.24), which can be written more explicitly:

$$[E_1^+ - \frac{q_t^2}{x^- E_2^-}][\frac{m_1^2}{E_1^+} + \frac{q_t^2}{x^+ E_1^+}] \geq m_{h1}^2 + q_t^2 \tag{15.25}$$

and

$$[E_2^- + \frac{q_t^2}{x^- E_2^-}][\frac{m_2^2}{E_2^-} - \frac{q_t^2}{x^+ E_1^+}] \geq m_{h1}^2 + q_t^2. \tag{15.26}$$

15.3.7 The string excitation by parton rearrangement.

In this approach [7] strings (as result of parton rearrangement) should be spanned not only between valence quarks of colliding hadrons, but also between valence and sea quarks and between sea quarks. The each participant hadron or nucleon should be splitted into set of partons: valence quark and antiquark for meson or valence quark (antiquark) and diquark

(antidiquark) for baryon (antibaryon) and additionaly the $(n-1)$ sea quark-antiquark pairs (their flavours are selected according to probability ratios $u:d:s=1:1:0.35$), if hadron or nucleon is participating in the n inelastic collisions. Thus for each participant hadron or nucleon we have to generate a set of light cone variables x_{2n}, where $x_{2n}=x_{2n}^{+}$ or $x_{2n}=x_{2n}^{-}$ according to distribution:

$$f^h(x_1,x_2,...,x_{2n})=f_0\prod_{i=1}^{2n}u_{q_i}^h(x_i)\delta(1-\sum_{i=1}^{2n}x_i), \tag{15.27}$$

where f_0 is the normalization constant. Here, the quark structure functions $u_{q_i}^h(x_i)$ for valence quark (antiquark) q_v, sea quark and antiquark q_s and valence diquark (antidiquark) qq are:

$$u_{q_v}^h(x_v)=x_v^{\alpha_v},\ u_{q_s}^h(x_s)=x_s^{\alpha_s},\ u_{qq}^h(x_{qq})=x_{qq}^{\beta_{qq}}, \tag{15.28}$$

where $\alpha_v=-0.5$ and $\alpha_s=-0.5$ [10] for the non-strange quarks (antiquarks) and $\alpha_v=0$ and $\alpha_s=0$ for strange quarks (antiquarks), $\beta_{uu}=1.5$ and $\beta_{ud}=2.5$ for proton (antiproton) and $\beta_{dd}=1.5$ and $\beta_{ud}=2.5$ for neutron (antineutron). Usualy x_i are selected between $x_i^{min}\le x_i\le 1$, where model parameter x^{min} is a function of initial energy, to prevent from production of strings with low masses (less than hadron masses), when whole selection procedure should be repeated. Then the transverse momenta of partons $\mathbf{q_{it}}$ are generated according to the Gaussian probability Eq. (15.21) with $a=1/4\Lambda(s)$ and under the constraint: $\sum_{i=1}^{2n}\mathbf{q_{it}}=0$. The partons are considered as the off-shell partons, i. e. $m_i^2\neq 0$.

15.4 Longitudinal string decay.

15.4.1 Hadron production by string fragmentation.

A string is stretched between flying away constituents: quark and antiquark or quark and diquark or diquark and antidiquark or antiquark and antidiquark. From knowledge of the constituents longitudinal $p_{3i}=p_{zi}$ and transversal $p_{1i}=p_{xi}$, $p_{2i}=p_{yi}$ momenta as well as their energies $p_{0i}=E_i$, where $i=1,2$, we can calculate string mass squared:

$$M_S^2=p^\mu p_\mu=p_0^2-p_1^2-p_2^2-p_3^2, \tag{15.29}$$

where $p_\mu=p_{\mu 1}+p_{\mu 2}$ is the string four momentum and $\mu=0,1,2,3$.

The fragmentation of a string follows an iterative scheme:

$$string\Rightarrow hadron+new\ string, \tag{15.30}$$

i. e. a quark-antiquark (or diquark-antidiquark) pair is created and placed between leading quark-antiquark (or diquark-quark or diquark-antidiquark or antiquark-antidiquark) pair.

The values of the strangeness suppression and diquark suppression factors are

$$u : d : s : qq = 1 : 1 : 0.35 : 0.1. \tag{15.31}$$

A hadron is formed randomly on one of the end-points of the string. The quark content of the hadrons determines its species and charge. In the chosen fragmentation scheme we can produce not only the groundstates of baryons and mesons, but also their lowest excited states. If for baryons the quark-content does not determine whether the state belongs to the lowest octet or to the lowest decuplet, then octet or decuplet are choosen with equal probabilities. In the case of mesons the multiplet must also be determined before a type of hadron can be assigned. The probability of choosing a certain multiplet depends on the spin of the multiplet.

The zero transverse momentum of created quark-antiquark (or diquark-antidiquark) pair is defined by the sum of an equal and opposite directed transverse momenta of quark and antiquark.

The transverse momentum of created quark is randomly sampled according to probability (15.21) with the parameter $a = 0.25$ GeV^{-2}. Then a hadron transverse momentum $\mathbf{p_t}$ is determined by the sum of the transverse momenta of its constituents.

The fragmentation function $f^h(z, p_t)$ represents the probability distribution for hadrons with the transverse momenta $\mathbf{p_t}$ to aquire the light cone momentum fraction $z = z^{\pm} = (E^h \pm p_z^h/(E^q \pm p_z^q)$, where E^h and E^q are the hadron and fragmented quark energies, respectively and p_z^h and p_z^q are hadron and fragmented quark longitudinal momenta, respectively, and $z_{min}^{\pm} \leq z^{\pm} \leq z_{max}^{\pm}$, from the fragmenting string. The values of $z_{min,max}^{\pm}$ are determined by hadron m_h and constituent transverse masses and the available string mass. One of the most common fragmentation function is used in the LUND model [12]:

$$f^h(z, p_t) \sim \frac{1}{z}(1-z)^a \exp\,[-\frac{b(m_h^2 + p_t^2)}{z}]. \tag{15.32}$$

One can use this fragmentation function for the decay of the excited string.

One can use also the fragmentation functions are derived in [13]:

$$f_q^h(z, p_t) = [1 + \alpha_q^h(< p_t >)](1-z)^{\alpha_q^h(<p_t>)}. \tag{15.33}$$

The advantage of these functions as compared to the LUND fragmentation function is that they have correct three–reggeon behaviour at $z \to 1$ [13].

15.4.2 The hadron formation time and coordinate.

To calculate produced hadron formation times and longitudinal coordinates we consider the (1 + 1)-string with mass M_S and string tension κ, which decays into hadrons at string rest frame. The i-th produced hadron

has energy E_i and its longitudinal momentum p_{zi}, respectively. Introducing light cone variables $p_i^{\pm} = E_i \pm p_{iz}$ and numbering string breaking points consecutively from right to left we obtain $p_0^+ = M_S$, $p_i^+ = \kappa(z_{i-1}^+ - z_i^+)$ and $p_i^- = \kappa x_i^-$.

We can identify the hadron formation point coordinate and time as the point in space-time, where the quark lines of the quark-antiquark pair forming the hadron meet for the first time (the so-called 'yo-yo' formation point [12]):

$$t_i = \frac{1}{2\kappa}[M_S - 2\sum_{j=1}^{i-1} p_{zj} + E_i - p_{zi}] \tag{15.34}$$

and coordinate

$$z_i = \frac{1}{2\kappa}[M_S - 2\sum_{j=1}^{i-1} E_j + p_{zi} - E_i]. \tag{15.35}$$

15.5 Status of this document.

9.10.98 created by N. Amelin. 5.12.98 editing by J.P. Wellisch. 19.01.99 revised by N. Amelin.

Bibliography

[1] Grypeos M. E., Lalazissis G. A., Massen S. E., Panos C. P., J. Phys. **G17** 1093 (1991).

[2] Elton L. R. B., Nuclear Sizes, Oxford University Press, Oxford, 1961.

[3] DeShalit A., Feshbach H., Theoretical Nuclear Physics, Vol. 1: Nuclear Structure, Wyley, 1974.

[4] Bohr A., Mottelson B. R., Nuclear Structure, W. A. Benjamin, New York, Vol. 1, 1969.

[5] Capella A. and Krzywicki A., Phys. Rev. **D18** (1978) 4120.

[6] Baker M. and Ter–Martirosyan K. A., Phys. Rep. **28C** (1976) 1.

[7] Amelin N. S., Gudima K. K., Toneev V. D., Sov. J. Nucl. Phys. **51** (1990) 327; Amelin N. S., JINR Report **P2-86-56** (1986).

[8] Abramovskii V. A., Gribov V. N., Kancheli O. V., Sov. J. Nucl. Phys. **18** (1974) 308.

[9] Andersson B., Gustafson G., Nielsson-Almquist, Nucl. Phys. **281** 289 (1987).

[10] Kaidalov A. B., Ter-Martirosyan K. A., Phys. Lett. **B117** 247 (1982).

[11] Capella A., Sukhatme U., Tan C. I., Tran Thanh Van. J., Phys. Rep. **236** 225 (1994).

[12] Andersson B., Gustafson G., Ingelman G., Sjöstrand T., Phys. Rep. **97** 31 (1983).

[13] Kaidalov A. B., Sov. J. Nucl. Phys. **45** 1452 (1987).

Chapter 16

Hadron kinetic model.

16.1 Reaction initial state simulation.

16.1.1 Allowed projectiles and bombarding energy range for interaction with nucleon and nuclear targets.

The GEANT4 kinetic model is capable to predict final states (produced hadrons which belong to the pseudoscalar meson nonet and the baryon (antibaryon) octet) of reactions on nucleon and nuclear targets with nucleon, pion and kaon projectiles. The allowed bombarding kinetic energy in the hadron–nucleon, hadron–nucleus is recommended to be more than 40 MeV in the laboratory frame. The upper limit of initial kinetic energy is approximately 10 GeV.

The initialization of each nucleus, consisting from A nucleons and Z protons ($N = A - Z$ neutrons) with coordinates is performed in similar way as it was described for the parton string model.

16.2 Hadron propagation.

So far the hadrons are transported along the straight line paths (cascade approach), i. e. particle coordinates $\mathbf{r}$ for time "shift" between t_0 and t_1 are updated according to

$$\mathbf{r}(t_1) = \mathbf{r}(t_0) + \frac{\mathbf{p}(t_0)}{E(t_0)}(t_1 - t_0), \tag{16.1}$$

where $\mathbf{p}$ and E denote particles momenta and energies. The intranuclear nucleons are assumed to be "frozen" before collision, i. e. they are allowed to move only with the c. m. nucleus velocity. However, their Fermi momenta are taken into account to find interaction cross sections or characteristics of secondary particles produced in the course of an intranuclear collision.

16.3 Selection of particle collisions and particle decays.

16.3.1 Particle collision criterion and collision time.

For each pair (i, j) of particles their total interaction cross section $\sigma_{tot}(s_{ij})$ is calculated. This cross section depends on the quantum numbers of the particles. It is also a function of the total particle c.m. energy squared $s_{ij} = (p_i + p_j)^2)$, where $p_i = (E_i, \mathbf{p_i})$ and $p_j = (E_j, \mathbf{p_j})$ are four momenta of particle i with mass $m_i = \sqrt{E_i^2 - \mathbf{p_i}^2}$ and particle j with mass $m_j = \sqrt{E_j^2 - \mathbf{p_j}^2}$, respectively. The cross section is interpreted geometrically as an interaction area with radius

$$b_{ij} = \sqrt{\frac{\sigma_{tot}(s_{ij})}{\pi}}. \tag{16.2}$$

It was assumed that two particles will collide, if their transverse (with regards to the relative velocity vector of the particles) distance d_{ij} fulfils the condition:

$$d_{ij} \leq b_{ij}. \tag{16.3}$$

For the distance d_{ij} we choose the relative distance between two particles at the time of closest approach calculated in the c.m. frame of two particles with coordinates $\mathbf{x_i^*}$ and $\mathbf{x_j^*}$ and momenta $\mathbf{p_i^*}$ and $\mathbf{p_j^*}$, respectively. It is determined by

$$d_{ij}^2 = (\mathbf{x_i^*} - \mathbf{x_j^*})^2 - \frac{[(\mathbf{x_i^*} - \mathbf{x_j^*})(\mathbf{p_i^*} - \mathbf{p_j^*})]^2}{(\mathbf{p_i^*} - \mathbf{p_j^*})^2}. \tag{16.4}$$

We order collisions in the reference frame of the hadron-nucleus or nucleus-nucleus interaction. Thus using the particle locations $\mathbf{x}$ and the particle momenta $\mathbf{p}$ in the reference frame of the hadron-nucleus or nucleus-nucleus interaction one can obtain for the time of closest approach of the two colliding particles:

$$\tau_{coll} = t_{ij} = t_{ji} = -\frac{(\mathbf{x_i} - \mathbf{x_j})(\mathbf{p_i}/E_i - \mathbf{p_j}/E_j)}{(\mathbf{p_i}/E_i - \mathbf{p_j}/E_j)^2}. \tag{16.5}$$

16.3.2 Hadron resonance lifetime.

The lifetime t for each particle with mass M_R was sampled according to probability:

$$P(t) = 1 - \exp\,(-\frac{t\Gamma_{tot}(m)}{\gamma\hbar}, \tag{16.6}$$

where $\gamma = E/m$ is the Lorentz factor, defined through particle total energy E. The particle (resonance) width $\Gamma_{tot}(m)$ is defined at table resonance mass

m. All pole masses and partial decay widths are taken from the Review of Particle Properties [1].

16.4 Hadron interaction cross sections.

The hadron interaction cross sections are a function of the incoming and outgoing particle types and their c. m. energy $\sqrt{s_{i,j}} = \sqrt{(p_i + p_j)^2}$, where $p_i = (E_i, \mathbf{p_i})$ and $p_j = (E_j, \mathbf{p_j})$ are denoting the four momenta of the incoming particle i with mass $m_i = \sqrt{E_i^2 - \mathbf{p_i}^2}$ and the incoming particle j with mass $m_j = \sqrt{E_j^2 - \mathbf{p_j}^2}$, respectively. The hadron interaction cross sections were either be tabulated, parametrized according to algebraic functions or extracted from other cross sections via general principles, such as isotopical invariance, detailed balance and additive quark model.

16.4.1 Hadron interaction tabulated and parametrized cross sections.

The total and elastic pp, pn, $\bar{p}p$, $\pi^{\pm}p$ and $K^{\pm}p$ cross sections are well known [1]. We tabulated pp and pn total and elastic cross sections at low energies $\sqrt{s_{i,j}} < 5$ GeV and at higher energies we use the CERN/HERA parametrizations [1]. The CERN/HERA parametrizations [1] are used to obtain the $\bar{p}p$ and $K^{+}p$ as well as the high energy non-resonance $\pi^{\pm}p$ and $K^{-}p$ total and elastic cross sections. The functional dependence of the total $\pi^{\pm}p$ and $K^{-}p$ cross sections on the total particle c.m. energy $\sqrt{s_{i,j}}$ shows at low energies the resonance behaviours. These cross sections are calculated. We calculate also nucleon-nucleon cross sections for resonance excitation processes. The calculation of other cross sections using general principles, such as isotopical invariance, detailed balance and additive quark model.

According to the detailed balance the cross sections of inverse $f \to i$ and direct $i \to f$ reactions, where i and f denote initial and final states, respectively, are related each other as follows:

$$\sigma_{f \to i} = \frac{\mathbf{p_i^2}}{\mathbf{p_f^2}} \frac{g_i}{g_f} \sigma_{i \to f}, \tag{16.7}$$

where $\mathbf{p_{i,f}^2}$ are the c. m. momenta of the initial and final states, $g_{i,f} = (2S_{i1,f1}+1)(2S_{i2,f2}+1)(2T_{i1,f1}+1)(2T_{i2,f2}+1)$ are denoting the spin-isospin degeneracy factors.

16.4.2 The interaction cross sections for meson-baryon collisions with quark annihilation.

The meson-baryon interactions going through quark annihilation are dominated by the formation of an intermediate resonance up to c.m. en-

ergies of 2.2 GeV. Thus the total meson-baryon cross section with quark annihilation can be approximated as follows [2]

$$\sigma_{tot}^{MB}(\sqrt{s_{MB}}) = \\ = \sum_{R=\Delta,N^*} < j_M, m_M, j_B, m_B || J_R, M_R > \frac{2T_R+1}{(2T_M+1)(2T_B+1)} \times \\ \times \frac{\pi}{p_{c.m.}^2} \frac{\Gamma_{tot}\Gamma_{R\to MB}}{(m_R-\sqrt{s_{MB}})^2+1/4\Gamma_{tot}^2} \qquad (16.8)$$

with the total and partial $\sqrt{s}$-dependent decay widths Γ_{tot} and $\Gamma_{R\to MB}$. In Eq. (16.8) $< j_M, m_M, j_B, m_B || J_R, M_R >$ denotes the Clebsch-Gordan coefficient determined by meson j_M, baryon j_B and resonance J_R angular momenta and their projections m_M, m_B and M_R, respectively. T_M, T_B and T_R are meson, baryon and resonance isospins, respectively, and $p_{c.m.}$ is c.m. momentum of incoming particles.

16.4.3 Nucleon-nucleon resonance interaction cross sections.

Up to incident beam energies of $4-5$ GeV/nucleon particle production in nucleon-nucleon collisions is dominated by resonance decays. To obtain resonance excitation cross sections we employ a practial approach of [2]. In this approach the resonance excitation cross sections are determined as

$$\sigma_{i,j\to k,l}(\sqrt{s_{i,j}}) = (2S_k+1)(2S_l+1)\frac{p_{k,l}}{p_{i,j}}\frac{1}{s_{i,j}}|M(\sqrt{s_{i,j}}, m_k, m_l)|^2, \qquad (16.9)$$

where S_k and S_l are spins of outgoing particles and $p_{k,l}$ and $p_{i,j}$ are ingoing and outgoing c.m. momenta. The matrix element $|M|^2$ is assumed to have no spin-dependence with free parameters are tuned [2] to experimental measurements.

16.5 Hadron collision simulation.

According to considered hadron interaction cross sections we should be able to simulate two-body hadron elastic scatterings as well as two-body inelastic scatterings and meson-barion resonance interaction.

16.5.1 Two-body hadron scatterings.

To simulate elastic scattering we need to know only the scattered angle distribution. To simulate the two-body scatterings with resonance excitation and deexcitation resonances we have to select a proper channel (according to calculated cross sections) and sample resonance mass (according to Breit-Wigner distribution with corresponding pole mass and pole width) and sample scattered angle.

It is assumed that angular distributions for all relevant two-body processes are similar and can be approximated by the differential cross-section of NN elastic scattering. This cross section is written in [2].

From knowledge of resonance interaction meson-baryon cross section we are able to select a resonance, which should be created at given initial energy.

16.6 Resonance decay simulation.

Resonance decay channels are sampled according to the partial decay widths $\Gamma(m)$, which depend from masses m of resonances. All resonances decay isotropically in their rest frame. If resonance is among the outgoing particles, its mass is first determined according to a Breit-Wigner mass distribution:

$$F(m) = \frac{1}{2\pi} \frac{\Gamma(m_R)}{(m_R - m)^2 + \Gamma(m_R)^2/4}. \tag{16.10}$$

All pole masses m_R and partial decay widths Γ_R are taken from the Review of Particle Properties [1]. If the exit channel contains three or four particles, then the respective N-body phase-space is taken into account for their momenta.

16.7 Phenomenological potentials.

We have taken into account mean field nuclear potentials for nucleons. Thus we have a possibility to consider nuclear absorption of these particles and therefore to calculate nucleus excitation energy as well as the number of excitons, particles and holes.

16.7.1 The nucleon potential.

For nucleons this potential is defined by sum of the Fermi-potential depends from the proton or neutron density $\rho(r)$ according to

$$T_F(r) = \frac{(\hbar c)^2 (3\pi^2 \rho(r))^{2/3}}{2m}, \tag{16.11}$$

where m is the nucleon mass in MeV and $\hbar c = 0.197327$ MeVfm, the binding energy $B(A, Z)$ and the Coulomb potential $V_C(Z, r)$ (for protons):

$$V_i(A, Z, r) = T_F(r) + B(A, Z) + V_C(Z, r). \tag{16.12}$$

Nucleons are transported along the straight line paths, i. e. the curvatures of nucleon trajectories in the nuclear and Coulomb potentials are neglected (Usualy the curvature effects are simplified in a cascade model by taken into account the refraction and reflection of nucleons due to a jump of potential [3]). The influence of intranuclear nucleons on the incoming nucleon is taken into account by adding to its kinetic energy this effective nuclear potential, i.e. the kinetic energy of a nucleon is calculated from the bottom of potential

well. For a proton leaving the nucleus the kinetic energy of this proton has to be sufficiently high to overcome the Coulomb barrier (in MeV) given by

$$V_C(A,Z) = C\frac{Z}{r_0(1+A^{1/3})}, \tag{16.13}$$

where $C = 1.44$ MeVfm and $r_0 = 1.2$ fm.

16.8 Pauli blocking procedure.

A free particle interaction cross section is reduced to an effective cross section by the Pauli-blocking due to Fermi statistics. For each collision the phase-space densities f_i, where i means fermion, in the final states should be checked in order to assure that the final distribution in phase space is in agreement with the Pauli principle, which rules out the posibility of finding more than one fermion in a single quantum state.

In this procedure, a nucleus with atomic number A and charge Z is treated as an ideal local completely degenerate Fermi gas of nucleons with coordinates $\mathbf{r}$, momenta $\mathbf{p}$. The nucleon phase-space density is approximated by

$$f_i(\mathbf{r},\mathbf{p}) = \Theta(\mathbf{p}_i^F(\mathbf{r}) - \mathbf{p}). \tag{16.14}$$

Because all states below Fermi-level are already occupyied, after each interaction one should check that the momenta $\mathbf{p'}_i$ of all secondary nucleons are above the Fermi-level, i. e.

$$p'_i > p_i^F(r). \tag{16.15}$$

If among the secondary nucleons there is a nucleon with momentum lower the the Fermi-level, then this collision is considered as prohibited (Pauli-blocked).

16.9 Residual nucleus parameters in the hadron-nucleus collision.

The number of nucleons A_{res} as well as the number of protons Z_{res} and total momentum P_{res} of the residual nucleus are determined by the relations:

$$A_{res} = A + q_p - \sum_{i=1}^{N_{out}} q_i^c, \tag{16.16}$$

$$Z_{res} = Z + e_p - \sum_{i=1}^{N_{out}} e_i^c, \tag{16.17}$$

$$\mathbf{P}_{res} = \mathbf{p}_p - \sum_{i=1}^{N_{out}} \mathbf{p_i^c}, \tag{16.18}$$

Here A, Z are the numbers of target nucleons and protons, $q_p, e_p, \mathbf{p}_p$ are the baryon number, the charge and momentum of incoming particle, respectively, and $q_i, e_i, \mathbf{p}_i$ denote, correspondingly, the baryon number, charge and momentum carried away by the ith outgoing particle and N_{out} is total number of the outgoing nucleons.

16.10 Calculation of a residual nucleus excitation energy.

The excitation energy U of the residual nucleus is defined as the energy above the ground state energy (mass) of residual nucleus. This energy is defined by sum of the particle kinetic energies T_p and hole kinetic energies T_h:

$$U = \sum_{i=1}^{N_p} T_p + \sum_{i=1}^{N_h} T_h, \tag{16.19}$$

where N_p is the number of "particles" and N_h is the number of "holes".

The located at r particle and hole energies are calculated from the Fermi energy $T_F(r)$. All cascade nucleons with kinetic energies above T_F and less than $T < T_F + B + V_C$, where $B(A, Z)$ is binding energy, V_C is Coulomb energy for proton, are called "particles". The "holes" are results of cascade interactions, when particles stroke nucleons from nucleus and they occupy states below T_F.

16.11 Status of this document.

9.10.98 created by N. Amelin.
27.01.99 revised by N. Amelin.

Bibliography

[1] Particle-Data-Group, Phys. Rev. **D54** 1 (1996).

[2] Bass S. A. *et al.*, Prog. Part. Nucl. Phys. **V. 41** 225 (1998).

[3] Barashenkov V. S., Iljinov A. S., Sobolevsky N. M., Toneev V. D., Usp. (Sov. Phys.), **16** 31 (1973).

Chapter 17

Precompound model.

17.1 Reaction initial state.

The GEANT4 precompound model is considered as an extension of the hadron kinetic model. It gives a possibility to extend the low energy range of the hadron kinetic model for nucleon-nucleus inelastic collision and it provides a "smooth" transition from kinetic stage of reaction described by the hadron kinetic model to the equilibrium stage of reaction described by the equilibrium deexcitation models.

The initial information for calculation of pre-compound nuclear stage consists from the atomic mass number A, charge Z of residual nucleus, its four momentum P_0, excitation energy U and number of excitons n equals the sum of number of particles p (from them p_Z are charged) and number of holes h.

At the preequilibrium stage of reaction, we following the [1] approach, take into account all possible nuclear transition the number of excitons n with $\Delta n = +2, -2, 0$ [1], which defined by transition probabilities. Only emmision of neutrons, protons, deutrons, thritium and helium nuclei are taken into account.

17.2 Simulation of pre-compound reaction.

The precompound stage of nuclear reaction is considered until nuclear system is not an equilibrium state. Further emission of nuclear fragments or photons from excited nucleus is simulated using an equilibrium model.

17.2.1 Statistical equilibrium condition.

In the state of statistical equilibrium, which is characterized by an eqilibrium number of excitons n_{eq}, all three type of transitions are equiprobable. Thus n_{eq} is fixed by $\omega_{+2}(n_{eq}, U) = \omega_{-2}(n_{eq}, U)$. From this condition we can

get

$$n_{eq} = \sqrt{0.5 + 2gU}. \tag{17.1}$$

17.2.2 Level density of excited (n-exciton) states.

To obtain Eq. (17.1) it was assumed an equidistant scheme of single-particle levels with the density $g \approx 0.595aA$, where a is the level density parameter, when we have the level density of the n-exciton state as

$$\rho_n(U) = \frac{g(gU)^{n-1}}{p!h!(n-1)!}. \tag{17.2}$$

17.2.3 Transition probabilities.

The partial transition probabilities changing the exciton number by Δn is determined by the squared matrix element averaged over allowed transitions $< |M|^2 >$ and the density of final states $\rho_{\Delta n}(n, U)$, which are really accessible in this transition. It can be defined as following:

$$\omega_{\Delta n}(n, U) = \frac{2\pi}{h} < |M|^2 > \rho_{\Delta n}(n, U). \tag{17.3}$$

The density of final states $\rho_{\Delta n}(n, U)$ were derived in paper [2] using the Eq. (17.2) for the level density of the n-exciton state and later corrected for the Pauli principle and indistinguishability of identical excitons in paper [3]:

$$\rho_{\Delta n=+2}(n, U) = \frac{1}{2}g\frac{[gU - F(p+1, h+1)]^2}{n+1}[\frac{gU - F(p+1, h+1)}{gU - F(p, h)}]^{n-1}, \tag{17.4}$$

$$\rho_{\Delta n=0}(n, U) = \frac{1}{2}g\frac{[gU - F(p, h)]}{n}[p(p-1) + 4ph + h(h-1)] \tag{17.5}$$

and

$$\rho_{\Delta n=-2}(n, U) = \frac{1}{2}gph(n-2), \tag{17.6}$$

where $F(p, h) = (p^2 + h^2 + p - h)/4 - h/2$ and it was taken to be equal zero. To avoid calculation of the averaged squared matrix element $< |M|^2 >$ it was assumed [1] that transition probability $\omega_{\Delta n=+2}(n, U)$ is the same as the probability for quasi-free scattering of a nucleon above the Fermi level on a nucleon of the target nucleus, i. e.

$$\omega_{\Delta n=+2}(n, U) = \frac{< \sigma(v_{rel})v_{rel} >}{V_{int}}. \tag{17.7}$$

In Eq. (17.7) the interaction volume is estimated as $V_{int} = \frac{4}{3}\pi(2r_c + \lambda/2\pi)^3$, with the De Broglie wave length $\lambda/2\pi$ corresponding to the relative velocity $< v_{rel} >= \sqrt{2T_{rel}/m}$, where m is nucleon mass and $r_c = 0.6$ fm.

The averaging in $< \sigma(v_{rel})v_{rel} >$ is further simplified by

$$< \sigma(v_{rel})v_{rel} >=< \sigma(v_{rel}) >< v_{rel} > . \tag{17.8}$$

For $\sigma(v_{rel})$ we take approximation:

$$\sigma(v_{rel}) = 0.5[\sigma_{pp}(v_{rel}) + \sigma_{pn}(v_{rel}]P(T_F/T_{rel}), \tag{17.9}$$

where factor $P(T_F/T_{rel})$ was introduced to take into account the Pauli principle. It is given by

$$P(T_F/T_{rel}) = 1 - \frac{7}{5}\frac{T_F}{T_{rel}} \tag{17.10}$$

for $\frac{T_F}{T_{rel}} \leq 0.5$ and

$$P(T_F/T_{rel}) = 1 - \frac{7}{5}\frac{T_F}{T_{rel}} + \frac{2}{5}\frac{T_F}{T_{rel}}(2 - \frac{T_{rel}}{T_F})^{5/2} \tag{17.11}$$

for $\frac{T_F}{T_{rel}} > 0.5$.

The free-particle proton-proton $\sigma_{pp}(v_{rel})$ and proton-neutron $\sigma_{pn}(v_{rel})$ interaction cross sections are estimated using the equations [4]:

$$\sigma_{pp}(v_{rel}) = \frac{10.63}{v_{rel}^2} - \frac{29.93}{v_{rel}} + 42.9 \tag{17.12}$$

and

$$\sigma_{pn}(v_{rel} = \frac{34.10}{v_{rel}^2} - \frac{82.2}{v_{rel}} + 82.2, \tag{17.13}$$

where cross sections are given in mbarn.

The mean relative kinetic energy T_{rel} is needed to calculate $< v_{rel} >$ and the factor $P(T_F/T_{rel})$ was computed as $T_{rel} = T_p + T_n$, where mean kinetic energies of projectile nucleons $T_p = T_F + U/n$ and target nucleons $T_N = 3T_F/5$, respecively.

Combining Eqs. (17.3) - (17.7) and assuming that $< |M|^2 >$ are the same for transitions with $\Delta n = 0$ and $\Delta n = \pm 2$ we obtain for another transition probabilities:

$$\omega_{\Delta n=0}(n, U) = \\ = \frac{<\sigma(v_{rel})v_{rel}>}{V_{int}}\frac{n+1}{n}[\frac{gU-F(p,h)}{gU-F(p+1,h+1)}]^{n+1}\frac{p(p-1)+4ph+h(h-1)}{gU-F(p,h)} \tag{17.14}$$

and

$$\omega_{\Delta n=-2}(n, U) = \\ = \frac{<\sigma(v_{rel})v_{rel}>}{V_{int}}[\frac{gU-F(p,h)}{gU-F(p+1,h+1)}]^{n+1}\frac{ph(n+1)(n-2)}{[gU-F(p,h)]^2}. \tag{17.15}$$

17.2.4 Emission probabilities for nucleons.

Emission process probability has been choosen similar as in the classical equilibrium Weisskopf-Ewing model [3]. Probability to emit nucleon b in the energy interval $(T_b, T_b + dT_b)$ is given

$$W_b(n, U, T_b) = \sigma_b(T_b)\frac{(2s_b+1)\mu_b}{\pi^2\hbar^3}R_b(p,h)\frac{\rho_{n-b}(E^*)}{\rho_n(U)}T_b, \tag{17.16}$$

where $\sigma_b(T_b)$ is the inverse (absorption of nucleon b) reaction cross section, s_b and m_b are nucleon spin and reduced mass, the factor $R_b(p,h)$ takes into account the condition for the exciton to be a proton or neutron, $\rho_{n-b}(E^*)$ and $\rho_n(U)$ are level densities of nucleus after and before nucleon emission are defined in the evaporation model, respectively and $E^* = U - Q_b - T_b$ is the excitation energy of nucleus after fragment emission.

17.2.5 Emission probabilities for complex fragments.

It was assumed [1] that nucleons inside excited nucleus are able to "condense" forming complex fragment. The "condensation" probability to create fragment consisting from N_b nucleons inside nucleus with A nucleons is given by

$$\gamma_{N_b} = N_b^3(V_b/V)^{N_b-1} = N_b^3(N_b/A)^{N_b-1}, \tag{17.17}$$

where V_b and V are fragment b and nucleus volumes, respectively. The last equation was estimated [1] as the overlap integral of (constant inside a volume) wave function of independent nucleons with that of the fragment.

During the prequilibrium stage a "condense" fragment can be emitted. The probability to emit a fragment can be written as [1]

$$W_b(n, U, T_b) = \gamma_{N_b}R_b(p,h)\frac{\rho(N_b, 0, T_b + Q_b)}{g_b(T_b)}\sigma_b(T_b)\frac{(2s_b+1)\mu_b}{\pi^2\hbar^3}\frac{\rho_{n-b}(E^*)}{\rho_n(U)}T_b, \tag{17.18}$$

where

$$g_b(T_b) = \frac{V_b(2s_b+1)(2\mu_b)^{3/2}}{4\pi^2\hbar^3}(T_b + Q_b)^{1/2} \tag{17.19}$$

is the single-particle density for complex fragment b, which is obtained by assuming that complex fragment moves inside volume V_b in the uniform potential well whose depth is equal to be Q_b, and the factor $R_b(p,h)$ garantees correct isotopic composition of a fragment b.

17.2.6 The total probability.

This probability is defined as

$$W_{tot}(n, U) = \sum_{\Delta n=+2,0,-2}\omega_{\Delta n}(n, U) + \sum_{b=1}^{6}W_b(n, U), \tag{17.20}$$

where total emission $W_b(n,U)$ probabilities to emit fragment b can be obtained from Eqs. (17.16) and (17.18) by integration over T_b:

$$W_b(n,U) = \int_{V_b}^{U-Q_b} W_b(n,U,T_b)dT_b. \tag{17.21}$$

17.2.7 Calculation of kinetic energies for emitted particle.

The equations (17.16) and (17.18) are used to sample kinetic energies of emitted fragment.

17.2.8 Parameters of residual nucleus.

After fragment emission we update parameter of decaying nucleus:

$$\begin{array}{c} A_f = A - A_b; Z_f = Z - Z_b; P_f = P_0 - p_b; \\ E_f^* = \sqrt{E_f^2 - \vec{P}_f^2} - M(A_f, Z_f). \end{array} \tag{17.22}$$

Here p_b is the evaporated fragment four momentum.

17.3 Status of this document.

3.11.98 created by N. Amelin.
3.02.99 revised by N. Amelin.

Bibliography

[1] Gudima K. K., Mashnik S. G., Toneev V. D., Nucl. Phys. **A401** 329 (1983).

[2] Williams F. C., Phys. Lett. **B31** 180 (1970).

[3] Ribanský I., Obložinský P., Bétaǩ E., Nucl. Phys. **A205** 545 (1973).

[4] Metropolis N. *et al.*, Phys. Rev. **100** 185 (1958).

[5] Weisskopf V. E., Ewing D. H. , Phys. Rev. 57 472 (1940).

Chapter 18

Evaporation model.

18.1 Reaction initial state.

The GEANT4 evaporation model is capable to predict final states as result of an excited nucleus with atomic number $A > 16$ break-up by the evaporation.

The initial information for calculation of evaporation stage consists from the atomic mass number A, charge Z of residual (e. g. after kinetic stage) nucleus, its four momentum P_0 and excitation energy E^*.

The evaporation of γ's,neutrons, protons, deutrons, thritiums, alphas, as well as the fission of heavy residual nuclei with $A > 65$ are taken into account.

18.2 Simulation of fragment evaporation.

The evaporation of neutron, proton, deutron, thritium and alpha fragments are taken into account.

18.2.1 Evaporation threshold.

One should take into account the energy condition for fragment emission, i. e. the nucleus excitation energy should be higher than the reaction threshold:

$$T_b^{\max} = E^* - Q_b - V_b > 0. \tag{18.1}$$

Here $T_b^{\max}$ is the maximal kinetic energy carried by emitted fragment b, $Q_b = M(A,Z) - M(A_f,Z_f) - M_b$ is the fragment b binding energy. V_b is the Coulomb potential energy, i. e. the Coulomb barrier for fragment b. $M(A,Z)$ is the mass of the initial nucleus, $M(A_f,Z_f)$ is the mass of the nucleus after emission of fragment b and M_b is the fragment b mass. It should be noted that expression (18.1) is only valid, when the recoil kinetic

energy equals zero. In our code we apply the condition:

$$T_b^{\max} = E_b^{\max} - M_b - V_b > 0, \tag{18.2}$$

where

$$E_b^{\max} = \frac{(M(A,Z)+E^*)^2 + M_b^2 - M^2(A_f,Z_f)}{2(M(A,Z)+E^*)}. \tag{18.3}$$

18.2.2 Nuclear and fragment mass defects.

We use neither the tabulated [1] or calculated according to the Cameron's liquid drop model formula [3] values of mass defects $dM(A,Z)$, $dM(A_f,Z_f)$ and dM_b, respectively.

18.2.3 Coulomb barrier calculation.

The Coulomb barrier:

$$V_b = C_b \frac{Z_b Z_f}{R_f + R_b}, \tag{18.4}$$

where $C_b = 1.44$ MeVfm, Z_b and R_b are charge and radius of nucleus after fragment emission, Z_f and R_f are charge and radius of fragment. The radii of nuclei are approximated by $R = r_C A^{1/3}$, where [**?**]

$$r_C = 2.173 \frac{1 + 0.006103 Z_b Z_f}{1 + 0.009443 Z_b Z_f}\ fm. \tag{18.5}$$

18.2.4 The fragment evaporation probability.

Evaporation process has been predicted by the statistical Weisskopf-Ewing model [3]. Probability to evaporate particle b in the energy interval $(T_b, T_b + dT_b)$ per unit of time is given

$$W_b(T_b) = \sigma_b(T_b) \frac{(2s_b+1)m_b}{\pi^2 h^3} \frac{\rho(E^* - Q_b - T_b)}{\rho(E^*)} T_b, \tag{18.6}$$

where $\sigma_b(T_b)$ is the inverse (absorption of particle b) reaction cross section, s_b and m_b are particle spin and mass, ρ is level densities of nucleus.

18.2.5 The inverse reaction cross section.

To calculate inverse reaction cross section it is assumed to have the form [4]

$$\sigma_b(T_b) = (1 + C_b)(1 - k_b V_b / T_b)\pi R^2 \tag{18.7}$$

for charged charged fragments with $A_f \leq 4$ interaction, where the k_b is the barrier penetration coefficient (its tabulated values are used), and

$$\sigma_b(T_b) = \alpha(1 + \beta/T_b)\pi R^2 \tag{18.8}$$

for neutrons. Here $R = r_0 A^{1/3}$ denotes the absorption radius, where $r_0 = 1.5$ fm, $\alpha = 0.76 + 2.2A^{-1/3}$ and $\beta = (2.12A^{-2/3} - 0.05)/(0.76 + 2.2A^{-1/3})$.

18.2.6 The level density.

The level density is approximated by Fermi-gas approach [**?**] for the nuclear level density:

$$\rho(E^*) = C\exp\left(2\sqrt{aE^*}\right), \tag{18.9}$$

where C is a constant, which does not depend from nucleus properties and excitation energy E^* and $a = A/8$ MeV^{-1} is the level density parameter.

18.2.7 The total evaporation probability.

The total probability W_b or total partial width $\Gamma_b = \hbar W_b$ to evaporate particle b can be obtained from Eq. (18.6) by integration over T_b:

$$W_b = \int_{V_b}^{E^*-Q_b} W_b(T_b)dT_b. \tag{18.10}$$

Here the summation is carried out over all excited states of the fragment.

Integration in Eq. (18.10) for probability to emit fragment b can be performed analiticaly, if we will use Eq. (18.7) for level density and the Eqs. (18.7)-(18.8) for inverse cross section. The probability to emit a charged particle:

$$\begin{gathered} W_b = \gamma_b A_b^{2/3} B\exp[-2\sqrt{aE^*}]\frac{(1+C_b)}{a_b^2}\{a_b T_b^{\max}[2\exp(2\sqrt{a_b T_b^{\max}})+1]- \\ -3\sqrt{a_b T_b^{\max}}\exp(2\sqrt{a_b T_b^{\max}}) - 3[1-\exp(2\sqrt{a_b T_b^{\max}})]/2\}, \end{gathered} \tag{18.11}$$

where T_b^{max} is defined by the equation (18.1). The following notations were introduced: $A_b = A - \Delta A_b$, $B = m_N r_0^2/(2\pi h^2)$, $\gamma_b = (2s_b+1)m_b/m_N$. ΔA_b is the number of nucleons in b particle. m_b, m_N and s_b are mass of particle b, mass of nucleon and spin of particle b respectively. The a_b is level density parameter for nucleus after emission of fragment b. Similarly for the neutron evaporation probability we obtain the following equation:

$$\begin{gathered} W_n = \gamma_n A_n^{2/3} B\frac{\alpha}{2a_n^2} \\ \exp[-2\sqrt{aE^*}+2\sqrt{a_n T_n^{\max}}][4a_n T_n^{\max}+(2a_n\beta-3)(2\exp(2\sqrt{a_n T_n^{\max}}-1)]. \end{gathered} \tag{18.12}$$

Using probabilities Eq. (18.11) and Eq. (18.12) we are able to choose randomly the type of emitted fragment.

18.2.8 Kinetic energy of emitted fragment.

The equation (18.6) can be used to sample kinetic energies of evaporated fragments. For example, keeping terms in Eq. (18.6), which depend from T_b and using the approximations for inverse cross section is given by Eq.

(18.7) and for level densities are given by Eq. (18.9), we obtain for charged fragments

$$W(x) = C_1 x \exp(2\sqrt{a(T_b^{\max} - x)} = C_2 T_b \exp(2\sqrt{aE^*}), \tag{18.13}$$

where C_1 and C_2 do not depend from T_b, $x = T_b - V_b$. To generate values of x we can use the next procedure, changing the expression for $W(x)$ to have $W(x^{\max}) = 1$ ($x^{\max} = [(a_b + T_b^{\max} + 1/4)^{1/2} - 1/2]/a_b$). Choose two random numbers ξ_1 and ξ_2 (distributed with equal probabilities between 0 and 1) and find kinetic energy of particle b as $T_b = T_b^{\max}\xi_1 + V_b$ at condition $\xi_2 \leq W(\xi_1 T_b^{\max})$. If this condition is not fulfilled we should choose another pair of random numbers.

18.2.9 Angular distribution of evaporated fragments.

We consider the angular distribution for emitted fragments as isotropical since we have no information about spin and polarization of nuclei.

18.2.10 Parameters of residual nucleus.

After fragment emission we update parameter of decaying nucleus:

$$\begin{gathered} A_f = A - A_b; Z_f = Z - Z_b; P_f = P_0 - p_b; \\ E_f^* = \sqrt{E_f^2 - \vec{P}_f^2} - M(A_f, Z_f). \end{gathered} \tag{18.14}$$

Here p_b is the evaporated fragment four momentum.

18.3 Fission probability calculation.

The fission decay channel (only for nuclei with $A > 65$) is taken into account as a competitor for fragment and photon evaporation channels.

18.3.1 The fission total probability.

hspace1.0emThe fission probability (per uni time) W_{fis} in the Bohr and Wheeler theory of fission [5] is proportional to the level density $\rho_{fis}(T)$ (approximation Eq. (18.9) is used) at the saddle point, i.e.

$$\begin{gathered} W_{fis} = \frac{1}{2\pi\hbar\rho_{fis}(E^*)} \int_0^{E^* - B_{fis}} \rho_{fis}(E^* - B_{fis} - T)dT = \\ = \frac{1 + (C_f - 1)\exp(C_f)}{4\pi a_{fis} \exp(2\sqrt{aE^*})}, \end{gathered} \tag{18.15}$$

where B_{fis} is the fission barrier height. The value of $C_f = 2\sqrt{a_{fis}(E^* - B_{fis})}$ and a, a_{fis} are the level density parameters of the compound and of the fission saddle point nuclei, respectively.

The value of the level density parameter is large at the saddle point, when excitation energy is given by initial excitation energy minus the fission barrier height, than in the ground state, i. e. $a_{fis} > a$. $a_{fis} = 1.08a$ for $Z < 85$, $a_{fis} = 1.04a$ for $Z \geq 89$ and $a_f = a[1.04 + 0.01(89. - Z)]$ for $85 \leq Z < 89$ is used.

18.3.2 The fission barrier.

The fission barrier is determined as difference between the saddle-point and ground state masses.

We use simple semiphenomenological approach was suggested by Barashenkov and Gereghi [6]. In their approach fission barrier $B_{fis}(A, Z)$ is approximated by

$$B_{fis} = B^0_{fis} + \Delta_g + \Delta_p. \tag{18.16}$$

The fission barrier height $B^0_{fis}(x)$ varies with the fissility parameter $x = Z^2/A$. $B^0_{fis}(x)$ is given by

$$B^0_{fis}(x) = 12.5 + 4.7(33.5 - x)^{0.75} \tag{18.17}$$

for $x \leq 33.5$ and

$$B^0_{fis}(x) = 12.5 - 2.7(x - 33.5)^{2/3} \tag{18.18}$$

for $x > 33.5$. The $\Delta_g = \Delta M(N) + \Delta M(Z)$, where $\Delta M(N)$ and $\Delta M(Z)$ are shell corrections for Cameron's liquid drop mass formula [3] and the pairing energy corrections: $\Delta_p = 1$ for odd-odd nuclei, $\Delta_p = 0$ for odd-even nuclei, $\Delta_p = 0.5$ for even-odd nuclei and $\Delta_p = -0.5$ for even-even nuclei.

18.4 The total probability for γ evaporation.

As the first approximation we assume that dipole $E1$–transitions is the main source of γ–quanta from highly–excited nuclei [7]. The probability to evaporate γ in the energy interval $(\epsilon_\gamma, \epsilon_\gamma + d\epsilon_\gamma)$ per unit of time is given

$$W_\gamma(\epsilon_\gamma) = \frac{1}{\pi^2(\hbar c)^3}\sigma_\gamma(\epsilon_\gamma)\frac{\rho(E^* - \epsilon_\gamma)}{\rho(E^*)}\epsilon^2_\gamma, \tag{18.19}$$

where $\sigma_\gamma(\epsilon_\gamma)$ is the inverse (absorption of γ) reaction cross section, ρ is a nucleus level density is defined by Eq. (18.9).

The photoabsorption reaction cross section is given by the expression

$$\sigma_\gamma(\epsilon_\gamma) = \frac{\sigma_0\epsilon^2_\gamma\Gamma^2_R}{(\epsilon^2_\gamma - E^2_{GDP})^2 + \Gamma^2_R\epsilon^2_\gamma}, \tag{18.20}$$

where $\sigma_0 = 2.5A$ mb, $\Gamma_R = 0.3E_{GDP}$ and $E_{GDP} = 40.3A^{-1/5}$ MeV are empirical parameters of the giant dipole resonance [7]. The total radiation

probability is

$$W_\gamma = \frac{3}{\pi^2(\hbar c)^3}\int_0^{E^*}\sigma_\gamma(\epsilon_\gamma)\frac{\rho(E^*-\epsilon_\gamma)}{\rho(E^*)}\epsilon_\gamma^2 d\epsilon_\gamma. \qquad (18.21)$$

The integration is performed numericaly.

18.4.1 Energy of evaporated photon.

The energy of γ-quantum is sampled according to the Eq. (18.19) distribution.

18.5 Discrete photon evaporation.

The last step of evaporation cascade consists of evaporation of photons with discrete energies. The competition between photons and fragments as well as giant resonance photons is neglected at this step. We consider the discrete E1, M1 and E2 photon transitions from tabulated isotopes. There are large number of isotopes [8] with the experimentally measured exited level energies, spins, parities and relative transitions probabilities. This information is implemented in the code.

18.6 Status of this document.

19.10.98 created by N. Amelin.
14.02.99 revised by N. Amelin.

Bibliography

[1] Audi G., Wapstra A. H., Nucl. Phys. **A595** V. 4 409 (1995).

[2] Cameron A. G. W. Canad. J. Phys., **35** 1021 (1957), **36** 1040 (1958).

[3] Weisskopf V. E., Ewing D. H. , Phys. Rev. 57 472 (1940).

[4] Dostrovsky L. I., Fraenkel Z., Friedlander G., Phys. Rev. **116** 683 (1959).

[5] Bohr N., Wheeler J. W., Phys. Rev., **56** 426 (1939).

[6] Barashenkov V. S., Iljinov A. S., Toneev V. D., Gereghi F. G, Nucl. Phys. **A206** 131 (1973).

[7] Iljinov A. S. *et al.*, Nucl. Phys. A543 517 (1992).

[8] Evaluated Nuclear Structure Data File (ENSDF) - a computer file of evaluated experimental nuclear structure data maintained by the National Nuclear Data Center, Brookhaven National Laboratory (http://www.nndc.bnl.gov/nndc/nudat/).

Chapter 19

Fission model.

19.1 Reaction initial state.

The GEANT4 fission model is capable to predict final excited fragments as result of an excited nucleus symmetric or asymmetric fission. The fission process (only for nuclei with atomic number $A \geq 65$) is considered as a competitor for evaporation process, when nucleus transits from an excited state to the ground state.

The initial information for calculation of fission decay consists from the atomic mass number A, charge Z of excited nucleus, its four momentum P_0 and excitation energy U.

19.2 Fission process simulation.

19.2.1 Atomic number distribution of fission products.

As follows from experimental data [1] mass distribution of fission products consists of the symmetric and the asymmetric components:

$$F(A_f) = F_{sym}(A_f) + \omega F_{asym}(A_f), \tag{19.1}$$

where $\omega(U, A, Z)$ defines relative contribution of each component and it depends from excitation energy U and A, Z of fissioning nucleus. It was found in [2] that experimental data can be approximated with a good accuracy, if one take

$$F_{sym}(A_f) = \exp\,[-\frac{(A_f - A_{sym})^2}{2\sigma_{sym}^2}] \tag{19.2}$$

and

$$\begin{aligned} F_{asym}(A_f) = \exp\,[-\tfrac{(A_f-A_2)^2}{2\sigma_2^2}] + \exp\,[-\tfrac{A_f-(A-A_2)^2}{2\sigma_2^2}] + \\ +C_{asym}\{\exp\,[-\tfrac{(A_f-A_1)^2}{2\sigma_1^2}] + \exp\,[-\tfrac{A_f-(A-A_1)^2}{2\sigma_2^2}]\}, \end{aligned} \tag{19.3}$$

where $A_{sym} = A/2$, A_1 and A_2 are the mean values and σ^2_{sim}, σ^2_1 and σ^2_2 are dispertions of the Gaussians respectively. From an analysis of experimental data [2] the parameter $C_{asym} \approx 0.5$ was defined and the next values for dispersions:

$$\sigma^2_{sym} = \exp(0.00553U + 2.1386), \tag{19.4}$$

where U in MeV,

$$2\sigma_1 = \sigma_2 = 5.6\ MeV \tag{19.5}$$

for $A \leq 235$ and

$$2\sigma_1 = \sigma_2 = 5.6 + 0.096(A - 235)\ MeV \tag{19.6}$$

for $A > 235$ were found.

The weight $\omega(U, A, Z)$ was approximated as follows

$$\omega = \frac{\omega_a - F_{asym}(A_{sym})}{1 - \omega_a F_{sym}((A_1 + A_2)/2)}. \tag{19.7}$$

The values of ω_a for nuclei with $96 \geq Z \geq 90$ were approximated by

$$\omega_a(U) = \exp(0.538U - 9.9564) \tag{19.8}$$

for $U \leq 16.25$ MeV,

$$\omega_a(U) = \exp(0.09197U - 2.7003) \tag{19.9}$$

for $U > 16.25$ MeV and

$$\omega_a(U) = \exp(0.09197U - 1.08808) \tag{19.10}$$

for $z = 89$. For nuclei with $Z \leq 88$ the authors of [2] constracted the following approximation:

$$\omega_a(U) = \exp[0.3(227 - a)] \exp\{0.09197[U - (B_{fis} - 7.5)] - 1.08808\}, \tag{19.11}$$

where for $A > 227$ and $U < B_{fis} - 7.5$ the corresponding factors occuring in exponential functions vanish.

19.2.2 Charge distribution of fission products.

At given mass of fragment A_f the experimental data [1] on the charge Z_f distribution of fragments are well approximated by Gaussian with dispertion $\sigma^2_z = 0.36$ and the average $< Z_f >$ is described by expression:

$$< Z_f >= \frac{A_f}{A} Z + \Delta Z, \tag{19.12}$$

when parameter $\Delta Z = -0.45$ for $A_f \geq 134$, $\Delta Z = -0.45(A_f - A/2)/(134 - A/2)$ for $A - 134 < A_f < 134$ and $\Delta Z = 0.45$ for $A \leq A - 134$.

After sampling of fragment atomic masses numbers and fragment charges, we have to check that fragment ground state masses do not exceed initial energy and calculate the maximal fragment kinetic energy

$$T^{max} < U + M(A,Z) - M_1(A_{f1},Z_{f1}) - M_2(A_{f2},Z_{f2}), \tag{19.13}$$

where U and $M(A,Z)$ are the excitation energy and mass of initial nucleus, $M_1(A_{f1},Z_{f1})$, and $M_2(A_{f2},Z_{f2})$ are masses of the first and second fragment, respectively.

19.2.3 Kinetic energy distribution of fission products.

We use the empiricaly defined [3] dependence of the average kinetic energy $< T_{kin} >$ (in MeV) of fission fragments on the mass and the charge of a fissioning nucleus:

$$< T_{kin} >= 0.1178Z^2/A^{1/3} + 5.8. \tag{19.14}$$

This energy is distributed differently in cases of symmetric and asymmetric modes of fission. It follows from the analysis of data [2] that in the asymmetric mode, the average kinetic energy of fragments is higher than that in the symmetric one by approximately 12.5 MeV. To approximate the average numbers of kinetic energies $< T_{kin}^{sym}$ and $< T_{kin}^{asym} >$ for the symmetric and asymmetric modes of fission the authors of [2] suggested empirical expressions:

$$< T_{kin}^{sym} >=< T_{kin} > -12.5W_{asim}, \tag{19.15}$$

$$< T_{kin}^{asym} >=< T_{kin} > +12.5W_{sim}, \tag{19.16}$$

where

$$W_{sim} = \omega \int F_{sim}(A)dA / \int F(A)dA \tag{19.17}$$

and

$$W_{asim} = \int F_{asim}(A)dA / \int F(A)dA, \tag{19.18}$$

respectively. In the symmetric fission the experimental data for the ratio of the average kinetic energy of fission fragments $< T_{kin}(A_f) >$ to this maximum energy $< T_{kin}^{max} >$ as a function of the mass of a larger fragment A_{max} can be approximated by expressions

$$< T_{kin}(A_f) > / < T_{kin}^{max} >= 1 - k[(A_f - A_{max})/A]^2 \tag{19.19}$$

for $A_{sim} \leq A_f \leq A_{max} + 10$ and

$$< T_{kin}(A_f) > / < T_{kin}^{max} >= 1 - k(10/A)^2 - 2(10/A)k(A_f - A_{max} - 10)/A \tag{19.20}$$

for $A_f > A_{max} + 10$, where $A_{max} = A_{sim}$ and $k = 5.32$ and $A_{max} = 134$ and $k = 23.5$ for symmetric and asymmetric fission respectively. For both modes

of fission the distribution over the kinetic energy of fragments T_{kin} is choosen Gaussian with their own average values $< T_{kin}(A_f) >=< T_{kin}^{sym}(A_f) >$ or $< T_{kin}(A_f) >=< T_{kin}^{asym}(A_f) >$ and dispersions σ_{kin}^2 equal 8^2 MeV or 10^2 MeV^2 for symmetrical and asymmetrical modes, respectively.

19.2.4 Calculation of the excitation energy of fission products.

The total excitation energy of fragments U_{frag} can be defined according to equation:

$$U_{frag} = U + M(A,Z) - M_1(A_{f1},Z_{f1}) - M_2(A_{f2},Z_{f2}) - T_{kin}, \qquad (19.21)$$

where U and $M(A,Z)$ are the excitation energy and mass of initial nucleus, T_{kin} is the fragments kinetic energy, $M_1(A_{f1},Z_{f1})$, and $M_2(A_{f2},Z_{f2})$ are masses of the first and second fragment, respectively.

The value of excitation energy of fragment U_f determines the fragment temperature ($T = \sqrt{U_f/a_f}$, where $a_f \sim A_f$ is the parameter of fragment level density). Assuming that after disintegration fragments have the same temperature as initial nucleus than the total excitation energy will be distributed between fragments in proportion to their mass numbers one obtains

$$U_f = U_{frag}\frac{A_f}{A}. \qquad (19.22)$$

19.2.5 Excited fragment momenta.

Assuming that fragment kinetic energy $T_f = P_f^2/(2(M(A_f,Z_f+U_f)$ we are able to calculate the absolute value of fragment c.m. momentum

$$P_f = \frac{(M_1(A_{f1},Z_{f1}+U_{f1})(M_2(A_{f2},Z_{f2}+U_{f2})}{M_1(A_{f1},Z_{f1})+U_{f1}+M_2(A_{f2},Z_{f2})+U_{f2}}T_{kin}. \qquad (19.23)$$

and its components, assuming fragment isotropical distribution.

19.3 Status of this document.

22.10.98 created by N. Amelin.
12.02.99 reviseed by N. Amelin.

Bibliography

[1] Vandenbosch R., Huizenga J. R., Nuclear Fission, Academic Press, New York, 1973.

[2] Adeev G. D. *et al.* Preprint INR 816/93, Moscow, 1993.

[3] Viola V. E., Kwiatkowski K. and Walker M, Phys. Rev. **C31** 1550 (1985).

Chapter 20

Fermi break-up model.

20.1 Fermi break-up simulation for light nuclei.

The GEANT4 Fermi break-up model is capable to predict final states as result of an excited nucleus with atomic number $A < 17$ statistical break-up.

For light nuclei the values of excitation energy per nucleon are often comparable with nucleon binding energy. Thus a light excited nucleus breaks into two or more fragments with branching given by available phase space. To describe a process of nuclear disassembling the so-called Fermi break-up model is used [1], [2], [3]. This statistical approach was first used by Fermi [1] to describe the multiple production in high energy nucleon collision.

The initial information for calculation of break-up stage consists from the atomic mass number A, charge Z and number of neutrons N of excited nucleus and its excitation energy U. The total energy of nucleus in the rest system is $E = U + M(A, Z)$.

20.1.1 Masses of nuclei.

The tabulated and calculated according to the liquid drop model [3] values of mass defects $\Delta M(A, Z)$ are used to calculate the masses of nuclei $M(A, Z)$ in ground states.

20.1.2 Allowed channel.

The channel will be allowed for decay, if the total kinetic energy E_{kin} of all fragments of the given channel at the moment of break-up is positive. This energy can be calculated according to equation:

$$E_{kin} = U + M(A, Z) - E_{Coulomb} - \sum_{b=1}^{n}(m_b + \epsilon_b), \qquad (20.1)$$

m_b and ϵ_b are masses and excitation energies of fragments, respectively, $E_{Coulomb}$ is the Coulomb barrier for a given channel. It is approximated by

$$E_{Coulomb} = \frac{3}{5}\frac{e^2}{r_0}(1+\frac{V}{V_0})^{-1/3}(\frac{Z^2}{A^{1/3}} - \sum_{b=1}^{n}\frac{Z^2}{A_b^{1/3}}), \tag{20.2}$$

where V_0 is the volume of the system corresponding to the normal nuclear matter density and $\kappa = \frac{V}{V_0}$ is a parameter ($\kappa = 1$ is used).

20.1.3 Break-up probability.

The total probability for nucleus to break-up into n componets (nucleons, deutrons, tritons, alphas etc) in the final state is given by

$$W(E,n) = (V/\Omega)^{n-1}\rho_n(E), \tag{20.3}$$

where $\rho_n(E)$ is the density of a number of final states, V is the volume of decaying system and $\Omega = (2\pi\hbar)^3$ is the normalization volume. The density $\rho_n(E)$ can be defined as a product of three factors:

$$\rho_n(E) = M_n(E)S_nG_n. \tag{20.4}$$

The first one is the phase space factor defined as

$$M_n = \int_{-\infty}^{+\infty}...\int_{-\infty}^{+\infty}\delta(\sum_{b=1}^{n}\mathbf{p_b})\delta(E-\sum_{b=1}^{n}\sqrt{p^2+m_b^2})\prod_{b=1}^{n}d^3p_b, \tag{20.5}$$

where $\mathbf{p_b}$ is fragment b momentum. The second one is the spin factor

$$S_n = \prod_{b=1}^{n}(2s_b+1), \tag{20.6}$$

which gives the number of states with different spin orientations. The last one is the permutation factor

$$G_n = \prod_{j=1}^{k}\frac{1}{n_j!}, \tag{20.7}$$

which takes into account identity of components in final state. n_j is a number of components of j- type particles and k is defined by $n = \sum_{j=1}^{k} n_j$).

In non-relativistic case (Eq. (20.10) the integration in Eq. (20.5) can be evaluated analiticaly (see e. g. [5]). The probability for a nucleus with energy E disassembling into n fragments with masses m_b, where $b = 1,2,3,...,n$ equals

$$W(E_{kin},n) = S_nG_n(\frac{V}{\Omega})^{n-1}(\frac{1}{\sum_{b=1}^{n}m_b}\prod_{b=1}^{n}m_b)^{3/2}\frac{(2\pi)^{3(n-1)/2}}{\Gamma(3(n-1)/2)}E_{kin}^{3n/2-5/2}, \tag{20.8}$$

where $\Gamma(x)$ is the gamma function.

20.1.4 Fermi break-up model parameter.

Thus the Fermi break-up model has only one free parameter V is the volume of decaying system, which can be calculated as follows:

$$V = 4\pi R^3/3 = 4\pi r_0^3 A/3, \tag{20.9}$$

where $r_0 = 1.4$ fm is used.

20.1.5 Fragment characteristics.

We take into account the formation of fragments in their ground and low-lying excited states, which are stable for nucleon emission. However, several unstable fragments with large lifetimes: ^5He, ^5Li, ^8Be, ^9B etc are also considered. Fragment characteristics A_b, Z_b, s_b and ϵ_b are taken from [6].

20.1.6 MC procedure.

The nucleus break-up is described by the Monte Carlo (MC) procedure. We randomly (according to probability Eq. (20.8) and condition Eq. (20.1)) select decay channel. Then for given channel we calculate kinematical quantities of each fragment according to n-body phase space distribution:

$$M_n = \int_{-\infty}^{+\infty} ... \int_{-\infty}^{+\infty} \delta(\sum_{b=1}^{n} \mathbf{p_b}) \delta(\sum_{b=1}^{n} \frac{p_b^2}{2m_b} - E_{kin}) \prod_{b=1}^{n} d^3 p_b. \tag{20.10}$$

The Kopylov's sampling procedure [7] is applied. The angular distributions for emitted fragments are considered to be isotropical.

20.2 Status of this document.

1.11.98 created by N. Amelin.
1.02.99 revised by N. Amelin.

Bibliography

[1] Fermi E., Prog. Theor. Phys. **5** 1570 (1950).

[2] Kretschmar M. Annual Rev. Nucl. Sci. **11** 1 (1961).

[3] Epherre M., Gradsztajn E., J. Physique **18** 48 (1967).

[4] Cameron A. G. W. Canad. J. Phys., **35** 1021 (1957), **36** 1040 (1958).

[5] Barashenkov V. S., Barbashov B. M., Bubelev E. G. Nuovo Cimento, **7** 117 (1958).

[6] Ajzenberg-Selone F., Nucl. Phys. 1 **360** (1981); **A375** (1982); **392** (1983); **A413** (1984); **A433** (1985).

[7] Kopylov G. I., Principles of resonance kinematics, Moscow, Nauka, 1970 (in Russian).

Chapter 21

Multifragmentation model.

21.1 Multifragmentation process simulation.

The GEANT4 multifragmentation model is capable to predict final states as result of an highly excited nucleus statistical break-up.

The initial information for calculation of multifragmentation stage consists from the atomic mass number A, charge Z of excited nucleus and its excitation energy U. At high excitation energies $U/A > 3$ MeV the multifragmentation mechanism, when nuclear system can eventually breaks down into fragments, becomes the dominant. Later on the excited primary fragments propagate independently in the mutual Coulomb field and undergo de-excitation. Detailed description of multifragmentation mechanism and model can be found in review [1].

21.1.1 Multifragmentation probability.

The probability of a breakup channel b is given by the expression (in the so-called microcanonical approach [1], [2]):

$$W_b(U, A, Z) = \frac{1}{\sum_b \exp[S_b(U, A, Z)]} \exp[S_b(U, A, Z)], \tag{21.1}$$

where $S_b(U, A, Z)$ is the entropy of a multifragment state corresponding to the breakup channel b. The channels $\{b\}$ can be parametrized by set of fragment multiplicities N_{A_f,Z_f} for fragment with atomic number A_f and charge Z_f. All partitions $\{b\}$ should satisfy constraints on the total mass and charge:

$$\sum_f N_{A_f,Z_f} A_f = A \tag{21.2}$$

and

$$\sum_f N_{A_f,Z_f} Z_f = Z. \tag{21.3}$$

It is assumed [2] that thermodynamic equilibrium is established in every channel, which can be characterized by the channel temperature T_b.

The channel temperature T_b is determined by the equation constraining the average energy $E_b(T_b, V)$ associated with partition b:

$$E_b(T_b, V) = U + E_{ground} = U + M(A, Z), \tag{21.4}$$

where V is the system volume, E_{ground} is the ground state (at $T_b = 0$) energy of system and $M(A, Z)$ is the mass of nucleus.

To calculate mass $M(A, Z)$ of the initial nucleus and mass $M(A_b, Z_b)$ of the nucleus after emission of fragment b the so-called Cameron's liquid drop model formula [3], which includes shell and pairing effects corrections.

According to the conventional thermodinamical formulae the average energy of a partitition b is expressed through the system free energy F_b as follows

$$E_b(T_b, V) = F_b(T_b, V) + T_b S_b(T_b, V). \tag{21.5}$$

Thus, if free energy F_b of a partition b is known, we can find the channel temperature T_b from Eqs. (21.4) and (21.5), then the entropy $S_b = -dF_b/dT_b$ and hence, decay probability W_b defined by Eq. (21.1) can be calculated.

Calculation of the free energy is based on the use of the liquid-drop description of individual fragments [2]. The free energy of a partition b can be splitted into several terms:

$$F_b(T_b, V) = \sum_f F_f(T_b, V) + E_C(V), \tag{21.6}$$

where $F_f(T_b, V)$ is the average energy of an individual fragment including the volume

$$F_f^V = [-E_0 - T_b^2/\epsilon(A_f)]A_f, \tag{21.7}$$

surface

$$F_f^{Sur} = \beta_0[(T_c^2 - T_b^2)/(T_c^2 + T_b^2)]^{5/4} A_f^{2/3} = \beta(T_b)A_f^{2/3}, \tag{21.8}$$

symmetry

$$F_f^{Sim} = \gamma(A_f - 2Z_f)^2/A_f, \tag{21.9}$$

Coulomb

$$F_f^C = \frac{3}{5}\frac{Z_f^2 e^2}{r_0 A_f^{1/3}}[1 - (1 + \kappa_C)^{-1/3}] \tag{21.10}$$

and translational

$$F_f^t = -T_b \ln (g_f V_f/\lambda_{T_b}^3) + T_b \ln (N_{A_f,Z_f}!)/N_{A_f,Z_f} \tag{21.11}$$

terms and the last term

$$E_C(V) = \frac{3}{5}\frac{Z^2 e^2}{R} \tag{21.12}$$

is the Coulomb energy of the uniformly charged sphere with charge Ze and the radius $R = (3V/4\pi)^{1/3} = r_0 A^{1/3}(1+\kappa_C)^{1/3}$, where $\kappa_C = 2$ [2].

Parameters $E_0 = 16$ MeV, $\beta_0 = 18$ MeV, $\gamma = 25$ MeV are the coefficients of the Bethe-Weizsacker mass formula at $T_b = 0$. $g_f = (2S_f+1)(2I_f+1)$ is a spin S_f and isospin I_f degeneracy factor for fragment (fragments with $A_f > 1$ are treated as the Boltzmann particles), $\lambda_{T_b} = (2\pi h^2/m_N T_b)^{1/2}$ is the thermal wavelength, m_N is the nucleon mass, $r_0 = 1.17$ fm, $T_c = 18$ MeV is the critical temperature, which corresponds to the liquid-gas phase transition. $\epsilon(A_f) = \epsilon_0[1+3/(A_f-1)]$ is the inverse level density of the mass A_f fragment and $\epsilon_0 = 16$ MeV is considered as a variable model parameter, whose value depends on the fraction of energy transferred to the internal degrees of freedom of fragments [2]. The free volume $V_f = \kappa V = \kappa\frac{4}{3}\pi r_0^4 A$ available to the translational motion of fragment, where $\kappa \approx 1$ and its dependence on the multiplicity of fragments was taken from [2]:

$$\kappa = [1 + \frac{1.44}{r_0 A^{1/3}}(M^{1/3} - 1)]^3 - 1. \tag{21.13}$$

For $M = 1$ $\kappa = 0$.

The light fragments with $A_f < 4$, which have no excited states, are considered as elementary particles characterized by the empirical masses M_f, radii R_f, binding energies B_f, spin degeneracy factors g_f of ground states. They contribute to the translation free energy and Coulomb energy.

21.1.2 Direct simulation of the low multiplicity multifragment disintegration.

At comparatively low excitation energy (temperature) system will disintegrate into a small number of fragments $M \leq 4$ and number of channel is not huge. For such situation a direct (microcanonical) sorting of all decay channels can be performed. Then, using Eq. (21.1), the average multiplicity value $< M >$ can be found. To check that we really have the situation with the low excitation energy, the obtained value of $< M >$ is examined to obey the inequality $< M > \leq M_0$, where $M_0 = 3.3$ and $M_0 = 2.6$ for $A \sim 100$ and for $A \sim 200$, respectively [2]. If the discussed inequality is fulfilled, then the set of channels under consideration is belived to be able for a correct description of the break up. Then using calculated according Eq. (21.1) probabilities we can randomly select a specific channel with given values of A_f and Z_f.

21.1.3 Fragment multiplicity distribution.

The individual fragment multiplicities N_{A_f,Z_f} in the so-called macro-canonical ensemble [1] are distributed according to the Poisson distribution:

$$P(N_{A_f,Z_f}) = \exp\left(-\omega_{A_f,Z_f}\right)\frac{\omega_{A_f,Z_f}^{N_{A_f,Z_f}}}{N_{A_f,Z_f}!} \tag{21.14}$$

with mean value $< N_{A_f,Z_f} >= \omega_{A_f,Z_f}$ defined as

$$< N_{A_f,Z_f} >= g_f A_f^{3/2}\frac{V_f}{\lambda_{T_b}^3}\exp\left[\frac{1}{T_b}(F_f(T_b,V) - F_f^t(T_b,V) - \mu A_f - \nu Z_f)\right], \tag{21.15}$$

where μ and ν are chemical potentials. The chemical potential are found by substituting Eq. (21.15) into the system of constraints:

$$\sum_f < N_{A_f,Z_f} > A_f = A \tag{21.16}$$

and

$$\sum_f < N_{A_f,Z_f} > Z_f = Z \tag{21.17}$$

and solving it by iteration.

21.1.4 Atomic number distribution of fragments.

Fragment atomic numbers $A_f > 1$ are also distributed according to the Poisson distribution [1] (see Eq. (21.14)) with mean value $< N_{A_f} >$ defined as

$$< N_{A_f} >= A_f^{3/2}\frac{V_f}{\lambda_{T_b}^3}\exp\left[\frac{1}{T_b}(F_f(T_b,V) - F_f^t(T_f,V) - \mu A_f - \nu < Z_f >)\right], \tag{21.18}$$

where calculating the internal free energy $F_f(T_b,V) - F_f^t(T_b,V)$ one has to substitute $Z_f \rightarrow < Z_f >$. The average charge $< Z_f >$ for fragment having atomic number A_f is given by

$$< Z_f(A_f) >= \frac{(4\gamma + \nu)A_f}{8\gamma + 2[1 - (1+\kappa)^{-1/3}]A_f^{2/3}}. \tag{21.19}$$

21.1.5 Charge distribution of fragments.

At given mass of fragment $A_f > 1$ the charge Z_f distribution of fragments are described by Gaussian

$$P(Z_f(A_f)) \sim \exp\left[-\frac{(Z_f(A_f) - < Z_f(A_f) >)^2}{2(\sigma_{Z_f}(A_f))^2}\right] \tag{21.20}$$

with dispertion

$$\sigma_{Z_f(A_f)} = \sqrt{\frac{A_f T_b}{8\gamma + 2[1-(1+\kappa)^{-1/3}]A_f^{2/3}}} \approx \sqrt{\frac{A_f T_b}{8\gamma}}. \qquad (21.21)$$

and the average charge $< Z_f(A_f) >$ defined by Eq. (21.17).

21.1.6 Kinetic energy distribution of fragments.

It is assumed [2] that at the instant of the nucleus break-up the kinetic energy of the fragment T^f_{kin} in the rest of nucleus obeys the Boltzmann distribution at given temperature T_b:

$$\frac{dP(T^f_{kin})}{dT^f_{kin}} \sim \sqrt{T^f_{kin}} \exp\left(-T^f_{kin}/T_b\right). \qquad (21.22)$$

Under assumption of thermodynamic equilibrium the fragment have isotropic velocities distribution in the rest frame of nucleus. The total kinetic energy of fragments should be equal $\frac{3}{2}MT_b$, where M is fragment multiplicity, and the total fragment momentum should be equal zero. These conditions are fullfilled by choosing properly the momenta of two last fragments.

The initial conditions for the divergence of the fragment system are determined by random selection of fragment coordinates distributed with equal probabilities over the break-up volume $V_f = \kappa V$. It can be a sphere or prolongated ellipsoid. Then Newton's equations of motion are solved for all fragments in the self-consistent time-dependent Coulomb field [2]. Thus the asymptotic energies of fragments determined as result of this procedure differ from the initial values by the Coulomb repulsion energy.

21.1.7 Calculation of the fragment excitation energies.

The temparature T_b determines the average excitation energy of each fragment:

$$U_f(T_b) = E_f(T_b) - E_f(0) = \frac{T_b^2}{\epsilon_0} A_f + [\beta(T_b) - T_b \frac{d\beta(T_b)}{dT_b} - \beta_0] A_f^{2/3}, \quad (21.23)$$

where $E_f(T_b)$ is the average fragment energy at given temperature T_b and $\beta(T_b)$ is defined in Eq. (21.8). There is no excitation for fragment with $A_f < 4$, for ^4He excitation energy was taken as $U_{^4He} = 4T_b^2/\epsilon_o$.

21.2 Status of this document.

4.11.98 created by N. Amelin.
16.02.9 revised by N. Amelin.

Bibliography

[1] Bondorf J. P., Botvina A. S., Iljinov A. S., Mishustin I. N., Sneppen K., Phys. Rep. **257** 133 (1995).

[2] Botvina A. S. *et al.*, Nucl. Phys. **A475** 663 (1987).

[3] Cameron A. G. W. Canad. J. Phys., **35** 1021 (1957), **36** 1040 (1958).

Chapter 22

Low Energy Neutron Interactions

22.1 Introduction

The neutron transport class library described here simulates the interactions of neutrons with kinetic energies from thermal energies up to O(20 MeV). The upper limit is set by the comprehensive evaluated neutron scattering data libraries that the simulation is based on. The result is a set of secondary particles that can be passed on to the tracking sub-system for further geometric tracking within geant4.

The interactions of neutrons at low energies are split into four parts in analogy to the other hadronic processes in geant4. We consider radiative capture, elastic scattering, fission, and inelastic scattering as separate models. These models comply with the interface for use with the geant4 hadronic processes which enables their transparent use within the geant4 tool-kit together with all other geant4 compliant hadronic shower models.

22.2 Physics and Verification

22.2.1 Inclusive Cross-sections

All cross-section data are taken from the ENDF/B-VI[1] evaluated data library.

All inclusive cross-sections are treated as point-wise cross-sections for reasons of performance. For this purpose, the data from the evaluated data library have been processed, to explicitly include all neutron nuclear resonances in the form of point-like cross-sections rather than in the form of parametrisations. The resulting data have been transformed into a linearly interpolable format, such that the error due to linear interpolation between adjacent data points is smaller than a few percent.

The inclusive cross-sections comply with the cross-sections data set interface of the geant4 hadronic design. They are, when registered with the tool-kit at initialisation, used to select the basic process. In the case of fission and inelastic scattering, point-wise semi-inclusive cross-sections are also used in order to decide on the active channel for an individual interaction. As an example, in the case of fission this could be first, second, third, or forth chance fission.

22.2.2 Elastic Scattering

The final state of elastic scattering is described by sampling the differential scattering cross-sections $\frac{\mathrm{d}\sigma}{\mathrm{d}\Omega}$. Two representations are supported for the normalised differential cross-section for elastic scattering. The first is a tabulation of the differential cross-section, as a function of the cosine of the scattering angle θ and the kinetic energy E of the incoming neutron.

$$\frac{\mathrm{d}\sigma}{\mathrm{d}\Omega} \;=\; \frac{\mathrm{d}\sigma}{\mathrm{d}\Omega}\left(\cos\theta,\; E\right)$$

The tabulations used are normalised by $\sigma/(2\pi)$ so the integral of the differential cross-sections over the scattering angle yields unity.

In the second representation, the normalised cross-section are represented as a series of legendre polynomials $P_l(\cos\theta)$, and the legendre coefficients a_l are tabulated as a function of the incoming energy of the neutron.

$$\frac{2\pi}{\sigma(E)}\frac{\mathrm{d}\sigma}{\mathrm{d}\Omega}\left(\cos\theta,\; E\right) \;=\; \sum_{l=0}^{n_l}\frac{2l+1}{2}a_l(E)P_l(\cos\theta)$$

Describing the details of the sampling procedures is outside the scope of this paper.

An example of the result we show in figure 22.1 for the elastic scattering of 15 MeV neutrons off Uranium a comparison of the simulated angular distribution of the scattered neutrons with evaluated data. The points are the evaluated data, the histogram is the Monte Carlo prediction.

In order to provide full test-coverage for the algorithms, similar tests have been performed for ^{72}Ge, ^{126}Sn, ^{238}U, ^{4}He, and ^{27}Al for a set of neutron kinetic energies. The agreement is very good for all values of scattering angle and neutron energy investigated.

22.2.3 Radiative Capture

The final state of radiative capture is described by either photon multiplicities, or photon production cross-sections, and the discrete and continuous contributions to the photon energy spectra, along with the angular distributions of the emitted photons.

For the description of the photon multiplicity there are two supported data representations. It can either be tabulated as a function of the energy of the incoming neutron for each discrete photon as well as the eventual continuum contribution, or the full transition probability array is known, and used to determine the photon yields. If photon production cross-sections are used, only a tabulated form is supported.

The photon energies E_γ are associated to the multiplicities or the cross-sections for all discrete photon emissions. For the continuum contribution,

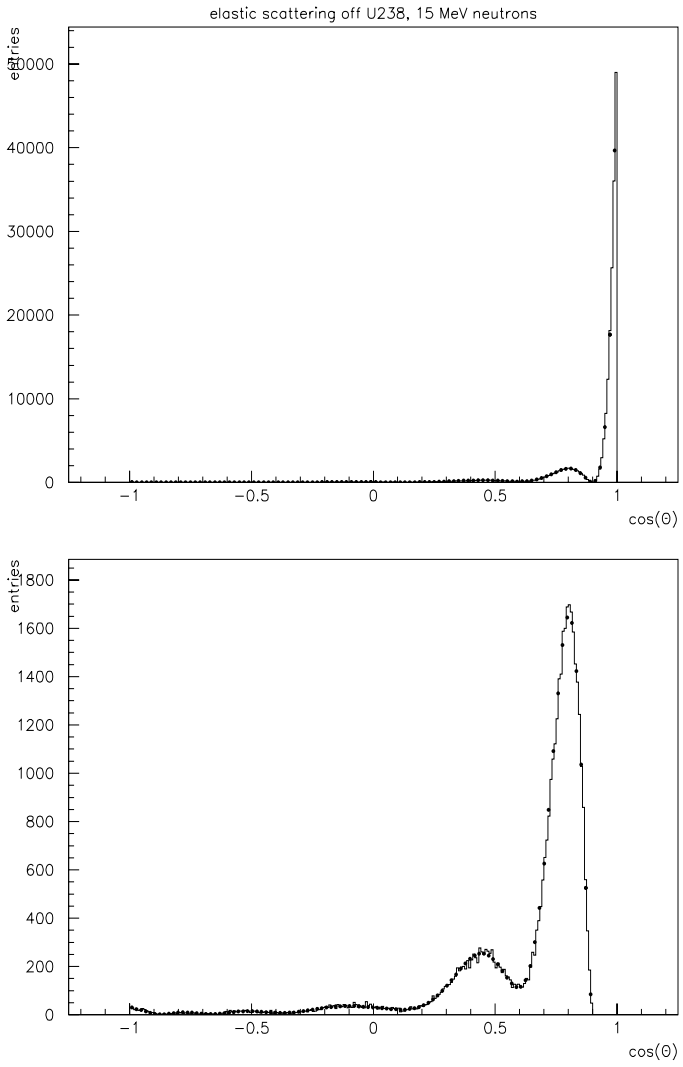


Figure 22.1: Comparison of data and Monte Carlo for the angular distribution of 15 MeV neutrons scattered elastically off Uranium (^{238}U). The points are evaluated data, and the histogram is the Monte Carlo prediction.

the normalised emission probability f is broken down into a weighted sum of normalised distributions g.

$$f\left(E \to E_\gamma\right) \;=\; \sum_i p_i(E) g_i(E \to E_\gamma)$$

The weights p_i are tabulated as a function of the energy E of the incoming neutron. For each neutron energy, the distributions g are tabulated as a function of the photon energy. As in the ENDF/B-VI data formats[1], several interpolation laws are used to minimise the amount of data, and optimise the descriptive power. All data are derived from evaluated data libraries.

The techniques used to describe and sample the angular distributions are identical to the case of elastic scattering, with the difference that there is either a tabulation or a set of legendre coefficients for each photon energy and continuum distribution.

As an example of the results is shown in figure22.2 the energy distribution of the emitted photons for the radiative capture of 15 MeV neutrons on Uranium (^{238}U). Similar comparisons for photon yields, energy and angular distributions have been performed for capture on ^{238}U, ^{235}U, ^{23}Na, and ^{14}N for a set of incoming neutron energies. In all cases investigated the agreement between evaluated data and Monte Carlo is very good.

22.2.4 Fission

For neutron induced fission, we take first chance, second chance, third chance and forth chance fission into account.

Neutron yields are tabulated as a function of both the incoming and outgoing neutron energy. The neutron angular distributions are either tabulated, or represented in terms of an expansion in legendre polynomials, similar to the angular distributions for neutron elastic scattering. In case no data are available on the angular distribution, isotropic emission in the centre of mass system of the collision is assumed.

There are six different possibilities implemented to represent the neutron energy distributions. The energy distribution of the fission neutrons $f(E \to E')$ can be tabulated as a normalised function of the incoming and outgoing neutron energy, again using the ENDF/B-VI interpolation schemes to minimise data volume and maximise precision.

The energy distribution can also be represented as a general evaporation spectrum,

$$f(E \to E') \;=\; f\left(E'/\Theta(E)\right).$$

Here E is the energy of the incoming neutron, E' is the energy of a fission neutron, and $\Theta(E)$ is effective temperature used to characterise the secondary neutron energy distribution. Both the effective temperature and the functional behaviour of the energy distribution are taken from tabulations.

Alternatively energy distribution can be represented as a Maxwell spectrum,

$$f(E \to E') \ \propto \ \sqrt{E'} \mathrm{e}^{E'/\Theta(E)},$$

or a evaporation spectrum

$$f(E \to E') \ \propto \ E' \mathrm{e}^{E'/\Theta(E)}.$$

In both these cases, the temperature is tabulated as a function of the incoming neutron energy.

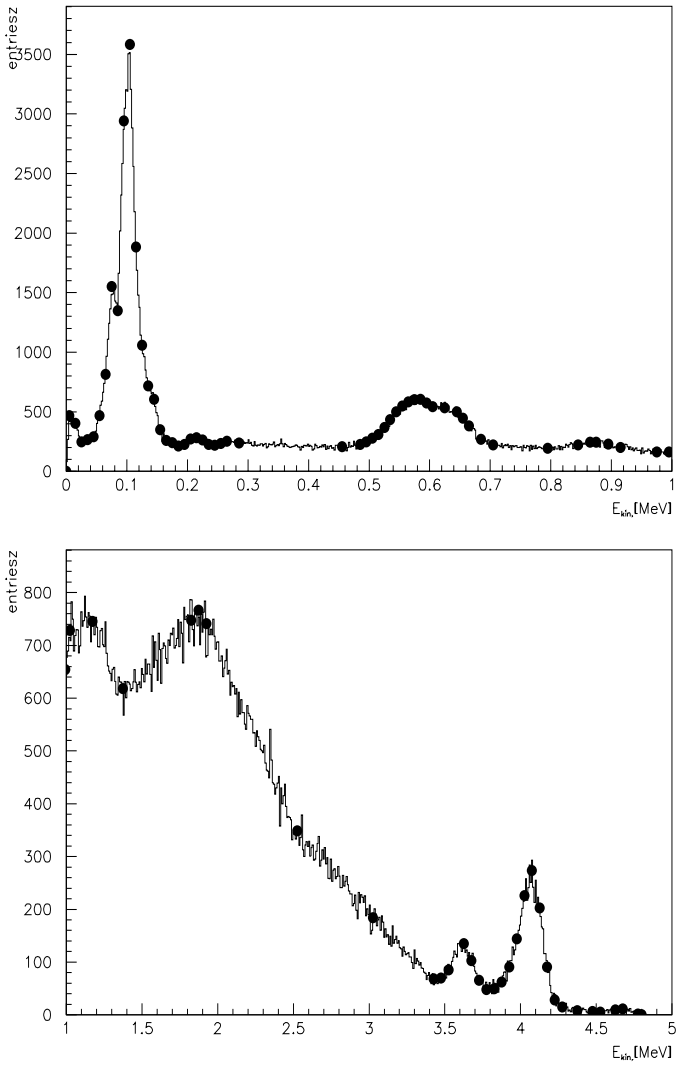


Figure 22.2: Comparison of data and Monte Carlo for photon energy distributions for radiative capture of 15 MeV neutrons on Uranium (^{238}U). The points are evaluated data, the histogram is the Monte Carlo prediction.

The last two options are the energy dependent Watt spectrum, and the Madland Nix spectrum. For the energy dependent Watt spectrum, the energy distribution is represented as

$$f(E \rightarrow E') \ \propto \ \mathrm{e}^{-E'/a(E)} \sinh \sqrt{b(E)E'}.$$

Here both the parameters a, and b are used from tabulation as function of the incoming neutron energy. In the case of the Madland Nix spectrum, the energy distribution is described as

$$f(E \rightarrow E') \ = \ \frac{1}{2} \left[g(E', < K_l >) \ + \ g(E', < K_h >) \right].$$

Here

$$g(E', < K >) \ = \ \frac{1}{3\sqrt{< K > \Theta}} \left[u_2^{3/2} E_1(u_2) - u_1^{3/2} E_1(u_1) + \gamma(3/2, u_2) - \gamma(3/2, u_1) \right],$$

$$u_1(E', < K >) = \frac{(\sqrt{E'} - \sqrt{< K >})^2}{\Theta}, \text{ and}$$

$$u_2(E', < K >) = \frac{(\sqrt{E'} + \sqrt{< K >})^2}{\Theta}.$$

Here K_l is the kinetic energy of light fragments and K_h the kinetic energy of heavy fragments, $E_1(x)$ is the exponential integral, and $\gamma(x)$ is the incomplete gamma function. The mean kinetic energies for light and heavy fragments are assumed to be energy independent. The temperature Θ is tabulated as a function of the kinetic energy of the incoming neutron.

Fission photons are describes in analogy to capture photons, where evaluated data are available. The measured nuclear excitation levels and transition probabilities are used otherwise, if available.

As an example of the results is shown in figure22.3 the energy distribution of the fission neutrons in third chance fission of 15 MeV neutrons on Uranium (^{238}U). This distribution contains two evaporation spectra and one Watt spectrum. Similar comparisons for neutron yields, energy and angular distributions, and well as fission photon yields, energy and angular distributions have been performed for ^{238}U, ^{235}U, ^{234}U, and ^{241}Am for a set of incoming neutron energies. In all cases the agreement between evaluated data and Monte Carlo is very good.

22.2.5 Inelastic Scattering

For inelastic scattering, the currently supported final states are (nA→) nγs (discrete and continuum), np, nd, nt, n^{3}He, nα, nd2α, nt2α, n2p, n2α, npα, n3α, 2n, 2np, 2nd, 2nα, 2n2α, nX, 3n, 3np, 3nα, 4n, p, pd, pα, 2p d, dα, d2α, dt, t, t2α, ^{3}He, α, 2α, and 3α.

The photon distributions are again described as in the case of radiative capture.

The possibility to describe the angular and energy distributions of the final state particles as in the case of fission is maintained, except that normally only the arbitrary tabulation of secondary energies is applicable.

In addition, we support the possibility to describe the energy angular correlations explicitly, in analogy with the ENDF/B-VI data formats. In this case, the production cross-section for reaction product n can be written as

$$\sigma_n(E, E', \cos(\theta)) \;=\; \sigma(E) Y_n(E) p(E, E', \cos(\theta)).$$

Here $Y_n(E)$ is the product multiplicity, $\sigma(E)$ is the inelastic cross-section, and $p(E, E', \cos(\theta))$ is the distribution probability. Azimuthal symmetry is assumed.

The representations for the distribution probability supported are isotropic emission, discrete two-body kinematics, N-body phase-space distribution, continuum energy-angle distributions, and continuum angle-energy distributions in the laboratory system.

The description of isotropic emission and discrete two-body kinematics

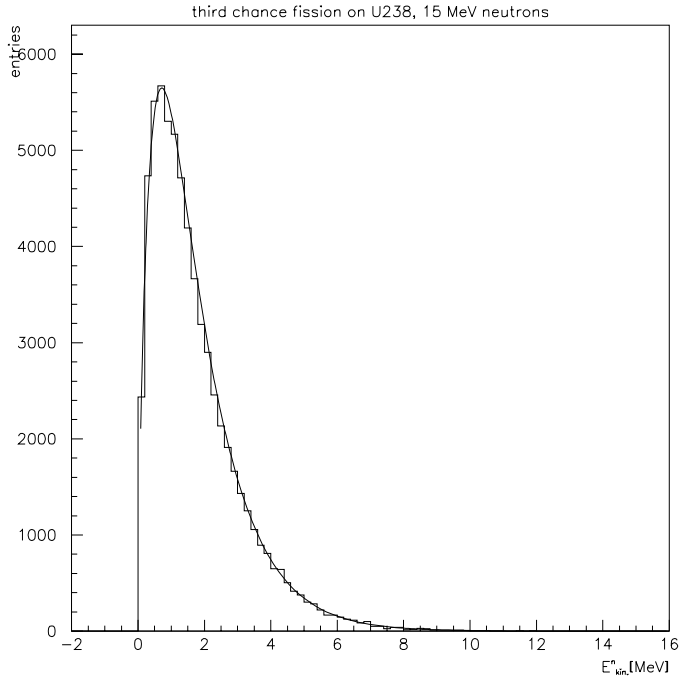


Figure 22.3: Comparison of data and Monte Carlo for fission neutron energy distributions for induced fission by 15 MeV neutrons on Uranium (^{238}U). The points are evaluated data, the histogram is the Monte Carlo prediction.

is possible without further information. In the case of N-body phase-space distribution, tabulated values for the number of particles being treated by the law, and the total mass of these particles are used. For the continuum energy-angle distributions, several options for representing the angular dependence are available. Apart from the already introduced methods of expansion in terms of legendre polynomials, and tabulation (here in both the incoming neutron energy, and the secondary energy), the Kalbach-Mann systematic is available. In the case of the continuum angle-energy distributions in the laboratory system, only the tabulated form in incoming neutron energy, product energy, and product angle is implemented.

First comparisons for product yields, energy and angular distributions have been performed for a set of incoming neutron energies, but full test coverage is still to be achieved. In all cases currently investigated, the agreement between evaluated data and Monte Carlo is very good.

22.3 Summary

By the way of abstraction and code reuse we minimised the amount of code to be written and maintained. The concept of container-sampling lead to abstraction and encapsulation of data representation and the corresponding random number generators. The Object Oriented design allows for easy extension of the cross-section base of the system, and the ENDF-B VI data evaluations have already been supplemented with evaluated data on nuclear excitation levels, thus improving the energy spectra of de-excitation photons. Other established data evaluations have been investigated, and extensions based on the JENDL[2], CENDL[4], and Brond[5] data libraries are foreseen for next year.

Bibliography

[1] ENDF/B-VI: Cross Section Evaluation Working Group, *ENDF/B-VI Summary Document*, Report **BNL-NCS-17541 (ENDF-201)** (1991), edited by P.F. Rose, National Nuclear Data Center, Brookhave National Laboratory, Upton, NY, USA.

[2] JENDL-3: T. Nakagawa, et al., *Japanese Evaluated Nuclear Data Library, Version 3, Revision 2,* **J. Nucl. Sci. Technol. 32**, 1259 (1995).

[3] Jef-2: C. Nordborg, M. Salvatores, *Status of the JEF Evaluated Data Library*, **Nuclear Data for Science and Technology**, edited by J. K. Dickens (American Nuclear Society, LaGrange, IL, 1994).

[4] CENDL-2: Chinese Nuclear Data Center, *CENDL-2, The Chinese Evaluated Nuclear Data Library for Neutron Reaction Data*, Report

IAEA-NDS-61, Rev. 3 (1996), International Atomic Energy Agency, Vienna, Austria.

[5] Brond-2.2: A.I Blokhin et al., *Current status of Russian Nuclear Data Libraries*, **Nuclear Data for Science and Technology**, Volume2, p.695. edited by J. K. Dickens (American Nuclear Society, LaGrange, IL, 1994)

Part V

Fast Shower Parametrizations

Chapter 23

Fast Shower Parametrizations